Aservice i Linköping
Orlunda Agro & IT
SWEDEN

WACO INVESTIGATION: IMAGE ANALYSIS AND VIDEO AUTHENTICATION

October 4 2000

Mrs. Lena KLASÉN
Orlunda Agro & IT
Skänninge, SWEDEN

Mr. Sten MADSEN
Aservice i Linköping
Linköping, SWEDEN

EXECUTIVE SUMMARY

The Office of Special Counsel, St. Louis, Missouri, U.S., was established to investigate the events that occurred at the Mt. Carmel complex on April 19, 1993, in Waco, Texas. As one part of the investigation, the Office of Special Counsel retained Mrs. Lena Klasén and Mr. Sten Madsen to perform image analysis and video authentication of the videotapes taken by the FBI Nightstalker surveillance aircraft on April 19, 1993. Mrs. Lena Klasén and Mr. Sten Madsen were retained January 13, 2000. This Executive Summary presents the results from an investigation of the flashes seen on the FLIR videotapes and the results from the FLIR video authentication, as requested by the Office of Special Counsel.

Image Analysis

Dr. Edward Allard, an expert for the Branch Davidians, initially compiled a list of questioned events or "flashes." Vector Data Systems (U.K.) Ltd., experts for the Office of Special Counsel later investigated this list. The Maryland Advanced Development Laboratory, experts for the U.S. government, have also investigated the list associated with Dr. Allard's declarations. The list of thermal events created by Vector Data Systems was provided to this investigation in February 2000 by the Office of Special Counsel, and served as a basis for the list used in this investigation. Vector Data Systems' list of flashes was updated within this investigation when appropriate.

In order to determine the cause of the flashes, a sophisticated computer hard and software systems solution was set up to analyze the FLIR imagery. The key issue to this investigation has been maintenance of the image quality and limitation of further degradation.

The technical approach for this investigation was to enhance the FLIR imagery in the area surrounding each questioned event. These enhancements were made to determine if any movement could be detected in relation to each flash. When moving objects were identified proximate to a flash, analytical methods were employed to determine whether the movement was human in form or nature. There is however no evidence of human movements in the area surrounding the flashes. There was, however, a lot of moving debris.

In the initial phase of the investigation it was discovered that several of the flashes appeared at fixed positions and on a regular basis. The timing of the flashes agreed with the FBI Nightstalker's circular movements over the Branch Davidian complex. This strongly suggested that the majority of the questioned events were caused by solar reflections. To confirm this hypothesis the reflection geometry of the day in question was reconstructed utilizing a 3D model based on the physical laws of reflection. The 3D model incorporated the positions of the Branch Davidian complex, the sun and the FBI Nightstalker. Based upon the striking correlation of the theoretical model and physical laws of reflection in comparison to the reconstructed geometry, it is concluded that the majority of the flashes were caused by solar specular reflections.

Four flashes of a pulsating nature could not be explained to be solar specular reflections from only the reconstructed data. To find the cause of these flashes, the imaging system itself was reviewed. Sophisticated and complex imaging technologies are not perfect. Imaging systems can create physical, electronic and mechanical phenomena, which were believed to cause undesired image artifacts and to affect the representation of small objects on the FLIR videotapes from April 19, 1993. To verify this assumption, the core of the FBI Nightstalker, the infrared SPRITE/TED detector elements and scanning mechanisms, were carefully studied. The interlaced video format used for recording the FLIR imagery was also studied carefully. The results from these studies confirmed the hypothesis that small objects cannot be assumed to be correctly represented on the FLIR videotapes. The Fort Hood flight trials were analyzed, as well, and pulsating flashes from reflecting debris were detected, similar to the flashes on the FLIR videotape from April 19, 1993. Based of the results from these examinations it is concluded that the remaining questioned flashes are reflections caused by solar or heat reflections, from single or multiple objects, subsequently distorted by the SPRITE/TED detectors and scanning mechanisms or the interlaced video format. Most likely there were complex combinations of these phenomena.

Many contradictory opinions exist as to the cause of the flashes seen on the FLIR videotape from April 19, 1993. Dr. Allard and Maurice Cox, among others, conclude that the flashes are gunfire. They also concluded that the FBI Nightstalker FLIR could not possibly record solar reflections. Dr. Allard stated "*nothing in nature could do this*" regarding the pulsating nature of thermal signatures. Mr. Allard and Mr. Cox's gunfire hypothesis is not only based on wrongful assumptions, but it also suffers from neglecting several important scientific parameters. For instance, (a) neglecting the FLIR sensor characteristics and scanning mechanisms, (b) impacts of the interlaced format of the video standard, (c) wrongful assumptions regarding solar reflections, (d) wrongful assumptions regarding the FBI Nightstalker aircraft ground speed and its position relative to the Branch Davidian complex. These factors have contributed to their misinterpretation of the flashes seen on the FLIR videotapes from April 19, 1993.

The Maryland Advanced Development Laboratory determined the flashes on the April 19, 1993, FLIR videotape, were too long to be muzzle blasts and instead were caused by a phenomena other than small-arm fire. The Maryland Advanced Development Laboratory further detected and proved solar specular reflections to be apparent on a watery surface. Their conclusions give a much more accurate and viable explanation for the flashes recorded on the FLIR imagery from April 19, 1993.

There are phenomena, unrelated to gunfire, that can cause flashes such as those seen on the April 19, 1993, FLIR videotapes. Solar reflections normally make little contribution in the thermal band in which the FBI Nightstalker surveillance system operated, but they are possible. The results of this investigation have proven that specular solar reflections do appear on the FLIR videotapes from April 19, 1993, between 10:41 a.m. - 12:16 p.m. The large amount of glass from broken windows and reflective debris from the demolished complex are believed to have contributed in a significant increase of the probability of specular solar reflections.

It is concluded with a confident level of certainty that all of the analyzed flashes seen on the FLIR videotapes from April 19, 1993, between 10:41 a.m. - 12:16 p.m., are caused by solar or heat reflections from single or multiple objects. The characteristics of the SPRITE/TED detectors and scanning mechanisms and the interlaced video format are factors that have contributed to distort the appearance of the flashes on the April 19, 1993, FLIR videotapes. Moreover, no humans were detected on the FLIR videotapes in any area in the vicinity of any of the flashes, only moving debris. The results from this investigation have shown, with a confident level of certainty, that the flashes on the FLIR videotapes from April 19, 1993, between 10:41 a.m. - 12:16 p.m., cannot form evidence of gunfire.

Originality and Authenticity of FLIR videotapes

The methods selected to investigate the originality and authenticity of FLIR videotapes Q-1, Q-2, Q-3, Q-4, Q-5, Q-6 and Q-7 were based on the characteristics of the electrical signals on the FLIR videotapes. The fact is, video machines leave individual and detectable traces on the videotape during recording. These traces can be measured and the measurements are like a fingerprint for a video machine. By analyzing these traces it can be determined whether a recordings has been interrupted, tampered with, erased, altered or recorded over. The following electrical signatures have been analyzed on the April 19, 1993, FLIR videotapes; RF-envelope for video signal, RF-signal carrier frequency for video signal, RF-envelope for FM-audio signal, RF-signal carrier frequency for FM-audio signal, dihedral error measurements and CTL-pulses.

Based on the analysis of the FLIR videotapes it is concluded, with a confident level of certainty, that only FLIR videotapes Q-1 – Q-5 are original recordings, in the sense that recorded portions are master recordings directly from the source, the FLIR sensor.

FLIR videotape Q-1 has at least three previous recordings found in the beginning of the tape, which all three have been over recorded. The recording made at 05:58:11-08:00:02 on April 19, 1993, is an original recording with no signs of edit or erasure on the recorded portion.

FLIR videotape Q-2 is an original recording with no signs of edit or erasure to the recorded portion.

FLIR videotape Q-3 is an original recording with no signs of edit or erasure to the recorded portion.

FLIR videotape Q-4 is an original recording with no signs of edit or erasure to the recorded portions. Although the recording is interrupted between 10:47:16 and 10:51:57, there is no sign that this portion of the tape was edited or erased.

FLIR videotape Q-5 is an original recording with no signs of edit or erasure to the recorded

portion.

FLIR videotape Q-6 is a first generation copy from an original master. There is no sign that the FLIR imagery has been edited. The master for this recording is not FLIR videotape Q-1 – Q-5.

FLIR videotape Q-7 is a first generation copy from an original master. Although the video sequence is interrupted between 10:47:15 and 10:51:57, there is no sign that this interruption in the recording is an edit point. There is no sign that any other part of the FLIR imagery has been edited or erased. The master for this recording is not FLIR videotape Q-1 – Q-5.

It is also concluded, with a confident level of certainty, that FLIR videotapes Q-1 – Q-5, are original recordings. There is no sign that the recorded portions on FLIR videotapes Q-1 – Q-5 have been edited or erased after they were produced. It is concluded, with a confident level of certainty that the interrupt on FLIR videotape Q-4, between 10:47:16 and 10:51:57, was not created afterwards but during the time of recording. It is also concluded, with a confident level of certainty, that FLIR videotapes Q-6 – Q-7, are copies.

CONTENTS

1. INTRODUCTION

In September 1999, the Attorney General of the United States appointed former United States Senator John C. Danforth to investigate the events at the Branch Davidian complex in Waco, Texas, 1993. Special Counsel Danforth established the Office of Special Counsel to carry out the investigation. As one part of the investigation, the Office of Special Counsel retained Mrs. Lena Klasén and Mr. Sten Madsen to perform image analysis and video authentication of the videotapes taken by the Federal Bureau of Investigation (FBI) Nightstalker surveillance aircraft on April 19, 1993. Mrs. Lena Klasén and Mr. Sten Madsen were retained January 13, 2000.

Based on her experience with defense reconnaissance applications, forensic casework and research on three-dimensional (3D) reconstruction of human shape and motion from video, the Office of Special Counsel asked Mrs. Lena Klasén to analyze the "flashes" on the FLIR videotapes, recorded April 19, 1993. Based on his vast experience with a variety of video technologies and forensic casework, the Office of Special Counsel asked Mr. Sten Madsen to investigate the originality and authenticity of the video track on each of the seven FLIR videotapes from April 19, 1993. Mrs. Klasén and Mr. Madsen have not been under a contract with the U.S. Government before this assignment. Neither have they been involved with any investigation of the events at the Branch Davidian complex in Waco, Texas, 1993, prior to this engagement. Mrs. Klasén's and Mr. Madsen's biographies are attached hereto as appendix 1.

1.1 Background

During the stand off the FBI Nightstalker FLIR imaging system recorded several videotapes of the Branch Davidian complex. According to information that was provided by the Office of Special Counsel, the FBI Nightstalker used April 19, 1993, was equipped with a Sea Owl long-range infrared (IR) imaging system. This Sea Owl long-range imaging system had as its core a SPRITE/TED IR detector. Thermal images from the FBI Nightstalker FLIR were simultaneously recorded onto VHS videotapes on April 19, 1993, FLIR videotapes Q-1 – Q-5. The masters for recordings Q-6 and Q-7 were also recorded on April 19, 1993.

The Branch Davidian complex appears on the FLIR imagery from a variety of viewing angles and distances as the FBI Nightstalker circled above the complex during surveillance. Conventional photos were also taken on April 19, 1993, from both aerial and ground views. Media covering the standoff also made video recordings of the events from morning to afternoon. Figure 1.1 is an image from FLIR videotape Q-4, a duplicate aerial color photo and a simplistic three-dimensional (3D) model from similar views. Figure 1.1 also illustrates the directional color-coding of the Branch Davidian complex used by the FBI, which will be referred to in this report.

This report describes the source data, the technical approach to the investigation, investigation procedures, results and conclusions.

Figure 1.1. A FLIR image (left), a duplicate photo (middle) and a simplistic 3D-reconstruction model of the Branch Davidian complex based on GPS stake coordinates (right), distances in meter [m].

1.2 Outline of Investigation

The Office of Special Counsel requested the following be determined: (1) the cause of the questioned events (also denoted as flashes or pulsating flashes) on FLIR videotape Q-4; (2) whether FLIR videotapes Q-1 – Q-7 are original and authentic; and (3) the location of any heat signatures associated with the start of the fire inside the Branch Davidian complex. After initial reviewing of the FLIR imagery and discussions with the Office of Special Counsel the tasks agreed upon were:

- to enhance image sequences from the FLIR videotapes and analyze the flashes seen on the FLIR videotape Q-4;
- to determine whether any persons appear on FLIR videotape Q-4 and to track and analyze their movements;
- to analyze the flashes on FLIR videotape Q-4 by reconstructing the geometrical relations of the Branch Davidian complex, sun and the FLIR sensor;
- to provide measurements and enhanced images for the fire development investigation;
- to determine if the FLIR videotapes are original recordings; and
- to determine if the FLIR videotapes have been edited or technically altered in any way.

Image processing for the fire investigation has been carried out in cooperation with Professor Ulf Wickström, SP, Swedish National Testing and Research Institute, an expert of the Office of Special Counsel, who received processed data from this investigation. Authentication of the FLIR video has been done in cooperation with Chris Mills, Network International Forensic Science Division, an expert of the Office of Special Counsel who analyzed the authenticity of the audio tracks on the FLIR videotapes.

2. INVESTIGATION MATERIAL

The Office of Special Counsel provided the source of data for this investigation. Appendix 2 contains a complete list of all material received. In this case only videotape Q-1 – Q-5 are original recordings, see chapter 6, which is why FLIR videotapes Q-1 – Q-5 provided the primary source of data in this investigation. Copy videotapes and duplicate imagery have been used as complementary source data rather than evidential images. Additional reference literature referred to in this investigation are included in the list of references at the end of this report.

2.1 Videotapes

FLIR videotapes Q-1 – Q-7, detailed in table 1, were made available for this investigation from February 29, 2000 to March 29, 2000. FLIR videotapes Q-1 – Q-7 are all in VHS format. FLIR videotapes Q-1 to Q-5 are original master recordings, while Q-6 and Q-7 are first order generation copies from original masters, see chapter 6.

Reference	**Notes and some of the text from cassette-labels**	**Time Information, Recorded Portions**
FLIR videotape Q-1	Videotape Q-1, VHS “Nightstalker - 4/19/93 Tape#1 -5:57 Am-8:00 Am Q-1”	05:58:11-08:00:02
FLIR videotape Q-2	Videotape Q-2, VHS “Nightstalker - 4/19/93 Tape #2 7:57A-9:30 AM Q-2”	07:57:42-09:28:20
FLIR videotape Q-3	Videotape Q-3, VHS “Q-3 Nightstalker 4/19/93 Tape #1 -5:57AM-7:57AM”	05:58:09-07:57:00
FLIR videotape Q-4	Videotape Q-4, VHS “Tape 1 ORIGINAL 4/19/93 appx 1:30 Q-4”	10:41:57-12:16:13
FLIR videotape Q-5	Videotape Q-5, VHS “4/19/93 Tape II Waco ORIGINAL appx 45 min Q-5”	12:16:37-13:39:07
FLIR videotape Q-6	Videotape Q-6, VHS “Tape #16 FBI aerial infra-red recording of Mt. Carmel’s Branch Davidian Compound on 4/19/93, 12:41 p.m. through 2:01 p.m. (2 of 2). Elsur #1B-319”	12:41:25-14:01:38
FLIR videotape Q-7	Videotape Q-7, VHS “Tape #15 FBI aerial infra-red recording of Mt. Carmel’s Branch Davidian Compound on 4/19/93, 10:41 a.m. through 12:41 p.m. (1 of 2). Elsur #1B-319”	10:41:56-12:41:07

Table 1. FLIR videotapes Q-1 – Q-7.

The Office of Special Counsel also provided copies of the April 19, 1993, FLIR videotapes (app. 2, items 8-11), one FLIR videotape recorded at the Branch Davidian complex on March 26, 1993, (app. 2, item 12), videotapes of major news footage (app. 2, items 13-14), a videotape concerning solar reflections in the far IR spectrum presented by the Maryland Advanced Development Laboratory (app. 2, item 15) and videotapes from the Fort Hood flight trials March 19, 2000, (app. 2, items16-26). All videotapes (app. 2, items 8-26) were in VHS format and were copies.

2.2 Digital Images, Photos and Duplicate Photos

The Office of Special Counsel also provided digital images of the complex before and during April 19, 1993, (app. 2, items 27-34). A hard disk with digitized video (app. 2, items 35), as well as requested primary FLIR images with temperature data from the flight trials at Fort Hood (app. 2, items 36) were received. All of the digital images of the Branch Davidian complex were, however, digitized from photos or reproductions from duplicates and were stored in compressed image formats. The negatives were unavailable to this investigation. Duplicate photos of the complex (app. 2, items 42-43) and photos of the Fort Hood trial site (app. 2, items 37-41) were further provided. The photos from the flight trials (app. 2, items 37-41) were produced directly from the negatives.

2.3 Maps and Drawings

Maps and drawings of the complex, both as paper copies (app. 2, items 44-49 and 52), stake positions of Mount Carmel complex (app. 2, item 50) and CAD data (app. 2, item 51) were requested and provided by the Office of Special Counsel.

2.4 Reports and Related Literature

The Office of Special Counsel provided expert reports for information and review (app. 2, items 53-65). Experts prepared these reports for the Branch Davidian, the U.S. Government and the Office of Special Counsel and concerned issues relevant to this investigation. Each of these reports was reviewed and a summary of the review is included in chapter 7.

Requested, and also provided by the Office of Special Counsel, were a summary of the NIIRS rating scale (app. 2, item 66), an abbreviated summary of the FBI Nightstalker FLIR system platform data (app. 2, item 67), the protocol for the Fort Hood flight trial (app. 2, item 68), a copy of the FBI Nightstalker aircraft handbook (app. 2, item 69) and audio transcripts of the April 19, 1993, FLIR videotapes (app. 2, item 70). A summary of public statements made by experts regarding the flashes seen on FLIR videotape Q-4 and the copy Q-6 (app. 2, item 71) were also provided.

2.5 Miscellaneous

Other data requested for the investigation were climatic information and daily weather reports for April 19, 1993, (app. 2, item 72), and March 18-19, 2000, (app. 2, item 73). An early and abbreviated version of the Vector Data Systems' (U.K.) Ltd. master event list was also received from Vector Data Systems, (app. 2, item 74).

3. TECHNICAL APPROACH

It is important to clarify the parameters that were considered important for analyzing the FLIR videotapes.

The FBI Nightstalker FLIR system generated thermal images of wavelength 8-13 μm, outside the visible range of human biological vision, which is 0.4-0.7 μm. CCD images and conventional photos are images captured within the range of our biological vision. As infrared (IR) wavelengths are captured outside our visual range, a thermal image can be defined as an image captured by an infrared detector and converted into a visual image by a thermal imaging system. The detector elements in the thermal imaging system convert infrared radiation into an electrical signal, which further is converted into a video signal that can be recorded and displayed.

Thermal images make the light naturally emitted by an object visible based on temperature differences rather than absolute temperatures. The temperature difference, in turn, depends on the objects energy exchange with the environment, self-heating, emissivity differences or reflections of other sources. Emissivity is explained as the magnitude of radiated thermal energy from a surface as a function of the surface property. Mathematical models that describe in detail how this radiated thermal energy is converted in the imaging system are well described in the literature. See [Fraden] and [Cuthbertson]. The advantage of a thermal imaging system is the ability to expand the human visual range into the infrared region. For example, thermal imaging can provide night vision. Another advantage is the ability to detect, track and recognize objects at a long range, provided a resolvable temperature difference relative to the background is available.

Thermal images cannot be directly compared to images taken directly in our visual range as the inputs from the real world are different. One major factor is the use of temperature differences instead of illumination in thermal imaging. In practice, this difference can cause hot water and cold water to look different on a thermal image, but on a conventional photo it will appear the same. Further explanations and illustrations of the differences are found in [HolstIR], [HolstCCD] and [Cuthbertson], but also in (app. 2 item 65) and in appendix C in (app. 2 item 58). Neglecting the significant difference in thermal images compared to CCD images and conventional photos can lead to unrealistic conclusions about what can be seen on the FLIR videotapes.

As "*nothing is as good as the original*" regarding imaging technologies in forensic applications, analyzing a low quality image requires specific methods to avoid further degradation in all phases of the investigation. This has been a key issue for this investigation. Signal-to-noise ratio (SNR) can be a useful measure of image quality degradations caused by a particular system or sub-system. Variations in image quality can originate, for example, from the varying performance of video recorders, video systems, equipment used to digitize and display the video, computer frame grabbers, image format, monitors, projectors and computer screens. Each of these systems will introduce some kind of degradation to the

image. Literatures on the subject are [HolstIR] and [HolstCCD] who discuss some of these variations.

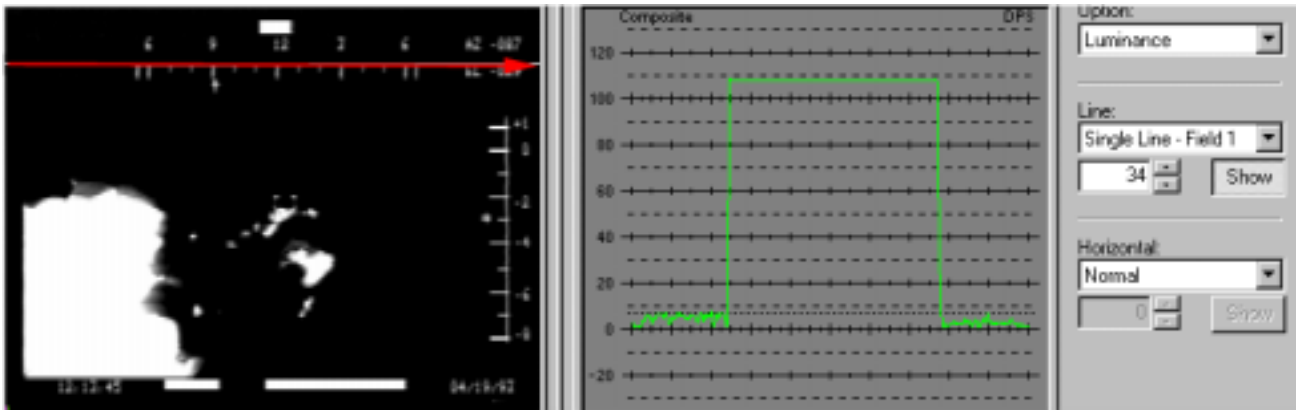

Figure 3.1. Signal levels in percentage (right image) measured at the red horizontal arrow in the FLIR image (left image).

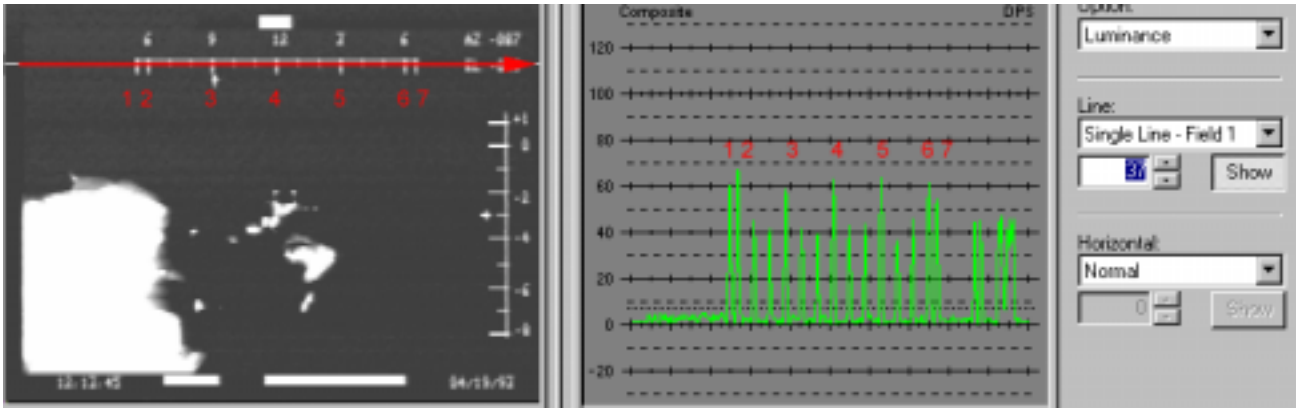

Figure 3.2. Variations between perceived visual information at the red horizontal arrow in the FLIR image (left image) and corresponding measured signal levels in percentage (right image).

Degradation of image quality had already been induced during recording of the FLIR videotapes. Figures 3.1 and 3.2 are images from FLIR videotape Q-4. The measurements are from an examination of the video signal levels before the FLIR videotapes were digitized. The AZ-presentation in the FLIR images indicates the azimuth angle of the FLIR sensor relative to the FBI Nightstalker aircraft. The video level on the FLIR videotapes was adjusted by using the video signal level of the AZ-presentation as a reference level. The white-level of the horizontal part in the AZ presentation became saturated at 109 %, measured by the system's built in waveform monitor. This corresponded to a pixel value of 255 in an 8-bit grey scale image, figure 3.1. In practice, this means that what we clearly perceive as "white" also remained "white" in the digitized images and that the image quality was maintained as desired. Figures

3.1 and 3.2 indicate two different kinds of problems; image degradation by the video format; and the difference between perceived and measured image information.

First, bandwidth limitations of the video format used when recording the FLIR videotapes degrades the recorded signal levels. Problems occur during rapid changes between "black" and "white," as an effect of the bandwidth limitations for the video format. This affects the representation of small objects. Figure 3.2 reveals this kind of degradation in the horizontal direction of small details, as the vertical parts of the AZ presentation, seen in figure 3.2, were limited to a maximum level (estimated to ≈65%) instead of "white" that was calibrated to 109%.

Secondly, there is a significant difference in how the human visual system perceives and processes visual information, compared to computer aided image analysis. The human visual system has the ability to process visual information beyond the capacity of today's computer vision methods. One example is the human eye's ability to deal with invariance caused by the varying scale of an item or changes in lighting conditions. This is a complex task to implement. In fact, it is so difficult that it is the subject of numerous ongoing research projects. There are, however, some weak points in our biological visual system. An example is our limited ability to resolve small quantitative differences, such as minor changes in contrast or in the size of an object. Computers can be used to assist the eye in making quantitative assessments. Computer based algorithms provides a consistent review of an image, compared to variations in each individual's ability to resolve small variations. The difference between visually perceived information and measured signal levels are illustrated in figure 3.2. The vertical bars (measured video signal level <65%) of the AZ-presentation appear the same "white" to the human eye as the horizontal bar (measured video signal level 109%). However, the measured video signal level shows a significant difference.

The use of image compression techniques can also introduce unwanted artifacts that can change the texture and geometrical shape of an object within an image. Normally we cannot see these data artifacts, but the introduction of these data artifacts can affect the integrity of the original image and threaten its reliability for forensic examination.

At this time and to the author's best knowledge, there is no formal standard for the use of evidential images. An overview of image analytical methods in criminal justice systems is presented in [Klasén], in which the urgent need for standardized forensic image procedures also is discussed. The Scientific Group on Imaging Technologies, [SWGIT], presented recommendations and guidelines in April 1999. In both documents it is suggested that original images and images to undergo image analysis, should not undergo "lossy" compression or other kinds of processing or copying that would case degradation to the original image. For this investigation, these general recommendations have been followed.

It is necessary to have knowledge of <u>all</u> phases of the imaging process and the behavior of the system components within the imaging system. The reason for this is to be aware of how objects in the

real world are represented and where the information from the real world might be degraded by the system's components. Examples of such components are the system's optics, detector elements, system electronics, storage media, digitizing procedures, computer based algorithms, display units, printers and the abilities of the system's operators. These factors all need consideration during any forensic examination. Imaging technologies are designed to achieve an optimal image quality, but features like noise patterns and deviations in signal-levels are often the key issues in forensic investigations.

The technical approach for this investigation was to first analyze the FLIR sensing system and, in particular, its SPRITE/TED detector. Some typical fixed pattern noise induced by the scanning mechanisms, among other factors, was immediately detected and recognized on the FLIR imagery. The results from this examination proved valuable in the digitizing process, noise reduction and for estimating the tracking error in the 3D reconstruction. The findings of the systems examination were also quite important to explain why small objects cannot be trusted to be correctly represented in the thermal images from the FLIR system.

The next step was to analyze the FLIR videotapes in depth. Because analyzing evidential images often means extracting information that is not directly obvious to our eyes and brain, image enhancement methods were used to provide images that were easier to interpret. Various analytical methods were used to provide complementary numerical values, such as the position of a flash or the FLIR sensor position. The main focus of this part of the investigation was to reconstruct the flash geometry. This work has been performed with awareness to the generic problems of detecting small objects, false detection, and the specific imperfections of the FBI Nightstalker's long-range thermal imaging system used on the April 19, 1993.

The electrical signals stored on the FLIR videotapes were successfully used to authenticate the April 19, 1993, FLIR recordings. Video machines leave individual and detectable traces on the videotape during recording. To determine if the recordings were interrupted, tampered with, erased, altered or recorded over, the following electrical signatures were analyzed; RF-envelope for video signal, RF-signal carrier frequency for video signal, RF-envelope for FM-audio signal, RF-signal carrier frequency for FM-audio signal, dihedral error measurements and control pulses (CTL- pulses).

4. IMAGING

The system used to digitize and analyze the recorded images on the April 19, 1993, FLIR videotapes utilized dpsReality/Velocity software and a frame grabber processing board. This was hosted in an Intel Pentium PC with a Windows NT 4.0 operating system. Data was stored uncompressed on an IBM SCSI raid disc with a capacity of 226 Gb. Seven additional IDE discs, of 20 to 26 Gb storage capacities were used for uncompressed storage of the remaining digitized video.

In order to digitize and store such a large amount of data, while retaining as much as the image quality as possible, analogue measurements and system tests were performed prior to digitizing. This was an important phase in the video authentication investigation, as deviations in measured values are also useful to trace technical tampering. Significant effort was put into creating sequences to be used for image enhancements. As a result, the FLIR videotapes were digitized at three different levels of the available video signal.

First, the dpsReality/Velocity systems default settings were used to maintain the FLIR videotapes' dynamic range. System defaults in this case resulted in some bit reduction. As the graphical presentations in the FLIR image peripherals were of slightly higher intensity than the saturation level by the FLIR sensor, this bit reduction was not critical. When digitizing the video signal, the white-level of the horizontal part in the AZ presentation, figure 3.1, was used as reference as this was the highest video signal level. This was set to correspond to pixel value 255 in an 8-bit grey scale image, which also corresponds to the cut of level of the system used for this investigation. Loss of single frames was only detected on three occasions, a rate that was considered small enough to be neglected considering the large amount of frames.

Secondly, interesting sequences from FLIR videotape Q-4 were digitized, with the dynamic range in low contrast areas stretched before digitizing. This saturated the upper and lower parts of the dynamic range. In this way, a significant enhancement of the contrast for the middle grey levels was achieved. These sequences were specifically designed to search for persons or other objects of very low contrast relative to the background and proximate to the flashes.

Third, several sequences from FLIR videotape Q-4 were digitized multiple times in the same manner to be used for noise reduction.

All of FLIR videotape Q-4 was digitized. Selected sequences from FLIR videotapes Q-1, Q-2 and Q-5 were also digitized. FLIR videotape Q-3 was omitted as the content and quality were similar to FLIR videotape Q-1. FLIR videotapes Q-6 and Q-7 were not used since they were first generation copies. In total, approximately 3 hours of video from the FLIR videotapes were digitized, which still left space on the system for temporary storage of processed sequences.

Each video frame was captured and stored in uncompressed YUV format. In this case it was unnecessary to use images of size 720 x 486 x 24 bit, as there is no color information on the FLIR videotapes to necessitate the use of 24 bit for color depth. However, there were many advantages with this system solution. For instance, it was a commercially available product with support facilities. A major functionality was that the system allowed access to stored images directly by other image analysis software, on arbitrary image formats and within very reasonable access times. The system also provided export facilities for different image formats. The system provided functions to view and export images at arbitrary speed and direction, either in frame or field mode. Images in BMP format were used throughout the investigation to avoid compression. For the three-dimensional reconstruction TGA images were needed, as BMP files were not accepted by the reconstruction software. ACDSee software was used to convert uncompressed BMP files to TGA, as the RLE compression option could be disabled for TGA files. No external image stabilization equipment beside the frame grabber was included in the system.

For image analysis Matlab by the MathWorks Inc. was used for benchmarking, measuring, mathematical calculations and for data visualization. Cognitech Video Investigator was used for image enhancement. MatchMover by Realviz was used for 3D reconstruction. ACDSee by ACD Systems Ltd. was used for viewing and image format conversions.

A 150 MHz, 4-channel Gould 3150 oscilloscope, a frequency counter, the dpsReality's built in waveform monitor and an external Leader LBO 5861 waveform monitor were all used for benchmarking and for accurate measurements of electrical signals from the FLIR videotapes. SONY PVM 1371 and Croma Monitor CM 151 video monitors and a variety of video projectors were used for viewing. JVC BP 5300EP and Panasonic AG 6200 video machines were also used, since these particular types of older video machines do not create or add any undesired signal processing to the final output. A Panasonic NV-W1E video machine was used to analyze the audio hi-fi tracks. A Panasonic alignment tape was used as a reference to calibrate the video machine. The built in oscilloscope in the dpsReality software was also used for benchmarking and monitoring the video signal.

5. IMAGE ANALYSIS

The first task was to enhance the sequences that included the flashes seen on the original FLIR videotape Q-4. Enhancements were achieved by applying image processing methods to deal with the various image distortions. The aim was to extract whatever visible information existed within the FLIR imagery. The FBI Nightstalker FLIR system not only created infrared video recordings, it also added a complex combination of noise and blur to the recorded images. As the characteristics of the FBI Nightstalker FLIR system have had a significant impact on the image quality, the FLIR imaging system itself needed to be investigated, section 5.1. Software specialized for investigative video processing was used to reduce and compensate for this noise and blur, see section 5.2. This software also provided techniques to achieve high-resolution images from FLIR videotape Q-4 based on "frame fusion for super-resolution".

In the case of alleged gunfire, it is reasonable to assume that persons would have to be present to fire the subject weapons. After a careful analysis of the areas surrounding the questioned events and careful tracking of movements of any type of objects near the flashes, it was concluded that no human type movement or activity occurred near any of the flashes on the April 19, 1993, FLIR videotape Q-4, see section 5.3.

In an early stage of the investigation it was discovered that the appearance of the flashes could actually be predicted. For example, some flashes on the single-story roof of the Branch Davidian complex occurred approximately every two minutes, figure 5.1. These flashes also occurred when the same part of the complex was in the FLIR sensor field of view and the FBI Nightstalker was in a similar position relative to the complex.

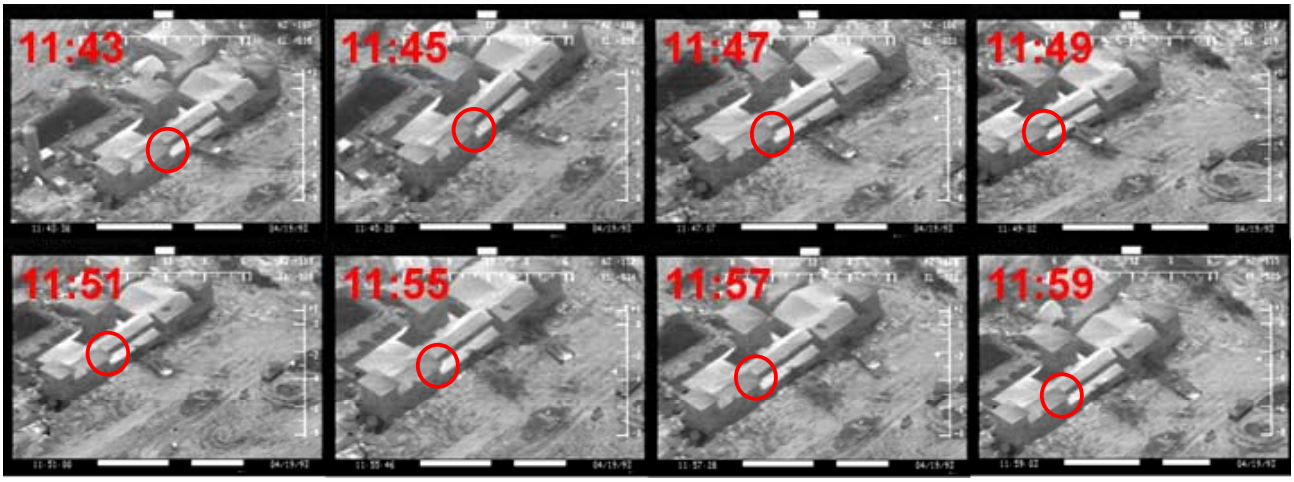

Figure 5.1. Regular appearance of flashes from the same part of the single story roof at 11:43:36, 11:45:20, at 11:47:07 the roof was partially clouded and a flash only faintly visible, at 11:49:02,

11:51:00, 11:55:46, 11:57:26 and 11:59:03. At 11:53 no reflection was detected. At 12:01 and 12:03 the single story roof was only partially seen in the FLIR images. At 12:05:15 a flash appeared again from this same part of the single story roof.

"Two-minute turns" are commonly used in aviation. From the FLIR imagery it was clearly seen that one turn of the FBI Nightstalker takes about two minutes to complete. See for example figure 5.1. On April 19, 1993, the FBI Nightstalker's pilot probably flew so the operator could keep the complex in the FLIR sensor's field of view. In all probability this caused the pilot to fly under visual flight rules (VFR). Variations in the FBI Nightstalker's flight path were believed to have been caused by the strong wind, which made the aircraft drift relative to the complex. As the flight path played an important role during recording of the FLIR videotapes, the first task was to investigate the various positions of the FBI Nightstalker and thereby the FLIR sensor, section 5.4.

It was discovered that the flashes seemed fixed in position relative to the complex. Based on the predictable nature of the flashes, it was decided to reconstruct the flash geometry in order to confirm the hypothesis that the flashes were reflections from glass or other kind of debris, section 5.5. Reconstructing the geometry for the flashes in table 2 became the main focus of this investigation due to the characteristics of the flashes, the results from the image enhancement and the lack of persons proximate to any of the analyzed events.

A three-dimensional (3D) reflection model based on the physical laws of reflection formed the basis for the reconstruction of the flash geometry. Essential parameters included the position of the complex, the position of the sun and the FBI Nightstalker's flight path from which the FLIR sensor position was determined. The reconstruction model was based on the geometrical relation between the two-dimensional (2D) information in the FLIR thermal images and the true size and location of objects existing in the real world. The time was set within the model based on the time information in the images and the reliable frame rate of the video standard. In all probability, the FLIR operator set the time and date information when he initialized the FLIR system.

One of the problems encountered when reconstructing 3D information from FLIR videotape Q-4 was the lack of detailed platform data. Fortunately, the Nightstalker's FLIR sensor is well described in research literature. Additional information requested and provided by the Office of Special Counsel, were reliable measurements of the complex and weather conditions for April 19, 1993.

As the solar specular reflection hypothesis did not fully explain the appearance of some of the flashes, the characteristics of the FLIR sensor and the video format were also studied. The Fort Hood flight trials were also analyzed, section 5.5. This analysis was motivated from the results in section 5.1, where it was concluded that the FLIR system could distort the image representation of small objects such as the flashes.

The image analysis confirmed that the analyzed flashes were specular solar reflections or other kinds of heat reflections from single or multiple objects. Moreover, the FLIR and video recording system induced image distortions, which affected several of the flashes seen on the FLIR images. The results from this investigation were confirmed by conducting an experiment, section 5.5. Due to the many contradictory conclusions by experts concerning the cause of the flashes, reports, statements and videotapes by Branch Davidian and government experts were carefully reviewed and summarized in chapter 7. This review supported the result from this investigation.

The flashes that have been analyzed are detailed in table 2. The table is based on the list provided by Vector Data Systems (U.K.) Ltd., updated with some additional observations from this investigation. The color-coding as illustrated in figure 1.1 has been used to roughly indicate the position of the flashes.

START	END	VDS #	NOTES	SIDE
10:53:24	10:53:25	1	Reflections from water surface towards gym	Black
10:54:20		2	Flash at damaged structure	Red
11:05:50	11:05:53	3	Flashes near a water storage tank	Green
11:14:10		4	Flashes at damaged structure	Red
11:18:21	11:18:23	5	Flash from left rear hull of Combat Engineering Vehicle 2 (CEV 2)	Black
11:18:48		6	Flash at demolished corner of gym	Black
11:23:25		7	Flash near left rear of CEV 2, close to gym	Black
11:24:30	11:24:35	8	Flashes directly to the rear of CEV 2	Black
11:24:50	11:24:51	9	Flashes on cafeteria roof	Black
11:25:02		10	Flash on chapel roof	Red
11:25:04		11	Flash on chapel roof	Red
11:26:27		12	Flashes near rear right drive sprocket of CEV 2	Black
11:28:04	12:28:14	13	Flashes in courtyard in front of central tower	Green
11:28:18	11:28:21	14	Flashes on cafeteria roof	Black
11:28:22		15	Flashes on cafeteria roof	Black
11:30:08	11:30:14	16	Flashes (weak) in courtyard in front of central tower	Green
11:30:26		17	Flashes on cafeteria roof	Black
11:34:32		18	Flash in courtyard in front of central tower	Green
11:34:32		19	Object moving from destroyed corner of gym to diving platform	Black
11:34:33		20	Flashes on cafeteria roof	Black
11:34:45		21	Flash on chapel roof	Red
11:38:31		22	Flash in front of CEV 2	Black
11:38:45		23	Flash at “black spot” at innermost penetration by CEV 2	Black

			into gym	
11:42:00	11:42:01	24	Flashes at damaged structure	Red
11:42:32	11:42:33	-	Flash in demolished gym area	Black
11:43:33		25	Flash on single-storey roof	White
11:43:35	11:43:38	26	Flashes on single-storey roof	White
11:44:48		27	Flash on cafeteria roof	Black
11:44:52	11:44:54	28	Flashes on cafeteria roof and courtyard near central tower	Black
11:45:15	11:45:24	29	Flashes on single-storey roof (flag pole end)	White
11:46:32	11:46:33	30	Flashes on ground at base of central tower and close to or on cafeteria roof	Black
11:46:34		31	Flash in courtyard	Green
11:46:36		32	Flash on cafeteria roof	Black
11:46:43		33	Flash near central tower	Black
11:47:05		34	Flash on single-storey roof	White
11:48:14		35	Flash on cafeteria roof	Black
11:49:01	11:49:08	36	Flashes on single-storey roof	White
11:50:17		37	Flash in courtyard near base of central tower	Green
11:50:27		38	Flash in courtyard near central tower	Black
11:50:59	11:51:04	39	Flashes on single-storey roof	White
11:55:46	11:55:47	40	Flashes on single-storey roof	White
11:57:25	11:57:28	41	Flashes on single-storey roof	White
11:58:04		42	“Flash” as CEV 1 withdraws from main door	White
11:59:03		43	Flashes on single-storey roof and also on roof near damaged area	White
12:00:40		44	Flash behind CEV2	Black
12:01:06		45	Flashes on ground in debris side of chapel	Red
12:05:13	12:05:17	46	Flashes on single-storey roof	White
12:08:31		50	Flashes near catwalk roof in gym	Black
12:08:48	12:08:50	51	Flashes near corner of damaged gym, closest to central tower	Green
12:08:51	12:08:52	52	Flashes next to CEV 2 at gym	Black
12:09:00		53	Flash on lean-to roof side of chapel	Black
12:09:23		54	Flash from inner courtyard, right of tower	Green
12:09:59		-	Flashes on CEV	Green
12:10:42		56	Person lying on single storey roof	Black
12:10:48	12:10:53	-	Multiple flashes in debris in courtyard	Green
12:10:58	12:11:23	57	Multiple flashes in debris in courtyard and on chapel roof	Green

Table 2. List of analyzed flashes.

All events in table 2 and in particular events 5, 50 and 53, have been thoroughly enhanced as described in section 5.2. Events 19, 50-52 and 56, as well as several additional sequences of low contrast, have been investigated in section 5.3. The flight path and the flashes were analyzed as described in section 5.4 and 5.5 respectively.

A second, primary image analysis task was to apply methods for tracking, pseudo-coloring and measuring the imagery at the initial phase of the fire. Events 47-49 and 55 have been excluded from table 2 as events related to the fire were analyzed separately as described in section 5.6.

The first time some of the events are visually detectable on the FLIR videotapes depends on the imaging techniques and display units, among other factors. This was considered in this investigation. All times for the first visual appearance of events stated in this report were based on the image quality, system configuration, display units and monitors as described in chapter 4.

The term “image” will be used for the reminder of this report to denote one field in a video frame. Fields have been used throughout this investigation for image processing and analysis. The reason for this was to avoid the motion blur induced by the video format that frequently disturbs the image quality. The video format is further explained in chapter 6. “Image” will also be used to denote a digitized photo, photo or duplicate image. “FLIR sensor” will be used as an acronym to the term “camera.”

5.1 Characteristics of the FBI Nightstalker FLIR Imaging System

The FLIR sensor in the FBI Nightstalker is different from an ordinary video camera equipped with a CCD sensor. The FBI Nightstalker FLIR is a serial/parallel scanner system, aimed for long-range and is based on a SPRITE/TED detector. The ability of this FLIR system to resolve small objects depends mainly on its spatial resolution and thermal sensitivity. Video format, monitoring devices and operator abilities can also affect resolution capabilities. For the SPRITE/TED some additional parameters were of great importance. For this reason, the characteristics of the FBI Nightstalker FLIR system and its SPRITE/TED detector, see figure 5.2, and scanning mechanisms were carefully reviewed.

Many of the commercially available computer programs for photogrammetry, three-dimensional (3D) reconstruction and video processing are based upon the use of “ordinary” short-range staring cameras. The known characteristics of the FLIR system and its impacts on the image quality were incorporated as part of the image analysis procedures described in the remaining of this chapter. It was also used for estimating errors in the algorithms on which the analytical methods were based.

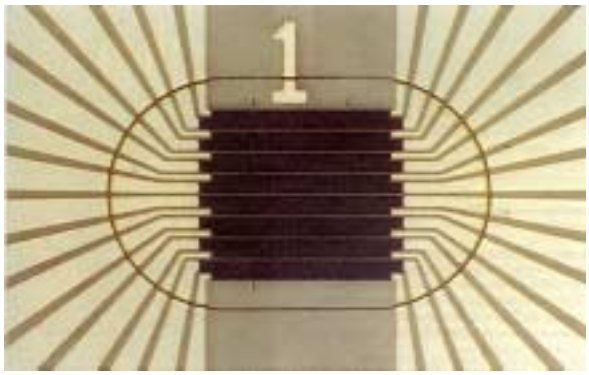

Figure 5.2. A SPRITE/TED array, from [Baker] p. 153.

5.1.1 The FBI Nightstalker FLIR Sensing System

The word ”FLIR” was originally used to denote airborne Forward-Looking InfraRed thermal imaging systems, but has since been adopted to denote thermal imaging system in general. Many early FLIR systems were mounted fixed relative to the aircraft and directed towards the target by directing the fuselage. The FBI Nightstalker FLIR is not only forward looking, an operator can also direct the FLIR sensor ±120° in the horizontal plane (azimuth angle, AZ) and -20° to -80° vertically (elevation, EL) relative to the carrier aircraft. According to information received from the Office of Special Counsel, the carrier was a multi-engine turboprop aircraft. An on-board operator maneuvered the FBI Nightstalker FLIR during the surveillance whilst the FLIR videotapes were recorded. This directional control of the sensor relative to the aircraft is seen on the FLIR images, both numerically and graphically, figure 5.3. The date and time information in this report refers to the numerical presentations seen in the FLIR images, figure 5.3.

Using a wide field of view provides a useful overview typically used for target detection. A narrow field of view is generally used for tracking and recognition of distant or small targets. The operator of the FBI Nightstalker FLIR could select either a wide field of view (WFOV) 9.7° x 6.5° or a narrow field of view (NFOV) 1.6° x 1.08°. WFOV was in use when capturing figure 5.3. NFOV was in use when the flashes in table 1 appeared on April 19, 1993. The concept of dual fields of view are in many cases inspired from the biological visual system of particularly sharp eyed birds, like hawks, as their center of the field of view provides a far better spatial resolution than peripheral views.

Normally, the term mid IR is used to denote wavelengths in the spectral range 3-5 μm, while far IR is used to denote 7-13 μm. The SPRITE/TED detector in the FBI Nightstalker FLIR system operated in the far IR band, 8-13 μm.

Figure 5.3. FLIR image graphics.

Thermal images are directly related to the thermal radiation variations from the scene, as illustrated in figure 5.4. To obtain optimal image quality the thermal window and the offset temperature can be adjusted to meet the dynamic requirements of a scene. "Gain" is often used to denote the instantaneously thermal range, or thermal window of the depicted scenery. In this case, "bias" defines the offset temperature in relation to the specified operating range of the system.

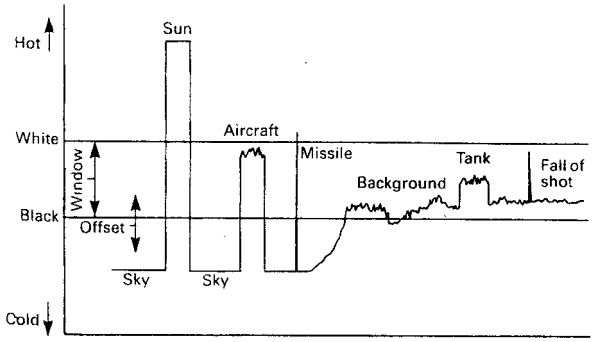

Figure 5.4. Dynamic range requirements of a typical scene illustrating the thermal window and offset bias, from [Cuthbertson] p. 25.

Two different dynamic range settings are illustrated in figure 5.5. The output signal from the FLIR sensor on April 19, 1993, varied sometimes very rapidly. This rapid variation in image intensity was related to the dynamic "gain" and "bias" that were automatically adjusted to the dynamic range of the

scene for almost the entire time FLIR videotape Q-4 was recorded. During the image processing for the fire investigation, the image intensity variation was measured for uniform temperatures at the Branch Davidian complex, section 5.6 figure 5.36. These variations were assumed to be related to the FBI Nightstalker's circular two-minute turns and the bearing to the sun. From this, it was concluded that it is very unrealistic to believe that an operator on board the FBI Nightstalker could have induced these rapid and regular variations in dynamic range.

Figure 5.5. Examples of two different thermal windows for the same scenery as indicated by the dynamic range scale (red circles).

There is nothing that corresponds to color in thermal images. As a result, FLIR images often are represented by a grey scale and recorded as a luminance signal on the videotape. The FBI Nightstalker FLIR operator could chose between using white to represent high temperatures in the thermal window and black for low, or the inverse, see figure 5.3. White was chosen by the FBI Nightstalker FLIR operator to represent hot for almost the entire recorded portion on FLIR videotape Q-4. Black represents hot in the two FLIR images in figure 5.8.

5.1.2 The SPRITE/TED Detector

The word “SPRITE” is an abbreviation for Signal Processing In The Element. C. T. ELLIOTT, [Elliott], originally developed the Thomas Elliott Device (TED) concept at Mullard, U.K.. The SPRITE/TED detector is also described in [Cuthbertson], [Baker] and [Philips].

The SPRITE/TED detector element is essentially a strip of infrared-sensitive material on a sapphire substrate. The detector elements are wide in the horizontal direction, see figure 5.2 and 5.6. The detector elements are of type Cadmium Mercury Telluride (CMT) and the integration time is fixed. There are only three electrical connections for each detector element. When a small region of the infrared sensitive strip

is exposed to infrared radiation, excess current carriers are generated in that region, see figure 5.6. The excess current drift towards the readout region, at a velocity determined by the magnitude of the bias current. The drift velocity is in fact quite high and matched to the velocity at which the infrared image is scanned along the strip. Under the TED concept, each of the eight elements were constructed for built in time delayed integration (TDI). With this construction the number of detector elements was reduced and there was no need for external TDI circuitry. The SPRITE/TED introduced a new technology in thermal imaging to overcome these problems. SPRITE/TED detectors became very popular and are used in a variety of applications.

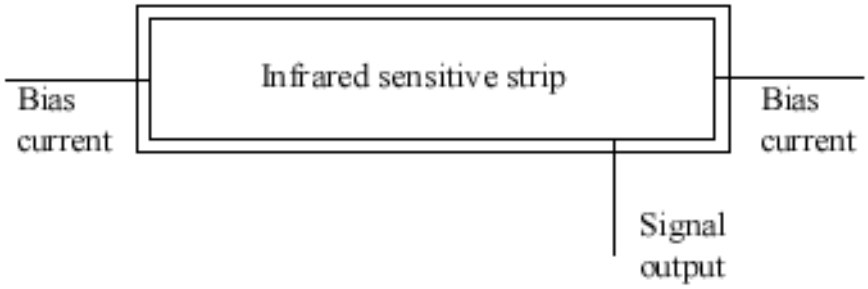

Figure 5.6. The SPRITE/TED detector element.

This particular kind of signal processing improves the signal-to-noise ratio, which in turn increases the ability to detect small or distant targets. It may, however, reduce the ability to resolve fine structural details.

Due to delay effects in the detector element itself, an exposure of thermal energy that is short in duration can appear in a longer time interval than the exposure itself. This phenomenon is known as time delay, not to be mixed up with TDI, and is expressed as a time constant, τ. This time constant τ of a detector is the time for the output signal to fall to 37% of its value after a radiation pulse has ceased, further described in [Philips]. The time constant τ can be estimated by applying a pulse of radiation to the detector and measuring the interval between the time of cut off and the time when the detector radiation output falls to 37% of its peak value. The true time delay for the FBI Nightstalker FLIR could not be measured, as the original FLIR was unavailable. However, the sensor element in the FLIR system is made of CMT and the time constant for such an element is less than 5 μs [Philips]. As eight detector elements are scanned in parallel, this reduces the scanning speed. The exact scanning speed of the FBI Nightstalker FLIR system is unknown, but, in general, this time delay could correspond to 1.6% of the scanning time for a video line in the FLIR-sensor.

Misalignment in bias current and the horizontal scanning speed are another phenomena that can also cause image details to be elongated in the direction of the scans.

It was concluded that thermal energy of short duration could appear longer in duration than in real

life. These phenomena will result in an elongation of small objects in the direction of the scans, which for the FBI Nightstalker FLIR was in the image's horizontal direction. In fact, several of the flashes in table 2 were elongated in their shape. Examples of flashes with an elongated shape are the events from 12:10:48 and onwards where the same part of the Branch Davidian complex was viewed from different positions. The horizontally elongated shape of these flashes remained the same, regardless of the FBI Nightstalker FLIR movements, illustrated in figure 5.7.

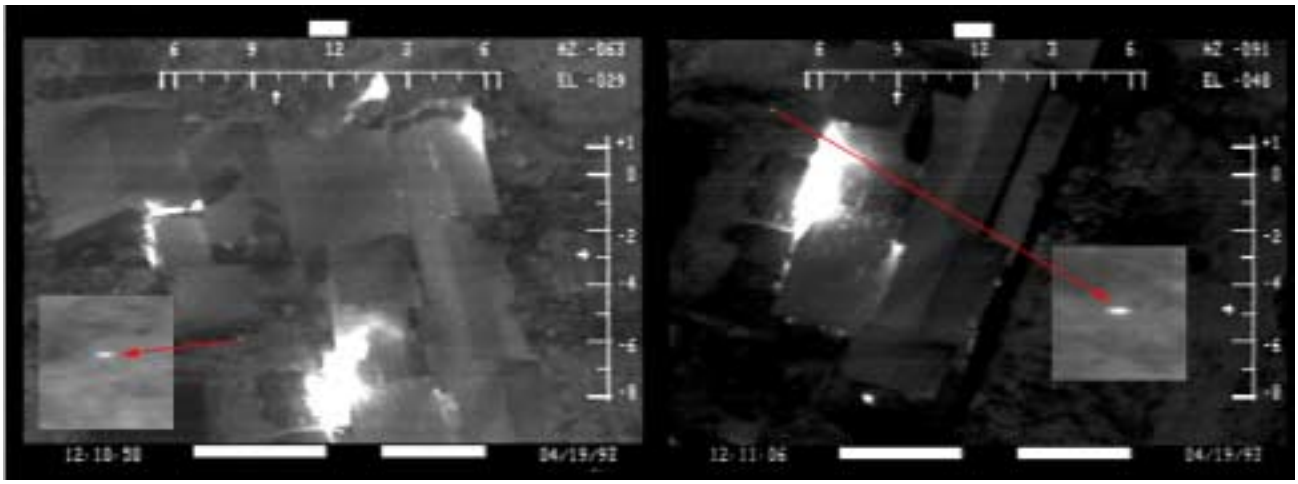

Figure 5.7. Horizontally elongated flashes from the same ground position, seen from two different aircraft positions at 12:10:50 and 12:11:06. The highlighted regions at the red arrows are unprocessed enlargements from the left and right image respectively.

In short, the effects from the FBI Nightstalker FLIR system, in particular the signal processing, time delay and the misalignment in bias current within the SPRITE/TED could be seen to contribute to the horizontal smearing of small objects of high thermal energy.

5.1.3 The Scanning Mechanisms

The FBI Nightstalker FLIR detector was mounted in a moveable turret on the carrier aircraft. The on-board operator directed this turret towards the Branch Davidian complex. The thermal radiation of the scenery passed through the optics and was projected onto the SPRITE/TED detector element by a combination of horizontally and vertically scanning mirrors. It takes several steps to project the thermal radiation onto the detector element. Each image was built up by serial/parallel scans to generate a full picture. Several serial scans in the horizontal direction are required to build up the full image where each scan generates eight video lines. Scanning mechanisms are known to degrade image quality more than conventional staring systems.

Amplification and further gain adjustments are applied within the FBI Nightstalker FLIR system to

remove any non-linear performance of the eight detector elements. Under sub-optimal operating conditions non-uniformity between detector elements has caused a striped noise pattern to be generated on the April 19, 1993, FLIR videotapes, see figure 5.8.

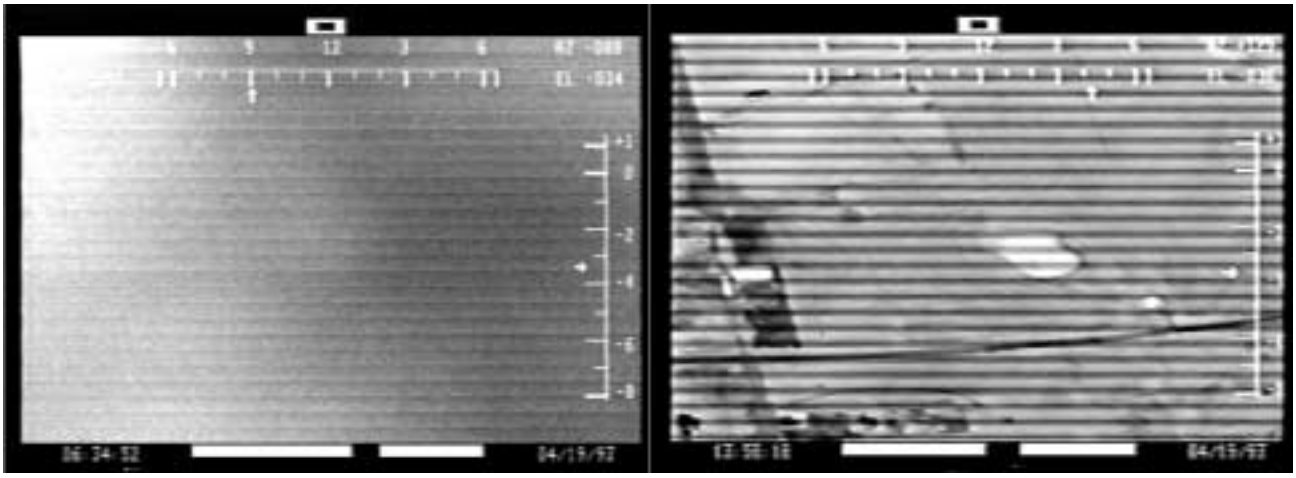

Figure 5.8. Artifacts from non-uniform outputs from the eight detector elements (left) and detector cooling problem (right) causing non-uniform outputs from serial scans.

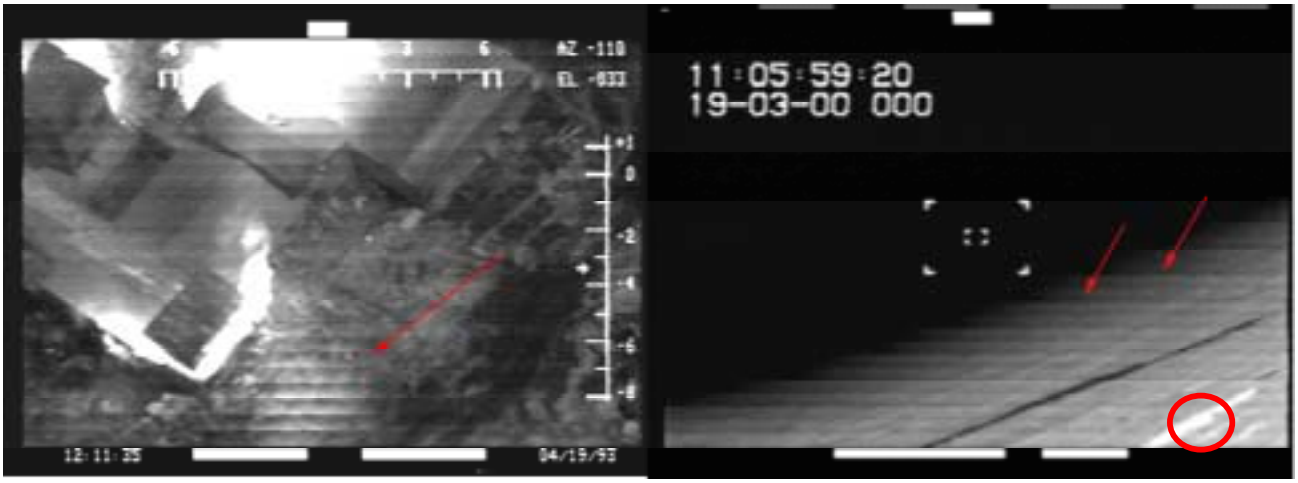

Figure 5.9. Artifacts caused by scanning mechanism in combination with flare from the optics (red arrow left image). Jagged edges (red arrows right image) from the scanning mechanism and detected horizontal displacements (red circle right image). The left image is from FLIR videotape Q-4. The Lynx FLIR recorded the right image during the FLIR Fort Hood trials, which are similar to the FLIR used to record FLIR videotapes Q-1 – Q-7.

Detector elements need cooling and can be quite sensitive to changes in operating temperature.

The effect of deviations from the optimal operating temperature could occasionally be seen in the FLIR images as non-uniform performance between raster scans, see figure 5.8. Another typical noise pattern appears when flare occurs within the system optics, figure 5.9. Spatial displacement in the image horizontal direction was detected, as an effect of the vertical jagged edges caused by the raster scans, illustrated in figure 5.9.

5.1.4 Effects of the FBI Nightstalker FLIR system on FLIR imagery

Imaging systems are not perfect. The functionality and the scanning mechanisms of the FBI Nightstalker FLIR created several kinds of distortions and noise patterns. In addition, mechanics of the video machine and the interlaced video format used to record the thermal images can also be a source of distortion and noise patterns. These distortions can seriously affect the representation of objects in the FLIR imagery that are about on the limit of the FLIR system's resolution capability.

The elongated shape of several of the questioned and small flashes, aligned to the image horizontal direction, was concluded to be a product of the FBI Nightstalker FLIR system. Therefore, it can not be trusted that the FLIR images represent the flashes' true shape, size and content.

5.2 Image Enhancement

Image enhancement of the flashes was performed to expose information present in the image sequences, but not directly obvious to the human eye. The aim was not only to analyze the flashes, as this would be a rather unrewarding process due to their nature. It was more important to analyze the region near the flashes.

To reduce some of the complex non-linear noise and blur pattern induced by the FLIR system, several combinations of noise and blur reduction techniques were tested. Sequences digitized several times from the same recorded portion of FLIR videotape Q-4 were arithmetically merged to further reduce the noise. It was found that the best way to deal with the complex noise pattern was to filter image sequences with an image restoration technique based on the total variation of all noise components, [Rudin]. This method successfully deals with more complex noise models and was most suitable for the noise characteristics apparent in the April 19, 1993, FLIR videotapes.

Super resolution was further used to enlarge the image sequences to produce images with higher resolution. Super resolution is one of the most promising and relatively new techniques for enlarging images digitized from video, [Guichard]. Matching image information from consecutive frames into a super-frame creates a higher-resolution image. In this way, the resolution can be increased, rather than just appear as larger pixels within an image. The super-resolution algorithm required prior estimation of the image motion to compensate for temporal variations in an image sequence.

"Motion" is an essential parameter for many image enhancement techniques. Basically there are two different kinds of motion: physical motion in the real world; and the apparent two-dimensional image motion induced by movements of the FLIR sensor, the FBI Nightstalker aircraft, and any local and global movements in the scenery.

There are several ways to model motion. For example, if a car is driving straight from the left to the right in an image. This is translating image motion. It is quite simple to estimate and reconstruct physical translating motion in the real world from image motion. If the car instead drives towards the camera, its scale will vary. Its scale will also vary if the camera moves relative to the car. If the car makes a turn, there will be a rotational motion. In this case, the motion of the Branch Davidian complex in the FLIR imagery was somewhat more complex, as both translating and rotating motion are apparent and with the scale varying nearly all the time. Therefore, a piecewise linear motion model ("affine model") was used to model the more complex motion. The affine motion model was used to match the image information in consecutive fields prior to super-resolution.

All events in table 2 were reviewed using the original FLIR videotapes. For the events on FLIR videotape Q-4 between 10:41:57 – 12:16:13, in table 2, the following procedures were utilized:

A) The sequences were digitized in an uncompressed format to an image width of 720 x height 486 x 24 bits. In this sequence the dynamic range of the grey levels were only slightly affected.

B) The sequences were digitized in an uncompressed format to an image width of 720 x height 486 x 24 bits. The dynamic range of FLIR videotape Q-4 was digitized without bit reduction.

C) The sequences were digitized in an uncompressed format to an image width of 720 x height 486 x 24 bits with stretched dynamics (before digitizing the video signal) to enhance the contrast.

D) Noise reduced sequence: noise was reduced in 10 iterations using a movie deblur noise reduction technique. These sequences play back at half the normal speed as each processed field was repeated twice to form one new frame.

E) Noise reduced sequence: noise was reduced in 10 iterations using a total noise variation technique. These sequences play back at half the normal speed as each processed field was repeated twice to form one new frame.

F) Super-resolution sequences were created using four consecutive image fields to increase the final resolution. These sequences play back at half the normal speed as each processed field was repeated twice to form one new frame.

G) Split-screen sequences were generated for comparison and review, see figure 5.10. These

sequences play back at half the normal speed as each processed field was repeated twice to form one new frame. The upper left quadrant of the screen contains a cropped version of the above sequence A. The upper right quadrant depicts the corresponding sequence with increased resolution, sequence F super-resolution using frame fusing techniques. The bottom left and right quadrant of the screen depicted from left to right shows:

- sequence C, with stretched dynamics to enhance the contrast
- sequence D, with motion deblur noise reduction technique applied
- sequence E with total variation noise reduction technique applied

Sequences D) -- G) utilized the sequences A) -- C) as input. The split sequences were created for comparison of processed sequences to the same unprocessed sequences. By analyzing the split sequences it was verified that no significant artifacts were induced.

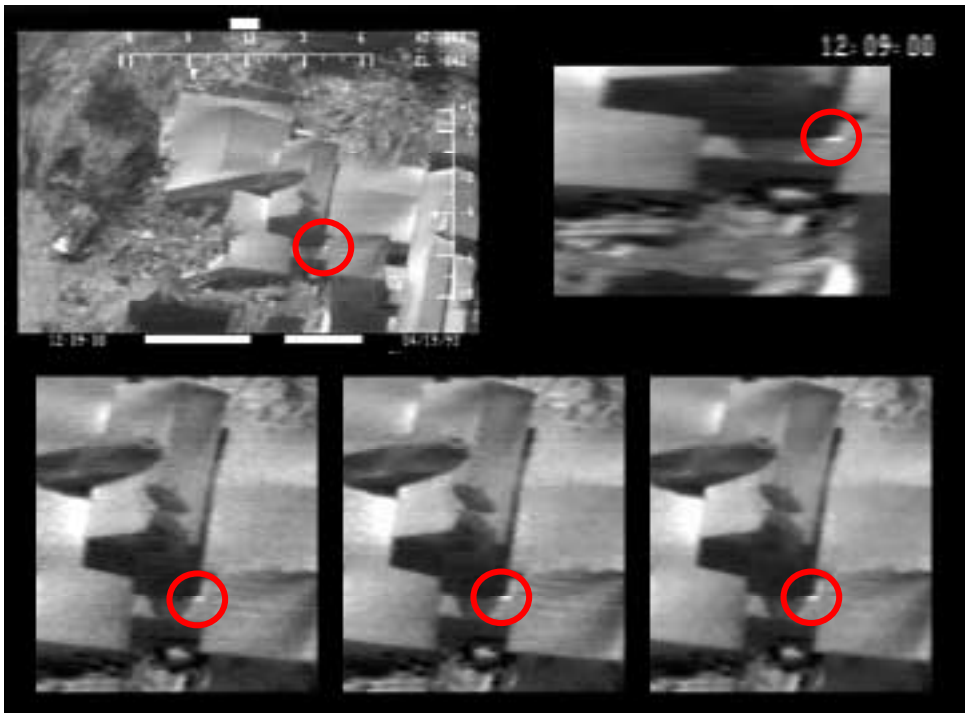

Figure 5.10. A view from the split-screen sequence from event 53 at 12:09:00.

The results from reviewing sequences A) – C) was that several moving objects were detected, however nothing was detected in close proximity to any of the listed flashes. Several events were also analyzed in depth utilizing the procedures D) – G). For example, event 5 during 11:18:20 – 24, event 50

during 12:08:30 – 34, and event 53 during 12:08:59 – 12:09:03. Nothing in close proximity to any of these three flashes was detected within any of these sequences.

When analyzing event 50, moving objects were detected and the sequence 12:08:34 – 12:08:39 were enhanced by the same techniques A) – G) and further investigated in section 5.3.

5.3 Motion Detection, Tracking and Analysis

An individual's radiated temperature difference relative to the background will vary as he moves. This can cause a person to appear alternately as colder or warmer than the background due to the wider temperature interval of the complex background. For this reason moving persons, in most cases, are easier to detect than persons standing still are. Occasionally a person's radiated temperature difference can be the same as the background. Consequently, a person can appear "thermally invisible." This same person, however, will most probably be traceable before and after entering the area where his temperature is about the same as the background. This is illustrated by an example from the Fort Hood Lynx copy videotape (app. 2 item 17), see figure 5.11. FLIR videotape Q-5 also contains several examples of this phenomenon where persons attending the fire momentarily "disappeared" when walking across the water-cooled roof of the tornado shelter.

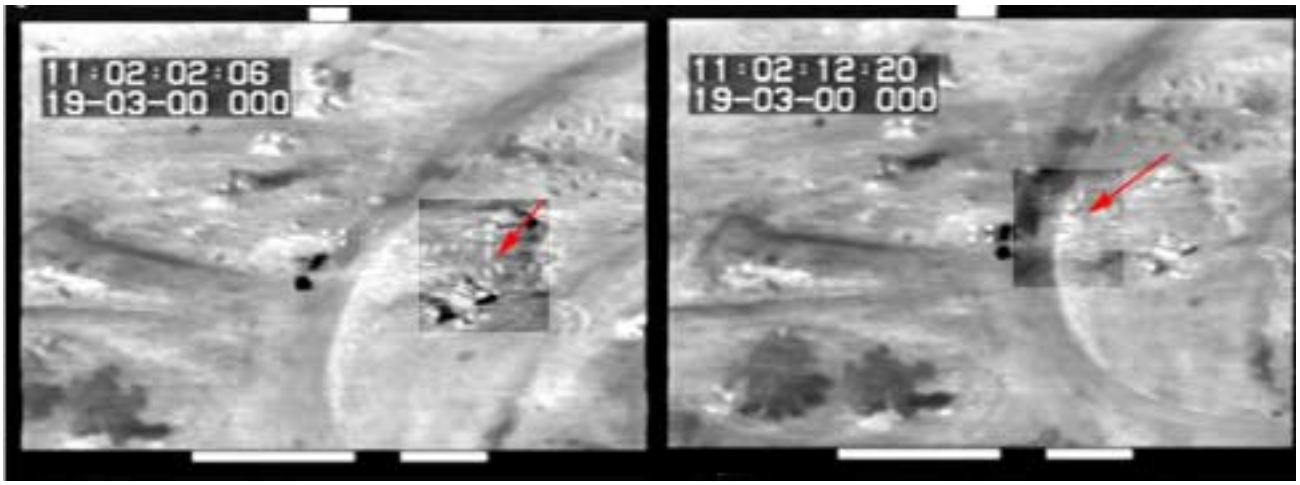

Figure 5.11. Examples of persons from the Fort Hood flight trials, Lynx helicopter. The persons moved from the initial position in the left image (red arrow in the highlighted part) to the position in the right image (red arrow in the highlighted part) where they are more difficult to detect.

Several videotapes and images were reviewed prior to the analysis of the April 19, 1993, FLIR videotape Q-4 in order to identify temperature intervals and spatial dimensions that correspond with a human's form and movement. The Office of Special Counsel prepared a ground FLIR recording of the flight trial which recorded absolute temperature measurements of ground activity during the trial, (app.2

item 36). The Fort Hood flight trial FLIR videotapes (app. 2, items 16-18) and FLIR temperature measurements provided a known source of data as persons were clearly seen on these videotapes. In addition, the duplicate photos and copy videotapes were reviewed. On FLIR videotape Q-1 and Q-3 persons were, for example, seen on a road crossing at 06:56:20. From reviewing the complementary source data, it was also verified that a person was seen on the single story-roof from 12:08:42, event 56 on FLIR videotape Q-4. After this time several persons attending the fire were clearly seen on the FLIR videotapes Q-4 and Q-5.

In the case of alleged gunfire on FLIR videotape Q-4, a reasonable assumption is that persons by necessity, need to appear close to the muzzle blast flashes. The Fort Hood flight trial results confirmed this assumption and clearly show individuals proximate to their weapon and the muzzle blast created by the weapon when the individual fired it. The trial videotapes also showed that different clothing types vary in contrast, figure 5.12. This phenomenon was less visible on the FLIR videotape created in the Lynx helicopter compared with the FLIR videotape created in the Nightstalker FLIR at the Fort Hood trials. The Lynx FLIR was of a less sophisticated design, but more similar to the FBI Nightstalker FLIR system used to record videotapes Q-1 – Q-5 on April 19, 1993.

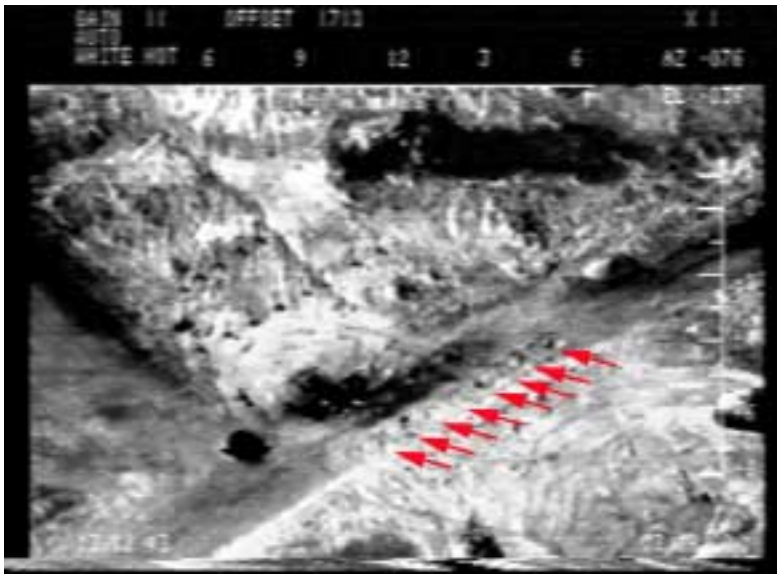

Figure 5.12. Contrast variations for suits worn at the Fort Hood flight trials.

In short, it is possible to detect persons on the FBI Nightstalker FLIR videotapes, regardless of the kind of suite worn, whenever the contrast relative to the background temperature and the imaging system configuration allows detection. The thermal sensitivity of the FLIR sensor, the radiated temperature of a person, the background temperature ranges, the spatial resolution of the FLIR system and the persons form are all contributing factors to the possibility of detecting persons. It is implausible to assume that a

moving person would have the same temperature as the adjacent background at all times on the FLIR videotapes.

The image motion between two consecutive video fields consists of two different kinds of motion from the real world; camera motion and physical motion. Since both background and objects move due to the moving FLIR sensor, detection and tracking of moving objects is difficult. However, moving objects and the Branch Davidian complex formed different motion and the tracking technique was designed only to track objects that moved relative to the Branch Davidian complex in the FLIR images.

Sophisticated tracking techniques were used to track moving objects, to separate moving objects relative to the motion of the Branch Davidian complex in the FLIR images, measure object sizes, analyze contrast variations and review the complementary imagery. Methods aimed to further analyze the characteristics of any detected humanlike motion pattern were not applied as no such motion was detected.

An initial review of the FLIR imagery was conducted. Special care was given to the sequences where the dynamic range had been expanded to enhance low contrast areas. Any movement in these areas would be less visually detectable, if it existed.

Based on the result of this initial review, several additional sequences were selected for analysis. The FBI Nightstalker FLIR system provided the on-board operator the ability to manually activate an event mark. The event mark can be seen as a white, square shaped graphics in the center of the image, similar to the event mark in figure 5.9. Because an event mark would suggest the operator had spotted some activity or event of interest on the FLIR imagery, those sequences from FLIR videotape Q-4 were also carefully reviewed. Table 3 includes a list of the sequences reviewed between 10:41:58 and 12:09:00. The entire picture area was reviewed unless otherwise stated in table 3.

TIME	VDS #	COMMENTS
10:41:58		Event mark, FLIR images in black hot mode
10:46:09		Event mark, searched the road crossing
10:53:00		Event mark, searched the low contrast area in courtyard towards chapel and surroundings
11:00:15		Event mark
11:04:50		Event mark, searched black side near damaged structure
11:08:53		Searched area left from CEV and debris area
11:09:34		Event mark, searched the nearby terrain
11:12:58		Event mark
11:15:02		Event mark
11:26:09		Event mark, searched the area where the CEV penetrates the building
11:27:00		Searched the area from corner of swimming-pool towards courtyard
11:27:44		Event mark, searched the area between pool and gym

11:30:15		Searched the area between swimming-pool and gym
11:34:32	19	Searched the debris area for low contrast objects
11:35:49		Event mark
11:39:40		Event mark
11:43:34		Searched the debris area for low contrast objects
11:50:07		Searched the area between the chapel and the central tower
11:50:54		Event mark
12:06:26		Searched the area between damaged structure and swimming-pool
12:06:42		Searched the area between damaged structure and swimming-pool
12:07:02		Searched the area between damaged structure and swimming-pool
12:08:31	50-52	Searched the area left of CEV and the debris area
12:09:00		Searched area left of CEV

Table 3. List of analyzed events.

Some of the events of low contrast to the background were analyzed in depth as a result from analyzing the sequences in table 3.

- Event 19 at 11:34:32 was concluded to be a square shaped debris blowing towards the diving platform. The diagonal size of the object was about 2’ 4” ± 2”. Human motion was not detected prior to, during or after this event.

- Moving objects seen at 12:06:26 – 55 appeared square in shape and does not have the spatial dimensions or temperature intervals associated with a human. It was concluded to be debris blowing in the wind, one example is seen in figure 5.13.

- At 12:08:31 – 12:08:56 several objects were moving among the debris in the demolished gym area. The objects were of both high and low contrast, relative to the background. Duplicate ground view photos were examined from which some of the moving objects could be identified. The estimated size of one object was about 2’ 4” ± 4”. This could be considered to be an approximate size for a person seen from the FLIR sensor field of view. However, it was concluded to be debris as some rapid variations of the object’s intensity were detected. These rapid variations make it implausible to be a person, but realistic to be a piece of debris. By reviewing the enhanced sequences described in section 5.2, tracking of objects, measuring object sizes and contrast variations and reviewing complementary imagery, it was concluded all of these detected objects were debris moving in the wind.

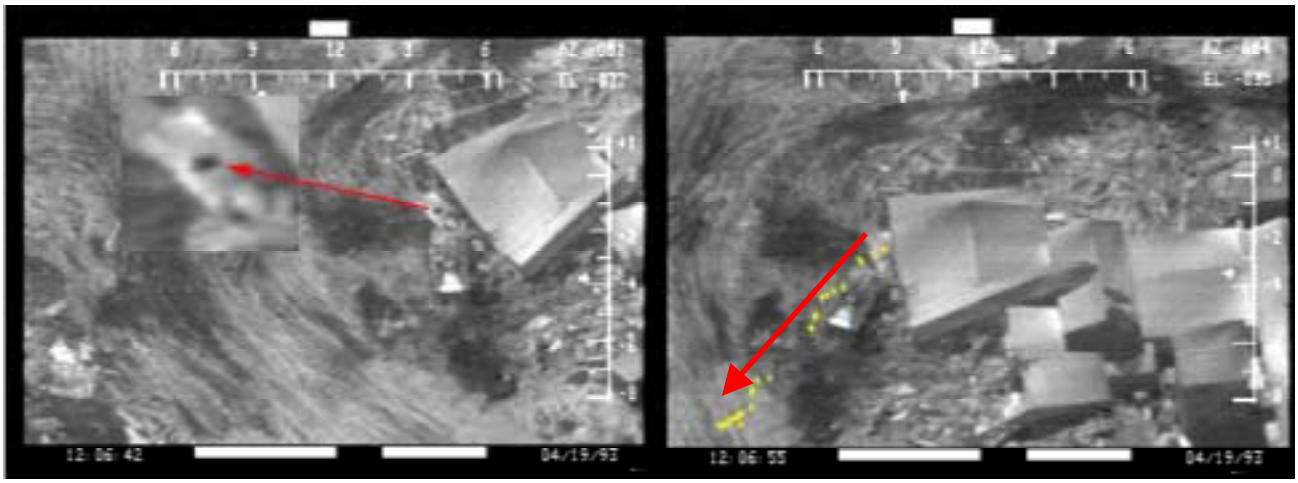

Figure 5.13. A square shaped debris (left, red arrow) seen blowing in the wind from 12:06:43 – 55 and its movements relative to the Branch Davidian complex (right, yellow dots, direction indicated by red arrow).

- At 12:09:00 – 01 an object moved close to the CEV. The size of the object was estimated to be about 3' – 5'. For the same reason as the object seen at 12:08:31 – 12:08:56, it was concluded to be debris from the demolished building.

The result from analyzing these events are based visual reviews of the FLIR videotapes, reviewing enhanced sequences, tracing the objects movements, measuring object sizes, analyzing contrast variations and reviewing the complementary imagery. It was concluded that all of the detected objects were debris from the demolished complex set in motion by a CEV and/or blowing in the wind. No activity that can be determined to be moving persons was detected on the sequences from FLIR videotape Q-4 in table 3 between 10:41:58 to 12:09:00, except the person seen lying on the single storey roof from 12:08:42. Neither were any activities that can be determined to be moving persons detected on complementary photos nor videotapes, bearing in mind their limited image quality.

5.4 Tracking of the FLIR Sensor Position

In the case of solar specular reflections, the variation in FBI Nightstalker's flight path gives a logical reason for the flashes intermittent appearance. The appearance of the flashes is closely related to variations in the FBI Nightstalker's flight path. Moreover, the duration-time of the flashes is closely related to the speed of the FBI Nightstalker. To further investigate these assumptions a three-dimensional (3D) model was needed. Constructing a 3D model of the FBI Nightstalker's flight path required a detailed review of both the pilot induced maneuvers and weather conditions existent on April 19, 1993. The parameters investigated were:

- aircraft positions relative the complex;
- aircraft ground speed; and
- wind strength, heading and variations at altitude.

In this 3D model, reconstructed flash data, the orientation of the Branch Davidian complex, the bearing to the sun and the instant positions of the FBI Nightstalker were incorporated to reconstruct the flash geometry, section 5.5. This computer model is illustrated in figure 5.14 and also in figure 1.1.

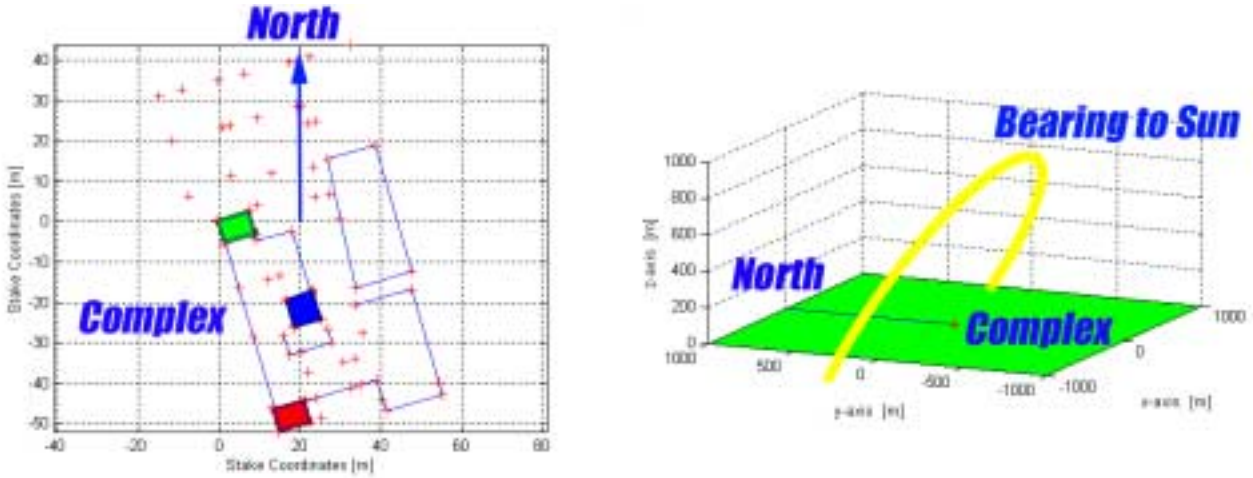

Figure 5.14. A 3D model of the complex (left) based on GPS stake coordinates seen from above. The model oriented towards north and incorporating the bearing to the sun from sunrise to sunset (right). All dimensions are in meter, [m].

Stake positions provided ground level stake coordinates of the complex, (app. 2, item 50). The FBI prepared the stake positions during their processing of evidence from the Branch Davidian crime scene. The bearing to North was obtained from aligning the stake positions for the complex to the bearing to the sun in a FLIR image at 11:39:02. In this image the azimuth bearing to the sun was aligned to the FLIR sensor position. The position of the sun on April 19, 1993, was obtained online from Astronomical Applications Dept. U.S. Naval Observatory [AA].

The size of the central tower roof was used for the 3D reconstruction of the flight path and the 3D reconstruction of flash geometry as seen from all directions. The size of central tower roof was estimated from the stake coordinates. The estimated values were confirmed from a CAD-model (app. 2, item 51) and additional measurements in the FLIR and complementary images. The heights of the three towers were estimated from the CAD-model and also from additional measurements in the FLIR images and complementary images.

To verify how the Nightstalker's flight path varied over time, the weather conditions for April 19, 1993, were also needed. Climatic data from U. S. Department of Commerce (app. 2, item 72) provided such information. Automated weather observations conducted by McGregor Municipal airport were also recorded onto the audio of FLIR videotape Q-1. The automated weather observation was confirmed by comparison to the audio transcripts (app. 2, item 70).

Comparing the ZULU time mentioned on the automated weather observations to the time on FLIR videotape Q-1 verified that the time on FLIR videotape Q-1 was given in Central Daylight Time (CDT). The error for the time information on FLIR videotape Q-1 was estimated to CDT ± 30 seconds. The time given on the remaining FLIR videotapes were assumed to be as reliable.

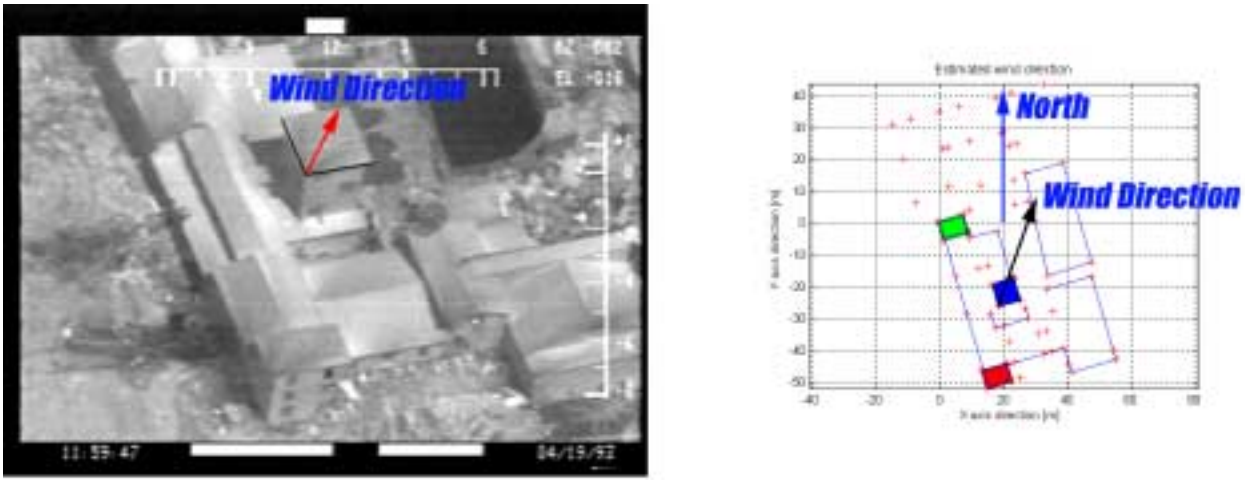

Figure 5.15. The average wind direction at ground level estimated from the cooling effect on the central tower roof (red and black arrow).

On April 19, 1993, the wind at ground level was quite strong. The instant wind direction can be assumed from the flag on the white side of the complex. According to the automated weather report recorded at 6:02 a.m., the wind direction is 180° degrees from true north, wind speed 24 knots and peak wind speed up to 28 knots. This was verified by the weather data. The average wind direction can also be seen on FLIR videotape Q-4, as the wind cools off the roof from the direction where the wind comes from, see figure 5.15. The average wind direction at the complex, at ground level during the time the flashes appeared was measured to 200° ± 20°, which agreed with the weather data for the same time.

Normally, the wind at altitude increases and changes in direction. This affected both the airspeed and flight heading of the FBI Nightstalker. Climatic data regarding the wind at altitude could not be found. However, at the FBI Nightstalker's operating altitude, the wind was estimated to come about 20°-30° more from the southwest than the ground level wind, 220 ± 25°. A 40°-50° variation in wind direction at the FBI Nightstalker's operating altitude was fully possible on April 19, 1993. This was

verified by visually reviewing the variations in image motion, variations in AZ- and EL-angle for the FLIR sensor relative to the aircraft movements and by observing the smoke from the fire on FLIR videotapes Q-4 and Q-5. Wind strengths up to 35 – 45 knots at the aircraft's operating altitude were fully possible on April 19, 1993.

The speed of an aircraft is a more complex parameter as there are several ways to define airspeed. The speed of the aircraft as shown by the aircraft's avionics is not necessarily the same as the aircraft's ground speed (GS). True airspeed (TAS) is the airspeed of an aircraft relative to undisturbed air and corrected for the aircraft's altitude, the temperature and other factors. Ground speed (GS) is explained as the aircraft's speed relative to the ground. TAS will, however, be equal to GS if there is no wind.

It was assumed that the FBI Nightstalker operated at an airspeed of about 160 knots, from studying the aircraft handbook (app. 2, item 69) and the image motion on FLIR videotape Q-4. Flying with a 40 knots head wind will result in 160 – 40=120 knots GS. Flying with a 40 knots tail wind will instead increase the ground speed to 160+40=200 knots GS. As a result, 160 knots gives a speed relative to the ground that will vary between 120 – 200 knots GS. Consequently, head wind has decreased the FBI Nightstalker ground speed and tail wind has increased the FBI Nightstalker ground speed.

By reconstructing the FLIR sensor position for three two-minute sequences (1) 10:55:23 – 10:57:57; (2) 11:34:20 – 11:36:18; and (3) 11:58:30 – 12:00:46, it was seen that the aircraft ground speed varied for the turns, see figure 5.16 and 5.17. This provided verification that the FBI Nightstalker circular movements had varied both in altitude and distance relative to the complex. The FBI Nightstalker ground speed was calculated from the reconstructed data. The calculated ground speed of the FBI Nightstalker during the reconstructed turns varied between 120 – 200 knots GS. The measurement error was estimated to ± 20 knots for the calculated GS.

The strong wind probably caused the FBI Nightstalker to drift off from an ideal path and thereby caused the variation in aircraft's position relative to the Branch Davidian complex seen in figures 5.15 and 5.16. The variations in aircraft altitude, seen on the reconstructed data in figure 5.17, are realistic altitude variations in such weather conditions.

On several occasions the FBI Nightstalker appeared to be directly above the complex. Reconstructing the position of the aircraft at 11:46:20 verified this, see figure 5.18.

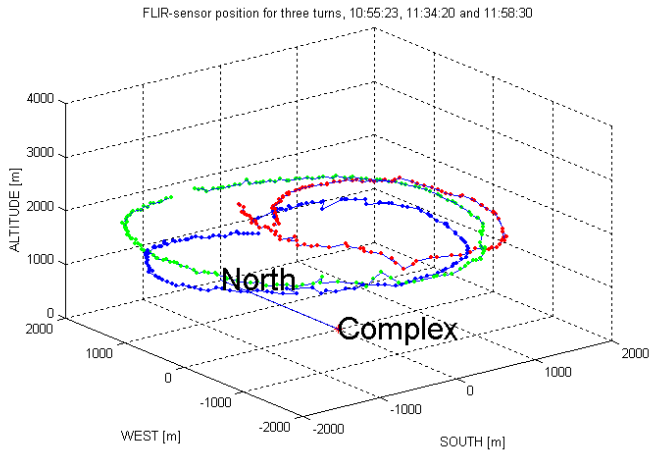

Figure 5.16. FBI Nightstalker circular movements relative to the complex at 10:55:23—10:57:57 (green), 11:34:20 – 11:36:18 (red) and 11:58:30 – 12:00:46 (blue), seen in 3D.

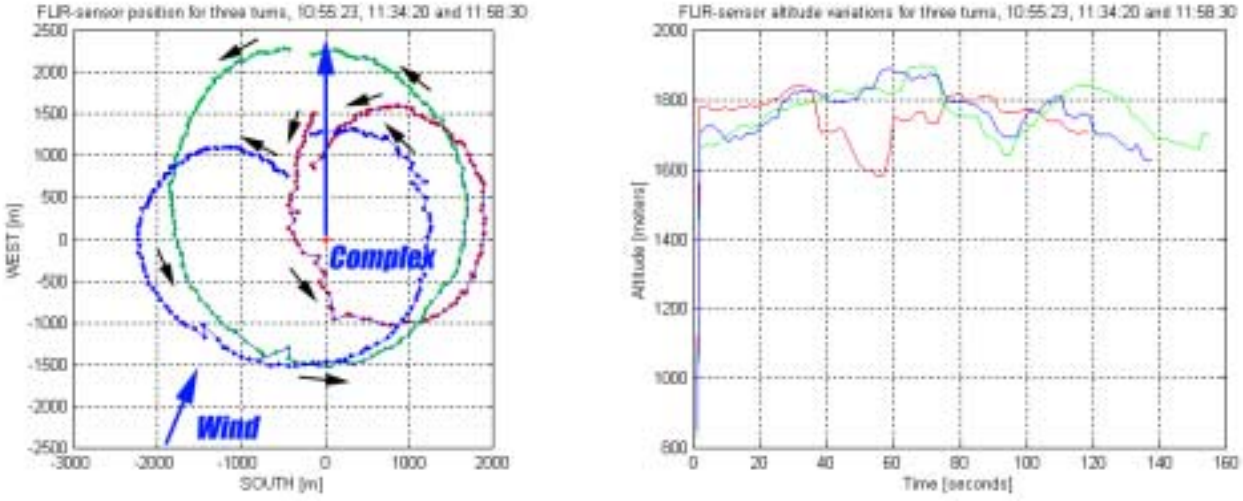

Figure 5.17. FBI Nightstalker's circular movements relative to the complex at 10:55:23—10:57:57 (green), 11:34:20 – 11:36:18 (red) and 11:58:30 – 12:00:46 (blue), seen from above (left) and the variations in altitude (right). Spatial displacements of 3D coordinates were mainly caused by the FBI Nightstalker's FLIR system. As a result, the altitudes (right) have been filtered, utilizing median filtering, to limit effects of object tracking errors.

From reconstructing the FBI Nightstalker's flight path it was concluded that the position, altitude and ground speed of the aircraft relative to the Branch Davidian complex varied significantly. This supported the hypothesis that the variation in FBI Nightstalker's flight path contributed to the flashes

intermittent appearance, as the aircraft sometimes flew through a solar specular reflection and sometimes flew beside the same reflection. The duration time of such reflections is significantly affected by the FBI Nightstalker's ground speed. Therefore, the FBI Nightstalker's flight path and airspeed can not be regarded as constants.

Figure 5.18. At 11:46:20 the FBI Nightstalker, and thereby the FLIR sensor, was right above the Branch Davidian complex at a distance of 1610 meter.

5.5 Three dimensional (3D) Reconstruction of the Flash Geometry

To investigate the potential for solar reflections in depth, the 3D model from section 5.4 was used to reconstruct the flashes' geometry. The theoretical approach for the complete reflection model is described in section 5.5.1. The 3D model was thereafter used to complete the reflection model, which included:

- the position of the sun;
- the position of the flashes on and around the Branch Davidian complex; and
- the FLIR sensor position.

The mathematical model and the results from the reconstructed flash geometry were verified by an additional experiment using a ThermaCAM infrared camera provided by FLIR Systems, Sweden, see section 5.5.8. The results from analyzing the reconstructed flash geometry are summarized in section 5.5.9.

5.5.1 Theoretical Approach

Thermal images are based on temperature difference of naturally emitted light, which depends on the objects' energy exchange with the environment, self-heating, emissivity differences or reflections of other sources. The physical law of reflection is historically attributed to Euclid [Frauen]. In short, the physical law of reflection explains that a ray of light that hits a planar boundary between two media is essentially divided in two parts. One part is reflected and the other part is passed on to the next media at a different angle.

One simple way to model light reflection components can be found in [Vince], see figure 5.19, which is widely used to create lighting effects in virtual images. This model formed the basis on which the geometry of the flashes on FLIR videotape Q-4 were reconstructed, see figure 5.20.

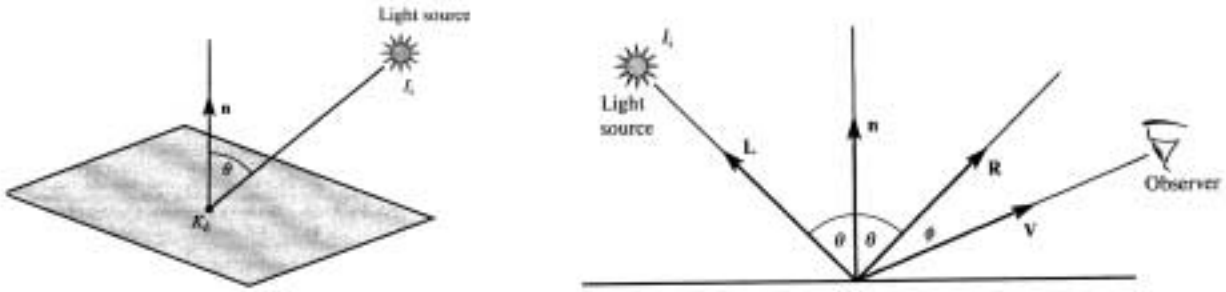

Figure 5.19. A simplistic model of the solar reflection from a planar surface, diffuse reflection component (upper left) and specular reflection component (upper right), from [Vince] p. 82-83.

The behavior of light reflection can simply be expressed as diffuse or specular reflections. Lights reflected by a diffuse surface will be radiated equally in all directions and are independent of the position of an observer. Rough surfaces, like carpets and textiles, exhibit mainly diffuse reflection properties. Specular reflections create a highlight that can be seen only within a limited distance from the reflection ray. Polished surfaces, like glass and metals, can cause specular reflections for which the visibility strongly depends on the position of the observer relative to the specular reflection ray. This reflection model holds for visual as well as infrared wavelength bands.

In the simplistic reflection model of one light reflection, the intensity ***I***, of a pixel at column *x,* row *y* and time *t* summarizes the reflection components of a light source; ambient; diffuse; and specular reflection components.

$$I(x,y,t)= I_{ambient}(x,y,t) + [I_{diffuse}(x,y,t)+ I_{specular}(x,y,t)] \quad (1)$$

$$I(x,y,t)= I_a(x,y,t)\, K_a + [I_i(x,y,t)^* K_d\, (L \bullet n)+ I_i(x,y,t)\, K_s \cos^g\Phi] \quad (2)$$

I_i is the intensity of the light source. K_a and K_d are surface reflection components. K_s is a color-independent specular coefficient. The angle Φ represents the observer **V** offset from the reflection ray **R**. **L** is the direction to the light source, **n** the surface normal and **L** • **n** denotes the scalar product. *g* is the materials reflection component and the factor $\cos^g\Phi$ and describes how the observation angle affects the intensity of the specular reflection component. The angle θ represents the angle of the reflection, which depends on the substance of the surface among other factors. This reflection model defines the intensity of image pixel values for an illuminated object as a function of the position of the camera and the intensity contributions from ambient, diffuse and specular reflections.

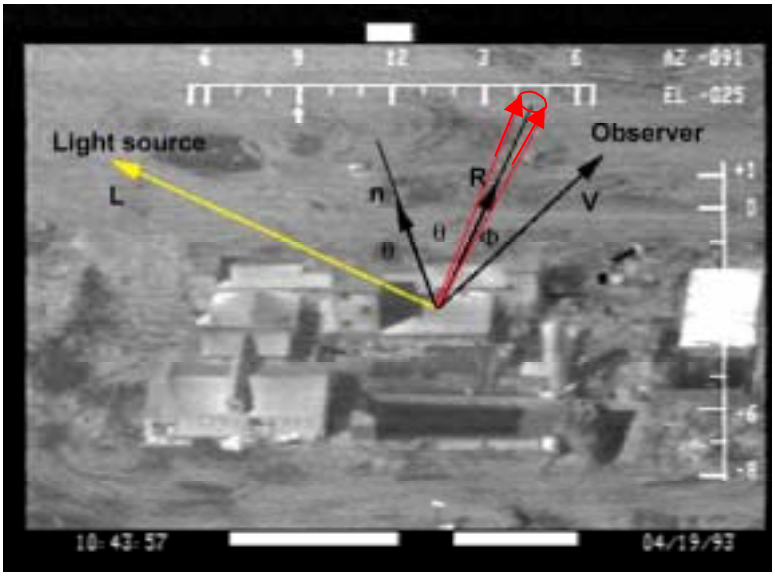

Figure 5.20. The expansion of the specular reflection model into 3D for reconstructing the geometry of the flashes on FLIR videotape Q-4 with the distribution "cone" of the solar specular reflection (red) in where the specular reflection can be observed.

On April 19, 1993, the sun was the light source and any solar specular reflections would have resulted in reflection "cones" in the air above the Branch Davidian complex. As the FBI Nightstalker aircraft approached one of these narrow cones where the flashes would be observable, the angle Φ between the reflection ray **R** and the observing FLIR sensor **V,** approached zero and the specular component became dominant. This agrees with the way a solar specular reflection is modulated by the $\cos^g\Phi$ function. In fact, equations (1) and (2) can in fact be further simplified.

$$\boldsymbol{I}(x,y,t) = c_1 + c_2 \cos^g\Phi \qquad (3)$$

In (3) the factor $c_2 \cos^g\Phi$ describes the specular part of the reflection and c_1 and c_2 are constants. Due to the high thermal energy of solar specular reflections, the ambient and diffuse reflection

components make little contribution to the reflection ray. Thus, the specular reflection component can be regarded as a point source with a very limited spatial distribution in the far IR band. Some examples of how *g* affects the size of the area where the specular reflection can be observed as shown in figure 5.21. However, for some of the analyzed flashes, the surface emissivity could not be fully neglected.

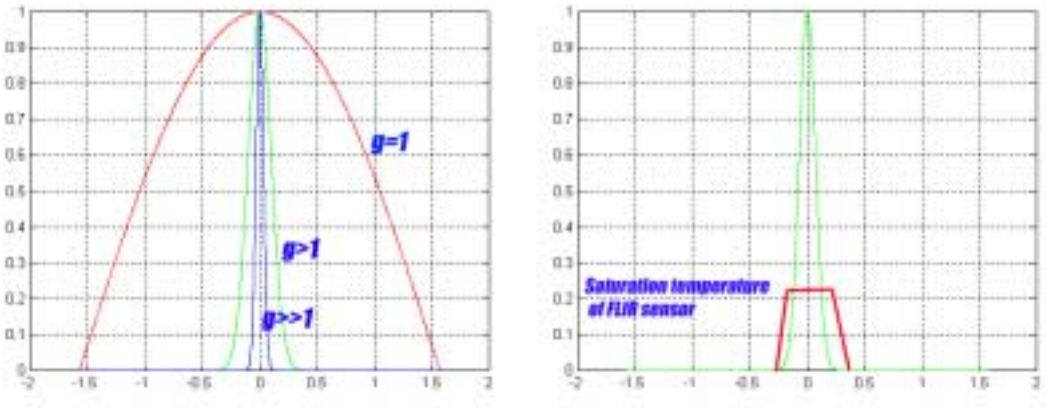

Figure 5.21. Examples of how the factor g affects the reflection geometry (left). The intensity of a reflection where the specular component is dominant (right, green line). An illustration of the intensity observed by a FLIR system (right, red line).

SPRITE/TED detector elements in the FBI Nightstalker FLIR were designed to operate within a temperature range far below the temperature of the sun, figure 5.4. When a solar specular reflections of high thermal energy in the far IR band falls onto the detector elements, the video signal on the FLIR videotapes normally become saturated. This, in turn, caused the corresponding pixels to became white in the FLIR images, as white was selected to represent hot temperatures. Studying [Cuthbertson] and [Philips] verified that the temperature of the sun is far outside the operating temperature range of the FLIR sensor. The intensity that would be observed by the FBI Nightstalker FLIR sensor is illustrated in figure 5.21.

The direction of a reflection ray is determined by the orientation of the reflective surface relative to the light source. Reflecting surfaces are most likely not aligned to the ground plane for the flashes on FLIR videotape Q-4. Moreover, the surface structure, shape and size of the reflecting surfaces were not known, which determines the size of the distribution cone. As a result, the flashes were modeled as sparse points. As the substance of the surface was unknown for the flashes on FLIR videotape Q-4, the reflection angle θ was compared mainly between flashes that appeared from similar positions relative to the complex.

Consequently, if the FLIR sensor captured a solar specular reflection, then the FBI Nightstalker must have entered, passed through and finally left the reflection cone. From a visual inspection of the flashes on FLIR videotape Q-4, listed in table 2, it was seen that the intensity of several flashes increased

and decreased in a way that agreed to the theoretical model of solar specular reflection. In fact, the relation between the duration of a specular solar reflection duration time and the speed and position of the FBI Nightstalker can be expressed as in equation (4).

$$N = 2\, m\, d \sin(\Phi) / s \cos(\theta+\Phi) \quad (4)$$

N is the number of frames in which the reflection highlight can be seen. *m* is the frame rate of the video format, which is 30 frames/second for NTSC. *s* is the ground speed or the aircraft [m/s]. *d* is the distance in meters between the complex and the aircraft. The angles θ and Φ are described in figure 5.20. For example, the number of frames in which the reflection can be seen decreases if the aircraft speed increases. Assume that a solar specular reflection can be seen for 10 frames and the aircraft's airspeed is 160 knots. In a 40 knots tail wind the same reflection will be seen for 8 frames at the same distance. In a 40 knots head wind the same reflection will be seen in 13-14 frames at the same distance.

Consequently, the duration time of a solar specular reflections strongly depends on the reflecting surface properties, the distance to the FLIR sensor and the speed and position of the aircraft. The incident positions of the aircraft determined which reflection cones the FLIR would have passed through and thereby what reflections would be recorded to the FLIR tape.

We all know that the position of the sun varies throughout the day and, therefore, the local time had to be incorporated in the reflection model. During the recording of the FLIR videotapes, the aircraft circled above the complex while the operator maneuvered the FLIR sensor. To deal with the various movements, the relation between the sun, the objects causing the flashes and the FLIR sensor position was modeled in 3D.

The geometrical relation between the pixel intensities, (x,y,t), can be related to the spatial position at the complex, $(X_{world}, Y_{world}, Z_{world})$, by using a suitable camera model, illustrated in figure 5.22 and 5.23. In the case of perspective image projection, the relation between an image pixel (x,y) and the position at the complex can be described as in equation (5) and (6).

$$x = f\ X_{world} / Z_{world} \quad (5)$$

$$y = f\, Y_{world} / Z_{world} \quad (6)$$

f denotes the focal length of the camera. The corresponding camera model is illustrated in figure 5.22. Even if the ideal camera model is mainly a theoretical model, it could be used to reconstruct the FLIR sensor position. The distance between the FLIR sensor and the complex was estimated directly from the images utilizing the FLIR system field of view and some reliable sizes of objects in the depicted scenery of the Branch Davidian complex. Thereby the geometrical relationship between the sun, the complex and the FLIR sensor could be numerically calculated for the flashes in table 2 utilizing specially developed software scripts.

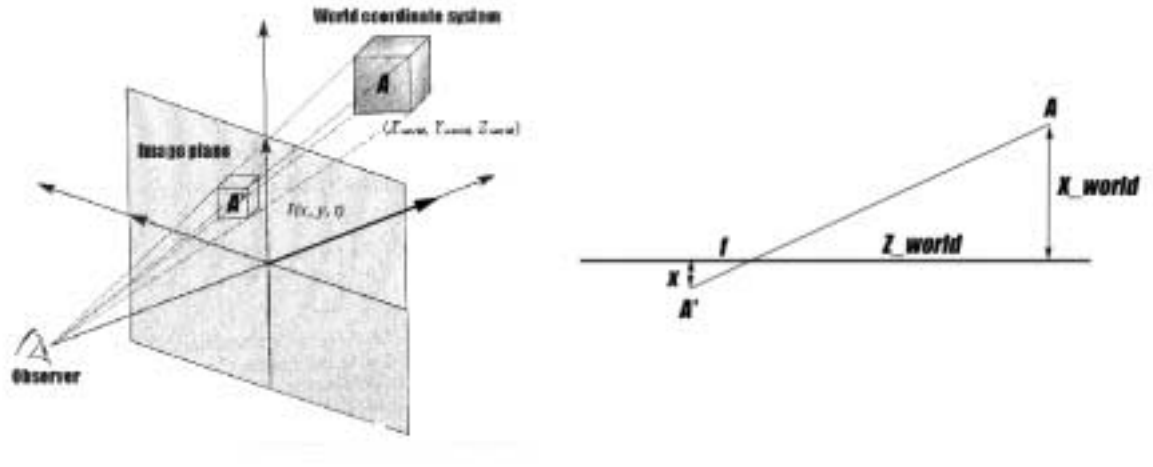

Figure 5.22. Perspective projection (left), initially from [Vince] p. 48, and the corresponding camera model (right).

The FLIR sensor position was estimated without considering the rotational movements of the image plane, which were believed to increase the error in the aircraft azimuth angle relative to the complex. To deal with the rotational movement of the FLIR sensor, MatchMover by Realviz was used to more accurately estimate the FLIR sensor positions. This software inserts virtual objects into a real-world video recording by reconstructing the camera positions. This technique is widely used in the movie industry. In this case only the 3D position of the FLIR sensor camera and the complex coordinates were of interest. The tracked FLIR sensor position from MatchMover and the 3D model was oriented towards North. Finally, the bearing to the sun was added to complete the reconstructed flash geometry.

The calculated distance between the complex and the FLIR sensor position varied. However, the reconstructed azimuth and elevation angles were accurate and reliable. By numerically calculating a set of reference distances from the image of the tower roof in figure 5.18, all tracked distances from MatchMover were calibrated for accurate distances.

The error in the reconstructed flash geometry was estimated to be somewhat larger than it would have been had a staring camera with known focal lengths been used instead of the FLIR system. The errors induced from the tracking procedure were mainly caused by misplacements of the 2D tracking points, see figure 5.23, or from image displacements caused by the FLIR system, illustrated in figure 5.9. By manually calculating the 3D points from the 2D FLIR images and comparing these data to the results, from both methods used for 3D reconstruction, the reconstructed flash geometry proved to be accurate and reliable.

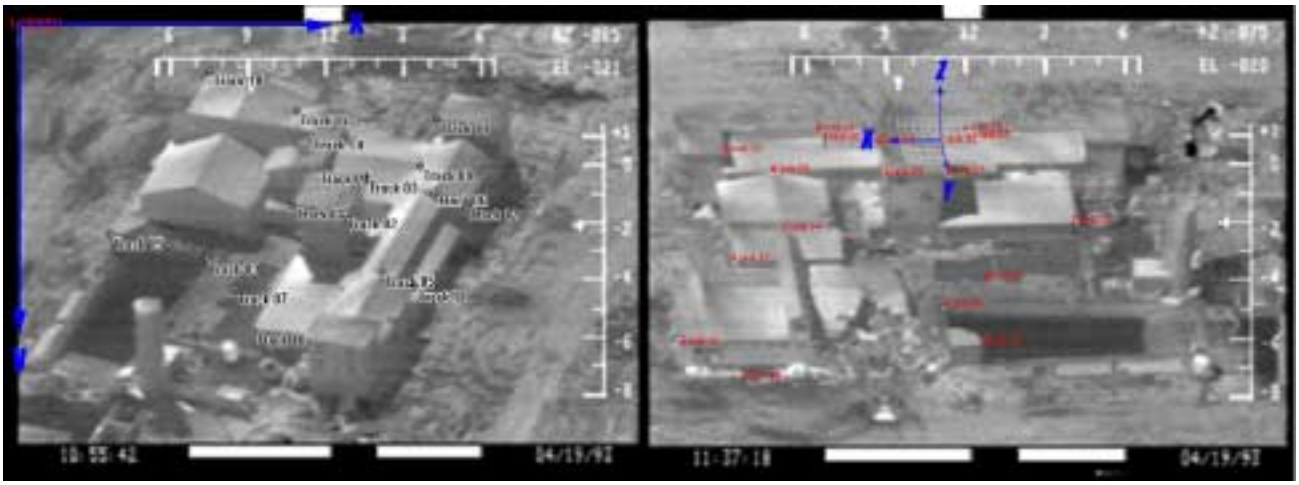

Figure 5.23. Tracked 2D points (left) and the image coordinate system (blue). Corresponding reconstructed 3D points (right) and the ground coordinate system (blue) at the Branch Davidian complex. Note that (X, Y, Z) denotes 3D points at the Branch Davidian complex which are related to the direction from the Branch Davidian complex to the FLIR sensor, (X_{world}, Y_{world}, Z_{world}), in the perspective projection model.

In short, there is only one possible reflection geometry per specular solar reflection at the time *t*. By reconstructing and comparing the reconstructed flash geometry it was possible to verify whether the flashes were of similar geometry, including the variations over time *t*.

5.5.2 Pre-review of the Flashes on FLIR Videotape Q-4

A review of the FLIR imagery was conducted prior to the numerical analysis. The results from the visual reviews of the flashes, the image enhancement, motion analysis and comparison to the complementary imagery were that;

- Event 1 was quite obviously caused by solar specular reflection.
- Events 6 at 11:18:48 and 42 at 11:58:04 were concluded to be only normal thermal radiation from debris/objects set in motion by the CEVs.

These two events, events 6 and 42, have been omitted from the remaining of the analysis.

5.5.3 Flashes in the Courtyard

Events 18 at 11:34:32 and 31 at 11:46:34 were the first to be tracked. To investigate why the flashes were not seen on successive aircraft turns, two additional sequences were tracked for which the positions of the FBI Nightstalker FLIR's field of view were similar to the positions for event 18 and 31.

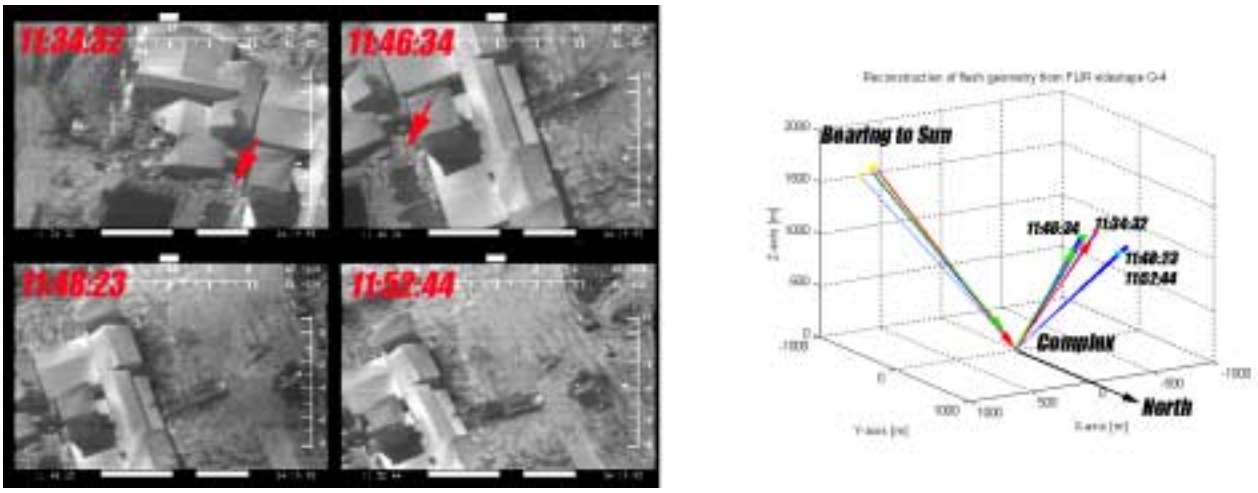

Figure 5.24. FLIR images (left) and the direction of the FBI Nightstalker and FLIR sensor position (right), event 18 at 11:34:32 (red) and event 31 at 11:46:34 (green) and two relative to similar fields of views at 11:48:23 (cyan) respectively 11:52:44 (magenta).

The result clearly shows that the FLIR sensor was at another position relative to the Branch Davidian complex for the latter two turns and that event 18 and 31 were actually very close in similar positions, see figure 5.24. The image planes were rotated in different ways for events 18 and 31, which was mainly caused by different FBI Nightstalker maneuvers. Twelve minutes passed between events 18 at 11:34:32 and event 31 at 11:46:34. The differences in the positions of the sun accurately account for the difference in positions for event 18 and 31. This clearly indicates that both event 18 and event 31 align extremely well to the reconstruction model and proves that the flashes 18 and 31 were caused by solar specular reflections. The size of the reflection cone for event 18 at 11:34:32 was estimated to be of a size of 30 – 45 meters at the FLIR sensor location, which is a very reasonable size for a solar specular reflection at that distance.

The remaining events in the courtyard also aligned well to the reflection geometry. These are events 16, 28, 30, 33, 37, 38, 51 and 54. It was concluded that these flashes also were caused by solar specular reflections. However, as the pulsating nature of the event 51 at 12:08:48 and event 52 at 12:08:51 could not be entirely explained from the reconstructed flash geometry, the appearance of these two flashes were further investigated in section 5.5.7.

5.5.4 Flashes within the Damaged Structure on the Red Tower

Events 2 at 10:54:20 and 4 at 11:14:10 were tracked next. From reviewing the reconstructed data, it was very clear that these two events in the damaged structure of the red tower at the red/white side of the complex were caused by solar specular reflections. Some very small debris probably caused these reflections. The pulsating nature of these flashes was concluded to be a product of the FBI Nightstalker

FLIR system, as explained in section 5.1 and section 5.5.7. Event 24 at 11:42:00 – 01 was very similar to events 2 and 4 in reconstructed geometry, but originated from another very close position relative to the Branch Davidian complex. Event 24 was probably caused by a closely located piece of similar reflective material. This part of the complex is not in the shadow.

5.5.5 Flashes on the Roofs

All events seen on roofs aligned extremely well to the reflection geometry as well. These events are;

- Events 9, 14, 15, 17, 20, 27, 28 the flashes on the roof, 32 and 35 on the cafeteria roof.
- Events 10, 11, 21 and 53 on the roof of the chapel. Event 53 at 12:09:00 was also analyzed in depth in section 5.2.
- Events 25, 26, 29, 34, 36, 39, 40, 41, 43 and 46 on the single storey roof on the white side.

Figure 5.25. Several hot spots on the cafeteria roof, 12:10:43 (highlighted square and at red arrows and other locations on the roof).

It was concluded that the events from 12:10:48, including the flashes in the courtyard and also event 57, were caused by heat reflections from the fire, even if solar specular reflections were believed to have contributed to causing some of the flashes. A large number of bright spots were detected on the cafeteria roof at this time, around 12:10:43, see figure 5.25, which coincided with the positions of the flashes on the cafeteria roof.

As no human-like activity was detected on any of the roofs, except event 56, and based on the

results from the image enhancement and motion analysis, and as all the events on the cafeteria, chapel and single-storey roofs aligned to the reflection geometry, it is concluded that the flashes on the roofs were caused by solar and heat reflections.

5.5.6 Flashes at Other Locations

Based on the results from the reconstructed flash geometry that aligned well to the reflection geometry, the results from visual reviews, image enhancements and the fact that there was no detected activity near any of these flashes, events 3, 7, 13, 22, 23, 11:42:32, 44, and 45 were also concluded to be caused by solar specular reflections. Event 13 at 11:28:04 was caused by at least two objects.

Event 5 at 11:18:21 was a flash from a CEV that was moving when the flash appeared. This flash was subject to an in depth review and image enhancement in section 5.2. This event was also similar to the sighting at 12:09:59. These two flashes appeared similar in their size relative to the CEV and they were both horizontally shaped. Based on these results and also from comparison to the other flashes, it was concluded that these flashes were caused by solar specular reflections.

Event 8 at 11:24:30 – 32 consisted of pulsating flashes from two close positions on the ground at the black side close to the demolished gym. At 11:24:35 heat combusts from the CEV was seen. Even thought there was a striking resemblance between those pulsating flashes and the flashes on FLIR videotape Q-4 that already were concluded to be solar or heat reflection, event 8 was further investigated in section 5.5.7. The pulsating flashes, event 12 at 11:26:27, were also further investigated.

Long duration flashes, like event 50 at 12:08:31, seen on the black side in the debris appeared only once. At 12:04:37 the CEV penetrates the gym at the black/red corner and the catwalk can be seen falling down to the ground. At 12:04:41 what is believed to be a window falls on the ground, which later is in the same position as is for the long duration flashes at 12:08:31. This flash was confirmed to be a window and can be seen in one of the ground view photos, figure 5.26.

At 12:06:33 and 12:10:35 no such flashes were seen even if the sensor position appears to be similar. When numerically compared the FLIR sensor position differed, figure 5.27. At 12:10:35 the sensor position was closer, but still different. This explains the lack of reflections at 12:06:33 and 12:10:35. Similar long duration flashes during the Fort Hood flight trial video, (app. 2 item 17), for example at 11:05:08, 11:16:33 and 11:17:49 are seen from the debris area, figure 5.28. Event 50 was also analyzed in depth in section 5.2. It was concluded that event 50 was caused by solar reflections from large pieces of glass.

Figure 5.26. The window from the demolished catwalk.

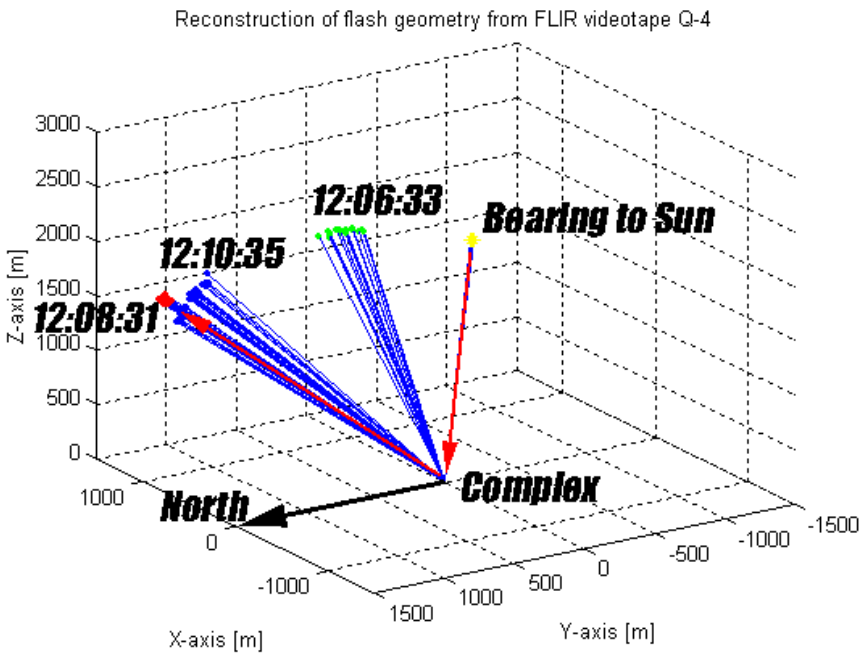

Figure 5.27. Event 50 at 12:08:31 tracked (red and red arrows) and compared FLIR sensor fields of view at 12:06:33 (green) and 12:10:35 (blue).

Figure 5.28. Debris causing reflections during the Fort Hood flight trial on the Lynx FLIR imagery. A flash that was small, elongated and short in duration (left) and a flash that was larger and longer in duration (right).

5.5.7 Appearance of Flashes

This section analyses the remaining flashes from the previous sections 5.5.3 and 5.5.6 in depth, by also taking into account the characteristics of the FLIR system and by comparing the flashes on the FLIR videotapes to the flashes seen on the imagery from the Fort Hood Flight trial, March 19, 2000. The remaining events were; event 8 at 11:24:30—35; event 12 at 11:26:27; event 51 at 12:08:48; and event 52 at 12:08:51. The aim was also to investigate any similarities between the analyzed flashes on FLIR videotape Q-4 and the muzzle blasts flashes seen on the videotapes from the Fort Hood flight trials March 19, 2000. The following data was reviewed: the trial imagery, protocol and report, Nightstalker FLIR videotape (app. 2, item 16), Lynx FLIR videotapes (app. 2, items 17-18), photos (app. 2, items 37-41), flight trial protocol (app. 2, item 68) and "Imagery Analysis report FLIR TRIAL Fort Hood, Texas 19 March 2000" in (app. 2 item 65). Noted was that (app. 2, items 17-18) were converted from PAL to NTSC, which have been considered in the investigation.

The results from an initial visual review was that the muzzle blast flashes that could be detected on the Fort Hood FLIR videotapes were different in appearance than the solar reflections in the debris area from the same videotape. The detected muzzle blast flashes on the Fort Hood trial videos were also different in appearance compared to the flashes seen on FLIR videotape Q-4, one example is shown in figure 5.29. Moreover, the flashes on FLIR videotape Q-4 were very similar in appearance to the solar reflections in the debris area from both the Fort Hood Lynx and Nightstalker FLIR videotapes, illustrated in figure 5.28. Noted was the similarity in the flashes horizontally elongated shape.

Pulsating solar reflections were detected on the Fort Hood Nightstalker videotape in the debris area. These pulsating solar reflections were similar to the pulsating flashes on FLIR videotape Q-4. Event 8 at 11:24:30 – 35, event 12 at 11:26:27 and the flashes from 12:08:48 and onwards, including event 57, on FLIR videotape Q-4 were compared to the pulsating solar specular reflection flashes recorded by the Fort Hood FBI Nightstalker. The visual review confirmed that events 8, 12, 51 and 52 on the FLIR videotape Q-4, were similar in appearance to the pulsating solar reflections in the debris area on the Fort

Hood trial videos, one example is shown in figure 5.30. Heat combust from the CEV can, however, have contributed in creating the flashes at events 8 and 12.

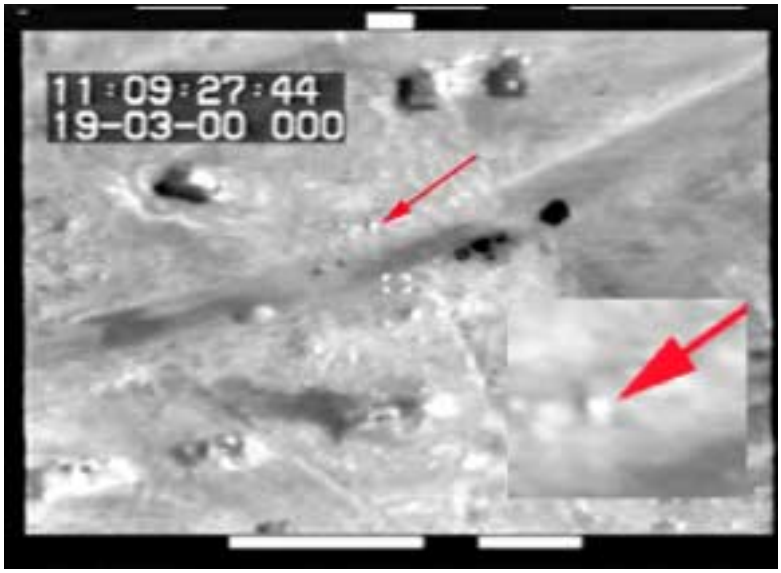

Figure 5.29. Muzzle blast flash (red arrow) from the Fort Hood FBI Lynx videotape and a highlighted enlargement of the same region.

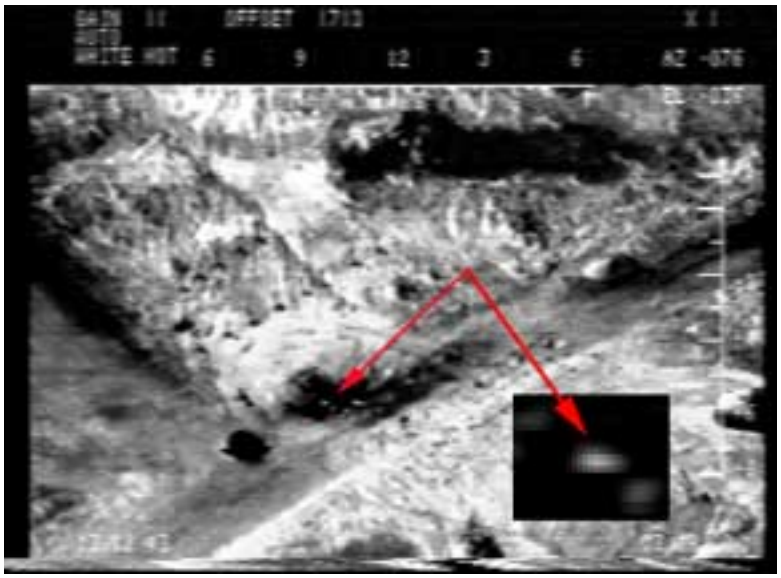

Figure 5.30. An illustration of pulsating flashes (red arrow) at the Fort Hood FBI Nightstalker videotape, enlarged in the lower right part of the image.

At 12:08:48, including event 57, several flashes appear from the same position in the courtyard near what once was the gym. From 12:10:48 onwards, multiple flashes are seen from that same position. The flashes from this position appear in one single horizontal line, regardless of the FBI Nightstalker's circular movement. This was verified by analyzing these flashes utilizing the analyzing system's built in waveform monitor. The object that caused the flash was obviously less than the size of the vertical resolution. It was concluded that the FLIR system smeared the flashes seen from 12:10:48 onwards, in the images horizontal direction. This effect was investigated in depth in section 5.1.2, see figure 5.7. The flashes from 12:08:48 and onwards, including event 57, from this position were concluded to be mainly reflections caused by heat from the fire, however, solar specular solar reflection cannot be entirely excluded.

Efforts were made to further determine the phenomena, beside multiple objects, that could cause the pulsating nature of the flashes seen on the FLIR respective to the Fort Hood videotapes. Measuring exact duration times from video is close to impossible for short duration flashes that are seen in one field or those appearing intermittent in multiple fields as pulsating flashes. Thus, counting fields does not, by itself, provide enough parameters to identify events from the FLIR videotape such as a small arm muzzle blast.

An object with a sharp horizontal edge might very well be presented in one field, but not in the next. This phenomenon is in the literature referred to as "twitter" on fine vertical details, [Watkinson]. Quantifying effects are known to cause variations in the image intensity, particularly when the size of a reflecting object is less than the FLIR system's spatial resolution. Such a small object can align well within one detector element, figure 5.2. For a high-energy flash like solar reflections, the pixel values will then be saturated, unless affected by limitations in the bandwidth of the video system. A small object might also fall between two elements in the vertical direction during parallel scan, see figure 5.2, and thereby become more or less invisible; or fall onto two (or more) detector elements and thereby become represented by two or more scanned lines. In these latter two cases, the pixel values will become a mixture of the object's and the surrounding background's thermal radiation.

The object can also fall on the edge between serial scans. This can affect the image intensity of the object, but also cause displacement of the representation of the object in the image as analyzed in section 5.1.3, figure 5.9.

Event 44, for example, is not of a pulsating nature. This flash was represented either as a rectangle in only one video line, or as a more diffuse rectangle that spanned several video lines, figure 5.31. The same effect appeared for larger flashes on FLIR videotape Q-4, but at the edges between the object and the background. Measuring the variations in intensity profile for several of the larger flashes verified this phenomena. According to the SPRITE tentative data in [Philips], the SPRITE/TED vertical element width is 62.5 μm. The exact size of the gap between the detector elements of this particular FLIR was unknown, but according to [Philips] this gap is about 12.5 μm or about 20 % of the vertical size of the SPRITE/TED

element. Phenomena that also can affect the appearance of small or distant objects are non-uniformity in signal processing within the FLIR system, described section 5.1.3, [Cuthbertson] and [Philips].

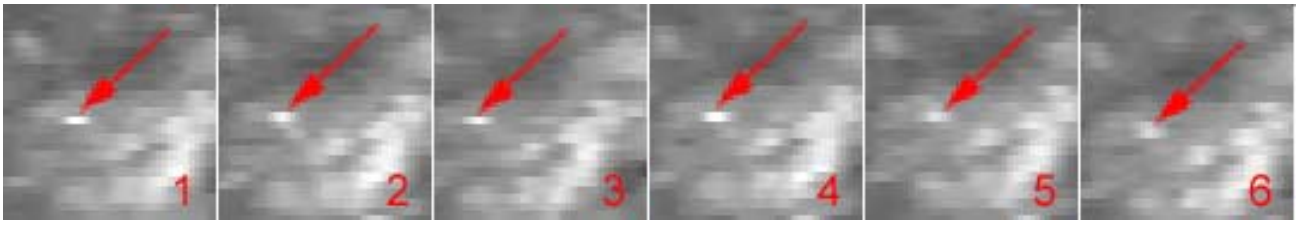

Figure 5.31. Event 44 at 12:00:40, six consecutive image fields with the flash represented by a varying number of video lines.

The effect of these phenomena can be illustrated by event 52 at 12:08:51, which is fixed in position relative to the Branch Davidian complex. The FLIR sensor moved significantly causing motion in the image. Tracking the flash showed a significant vertical motion in the image and thereby the thermal radiation was projected onto one or several consecutive detector elements, on the gap between two elements or between scans, illustrated in figure 5.32.

Figure 5.32. Vertical image motion for event 52 at 12:08:51 that is fixed in ground position, initial position (red arrow) and the trace (yellow dotted line) of the flashes from FLIR sensor movements.

Transient noise or electro-magnetic interference (EMI) from the aircraft avionics, connection cables and improper shieldings also cannot be excluded as factors contributing to image distortion. However, these kinds of image noise and distortions are unlikely to have had any significant impact on the flashes on FLIR videotape Q-4 due to the nature of the flashes.

In short, it is concluded that multiple reflecting objects can cause flashes of a pulsating nature. The result from comparing the analyzed flashes on FLIR videotape Q-4 to the flashes on the Fort Hood flight trial imagery confirmed this.

It is also concluded that the FLIR system and the video system can, and does, distort small objects of a high thermal energy and of a short duration time. Consequently, the SPRITE/TED detector, its scanning mechanisms, and the interlaced video format contributed to the intermittent and pulsating nature of the flashes on FLIR videotape Q-4. These effects, in combination with reflections from one or several close objects, or movements of reflecting objects, all contributed to the pulsating reflections. Complex combinations of these effects have most likely occurred.

Based on this results, it was concluded that event 8 at 11:24:30 – 35, event 12 at 11:26:27, event 51 at 12:08:48 and event 52 at 12:08:51 on FLIR videotape Q-4 also were caused by solar or heat reflections.

5.5.8 Experiments

To verify the results from the 3D reconstruction of the reflection geometry a test was performed utilizing a ThermaCAM PM595 IR camera from FLIR Systems, Sweden. The purpose was to further prove that systems like the FBI Nightstalker FLIR system, in fact, could capture solar specular reflections. The ThermaCAM operates in the spectral far IR band at 7.5 – 13 μm similar to the FBI Nightstalker FLIR sensor. The camera operates in the temperature range -40° to +120° C.

On July 25, 2000, around noon, a small masked mirror, less than 1 cm^2, was placed on a tripod and in a fixed position. This resulted in a very limited spatial distribution of the specular reflection. At a fixed $y \approx 17$ m the distribution cone was estimated to be ± 0.15 m in *x*- and *z*-axis direction, figure 5.33.

Figure 5.33. To the left is a ThermaCAM image taken at 12:14 p.m., where the specular solar reflection was captured. In the middle image, taken less than a minute later from another position at the about the same time, no visually detectable reflection was detected. To the right is a plot of the geometrical relation between the positions of the mirror, ThermaCAM camera and sun.

The solar specular reflection was located visually and captured by the ThermaCAM camera. Solar specular reflections were located and captured at 12:14 p.m. and could not be detected at any nearby position outside the distribution cone. The geometric relationship between the positions of the mirror, bearing to the sun, and the camera position were reconstructed, see figure 5.33. The positions of the sun and the camera position were reconstructed in the same manner as for the images from FLIR videotape Q-4. The results from the tests proved that the solar reflection could be detected in the far IR band. It further confirmed that solar reflections could be detected in the far IR band only within a limited distance from the reflection angle.

Solar specular reflections were further located and captured at 12:17 p.m. and later at 1:23 p.m. The geometrical relationship between the position of the mirror, bearing to the sun and camera position were reconstructed, figure 5.34. This result verified that the reflection geometry varies with the position relative to the sun in the same way as for the analyzed flashes on FLIR videotape Q-4.

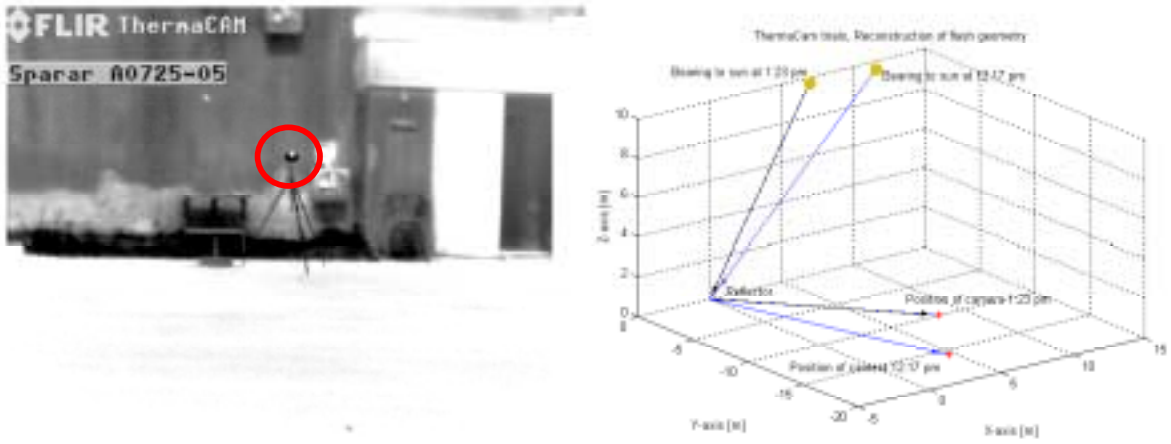

Figure 5.34. To the left is a ThermaCAM image taken at 12:17 p.m., in a position where the specular solar reflection was captured. To the right is a plot of the geometrical relation between the positions of the mirror, ThermaCAM camera and sun.

5.5.9 Results

Events 6 and 42 were only normal thermal radiation from debris/objects set in motion by the CEVs and were omitted from the remaining of the analysis of the flashes.

Based on the results from the visual reviews, the correlation of reconstructed data to the physical laws of solar specular reflection geometry, the fact that several long duration flashes fluctuate in intensity near their peak values, the lack of persons on the roofs and in other areas proximate to the flashes, and the results from the experiment, it is concluded that all of the analyzed flashes were caused by solar or heat reflections.

The sun appeared from under the clouds at the time FLIR videotape Q-4 was recorded on April 19, 1993. There was a lot of broken glass and other kinds of reflective debris from the demolished complex that was not present before April 19, 1993. The objects that caused the reflections were in many cases also seen from the other directions as "cold" objects. Several of the objects were also identified from the complementary duplicate photos and videotapes. Reflection cones have been reconstructed from FLIR videotape Q-4, in a variety of different directions as a result of the many different orientations of the reflecting surfaces. During the time FLIR videotape Q-4 was recorded there were probably several more reflection cones in space than the ones determined from FLIR videotape Q-4. Occasionally, the FBI Nightstalker flew through some of these rays of distributed solar specular reflection that appeared within the range of the aircraft's operating altitude. The strong wind contributed in causing the flashes to appear on an intermittent nature, as the aircraft drifted off from an ideal flight path. Quite simply, the FBI Nightstalker did not pass through all the possible reflection cones existing on April 19, 1993. If it had the number of flashes on FLIR videotape Q-4 would have increased.

5.6 Image Processing for Fire Investigation

The image processing of the Branch Davidian complex fire sequences from the April 19, 1993, FLIR videotapes were done in cooperation with Professor Ulf Wickström, SP, Swedish National Testing and Research Institute, Borås, Sweden. This section describes the approach to processing the FLIR videotapes from April 19, 1993. The results of this analysis have been provided to Professor Ulf Wickström for his analysis of the fire development. Besides discussing the matter by phone and e-mail conversations, meetings were held on three occasions, May 16 and July 13 in Linköping, Sweden, and June 27 in Borås, Sweden. The result from the tracking, pseudo-coloring and temperature measurements were presented and reviewed at these meetings. During these meetings duplicate photos and media footage were also reviewed.

To enhance the visibility of temperature variations on the building before and during the initial phase of the fire, a sequence of 25100 digitized images within the time interval 11:57:03 – 12:11:04 were pseudo-colored. One field per each frame was used to limit the motion blur that frequently disturbs the image quality caused by the interlaced video format. Pseudo-coloring is a process by which the shades of grey within the FLIR image are assigned colors. Because the human eye can not fully resolve small quantitative difference between the shades of grey depicted on the screen, pseudo-coloring can successfully be used to assist the eye to detect small objects or resolve temperature differences in the thermal images. When an object on the FLIR imagery increases in temperature, its shade of grey will become lighter. These small changes in temperature are, to some degree, easier to track when using the pseudo-coloring process, where the human eye could not detect the small change in grey levels.

However, the automatic gain and bias control of the FLIR caused rapidly changing variations in the grey scale, as mentioned in section 5.1. As a result, areas of uniform temperature do not always correspond to the same grey level intervals in the FLIR imagery. To overcome this problem, the sequence

was preprocessed. Four regions of interest were tracked, see figure 5.35, in which the temperature variations were assumed to remain relatively stable. As the fire spread, the central tower roof and the lawn in front of the central tower increased in temperature, measured relative to the water in the pool. The temperature of the water surface remained stable within the tracked time interval and was used for normalization of the gain variations. Normalization is here defined like in [HolstIR], as the "*process of reducing the measurements as nearly as possible to a common scale*".

Figure 5.35. Selected regions for normalization of grey levels illustrated in one of the frames, on the platform near the swimming pool, on the central tower roof, on the lawn in the courtyard and on the water surface in the swimming pool. An additional area was tracked on the soil of the red side.

This simplified normalization procedure adjusted the pixel values in the images according to the average intensity of the water surface. One field per 100 frames was tracked, except for 12:05:29 – 12:06:31 where each 50th frame was tracked. For the untracked fields between the tracked fields, the estimated pixel intensities were obtained from interpolation. The variations in the average grey levels for the four regions are shown in figure 5.36. Using this simplified normalization procedure, the variations caused by the automatic bias control were reduced, but not fully removed. The automatic gain function was also not fully corrected. Yet another region was tracked on the soil of the red side and some modifications of the normalization procedures were made to equalize the bias. The modified normalization procedure was applied for the interval 11:57:00-12:06:31. The remaining variations caused by the automatic bias and gain functions were determined negligible and not to have impact on the reliability of the results.

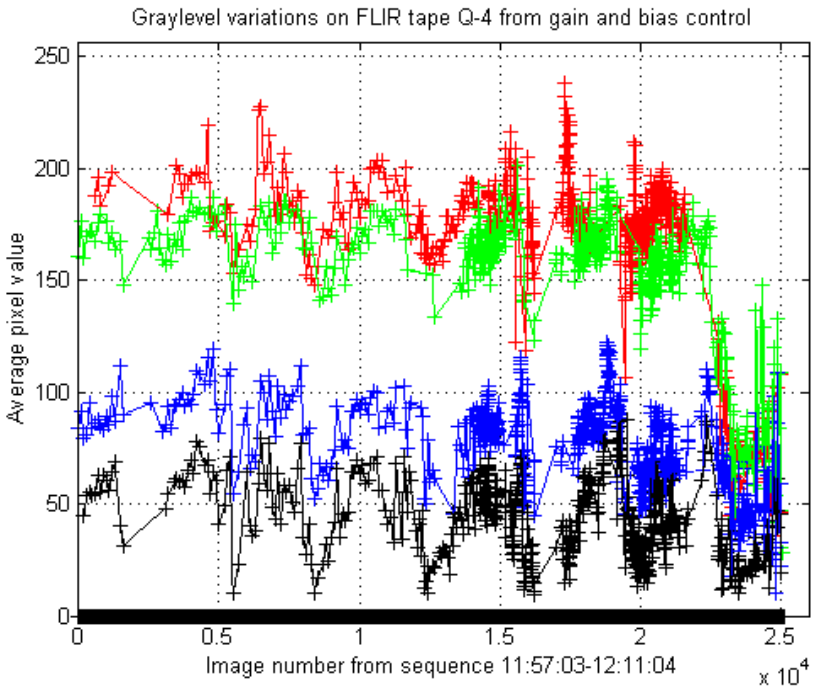

Figure 5.36. Variations of the average grey level of the tracked regions, as an effect from automatic gain and bias control of the FLIR at 11:57:03-12:11:04.

Finally, the sequence was pseudo-colored in three different ways, for both the unprocessed and the normalized sequence. First, a color-map was chosen to pseudo-color all grey levels. Second, the same color-map was used to pseudo-color only the highest temperature interval in the FLIR images. The third method applied red for the highest temperature interval in the FLIR images. The three pseudo-coloring techniques were applied both on unprocessed as well as processed sequences. Figure 5.37 shows some examples from the unprocessed and the pseudo-colored sequences.

The rather immediate outcome of the tracking and pseudo-coloring was the observations of heat on the white side of the red tower, the catwalk and the cafeteria.

To further analyze the temperature variations at lower intensity levels, a simple method was developed to detect a raise in temperature rather than just saturated pixels. From the first visible heat source, the FLIR sequences were tracked backwards in time until it was unable to detect the heat visually. An area to measure the image intensity was then selected where an intensity profile was created for several selected occasions. The occasions were selected based on the FLIR sensor field of view. Ten intensity profiles were created from consecutive images at each selected time. The intensity profiles were finally averaged to remove system noise. As a result, the relative variations in temperature could be compared over time. From figure 5.36 it was assumed that the variation caused by the automatic gain control had

impacts on the measured values, which had to be considered when interpreting the results. However, the impacts are not assumed to threaten the reliability of the result.

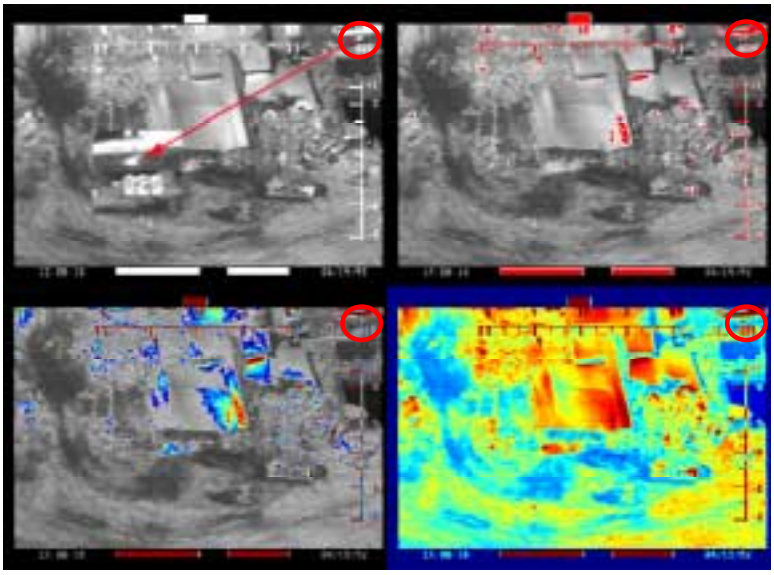

Figure 5.37. Detected heat sources at 12:08:10 (red circles), unprocessed (upper left) and enlarged (red arrow), and images pseudo-colored in three different ways (upper right, lower left and lower right).

Figure 5.38. Detected hot spots in the red tower 12:07:41 (left, red circle and enlarged) and 12:09:09 (right, red circle).

5.6.1 Red Tower

A heat source was detected from the pseudo-colored sequence at 12:07:41, in window B14 on the white side of the red tower. No significant variation in image intensity was detected on the white side wall of the tower before that, but was clearly seen when the white side appeared again in the FLIR field of view at about 12:09:09 figure 5.38.

5.6.2 Catwalk Roof

At the eave of the shaded side of the catwalk roof, a heated area was detected from reviewing the digitized FLIR sequences, faintly at 12:04:21 and 12:05:13 and more clearly at 12:06:13. The bright spot on the eave of the catwalk roof increases in heat until 12:10:21 when heat clearly were seen emerging from the catwalk and gym area.

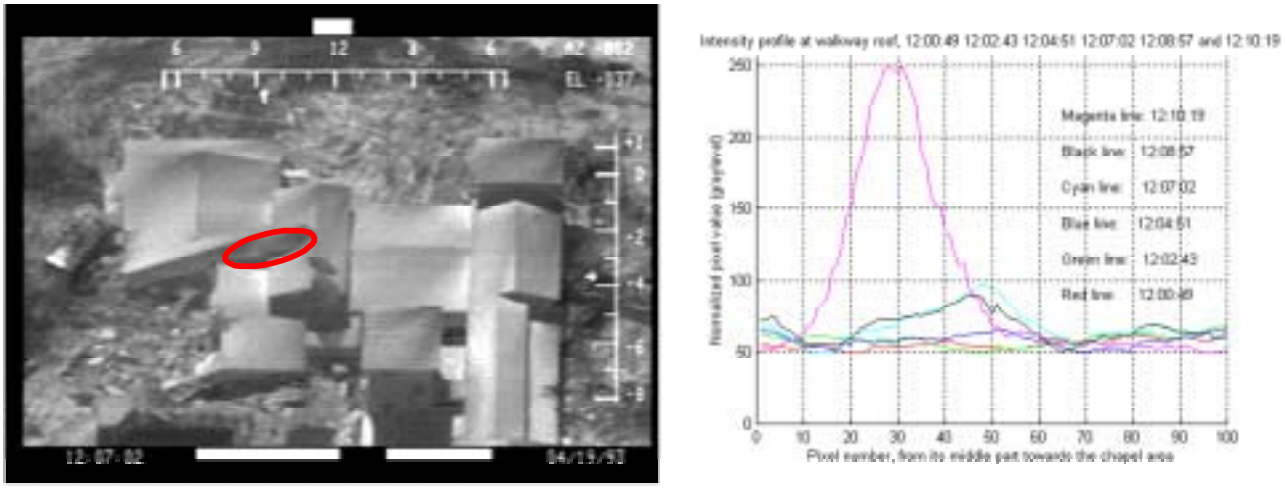

Figure 5.39. To the left a hot spot at the eave of the catwalk roof with the position for the measured intensity profile. To the right a plot of the measured temperature differences.

The relative difference in temperature was measured on a two-minute basis, utilizing the method described earlier. The decision to measure on a two-minute basis was simply motivated by the fact that the catwalk roof was not horizontally aligned on the FLIR images. In practice, measuring the intensity profiles from varying image directions would have increased the measurement error. Lower intensity values corresponding to unheated parts of the catwalk roof were assumed to be relatively stable in temperature and used to normalize the intensity profiles to approximately the same bias. According to the measured values, the first significant raise in temperature appears at 12:04:51, see figure 5.39. The first indication of increasing heat at the eave of the catwalk roof was verified by additional measurements utilizing a waveform monitor to measure the intensity profiles, but only when the roof was aligned to the images in the vertical direction. The result from this was that the heat increase on the catwalk roof was detected even earlier, at 12:04:05.

Figure 5.40. Duplicate photo of the demolished catwalk, taken from the black side.

Duplicate photos from the black side of the Branch Davidian complex were reviewed. One picture shows a fire in the structure towards the stage area at the rear of the chapel, see figure 5.40. It is reasonable to assume that this picture was taken after 12:04:43, as this is the time when the catwalk roof has fallen onto the ground but before 12:10:21 when heated plumes emerged. No CEV was detected in the picture. As a CEV are seen leaving the gym area at about 12:09:00 it is reasonable to believe the picture was taken some time between 12:09:10 and 12:10:21.

5.6.3 Cafeteria

A bright spot was detected at 12:08:10 on the pseudo-colored sequences, near the door into the cafeteria on the black side of the Branch Davidian complex, see figure 5.41. Later at 12:08:26, two heat sources were also detected, figure 5.41 and 5.37.

No detectable raise in temperature was detected at the cafeteria roof, neither from measuring the image intensities on the wall nor on the roof, see figure 5.42. Although some variations were measured, it could not be deduced whether heat or other phenomena, such as noise induced by the FLIR system, insufficient spatial resolution, or thermal sensitivity caused these deviations.

Figure 5.41. Hot spots near the door into the cafeteria at 12:08:10 (left) and 12:08:26 (right).

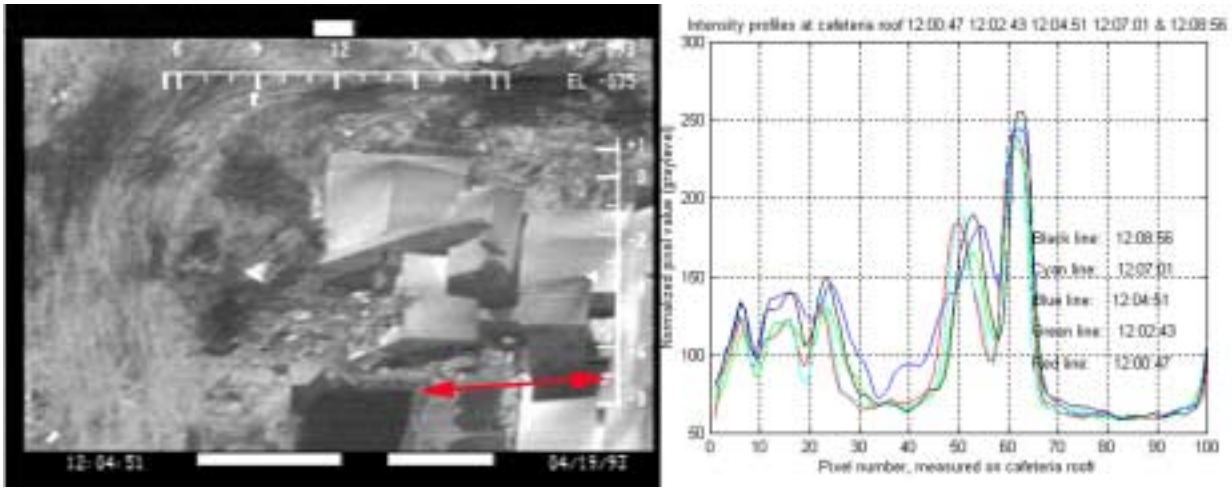

Figure 5.42. To the left is the cafeteria roof with the position for the measured intensity profile. To the right is a plot of the measured temperature differences.

6. VIDEO AUTHENTICATION

Recording an analog video signal is a very complex process. This section contains a short tutorial on video technology to introduce some of the parameters used for investigating whether videotapes are original, authentic, or have been technically manipulated. This section will further explain how the analysis was carried out on the April 19, 1993, FLIR videotapes, and the conclusion of that analysis.

6.1 Video Format

6.1.1 Picture Reproduction

The visible screen on a FLIR system is built up of images called frames. These frames are quickly and sequentially exposed to the viewer, much like the frames playing through a projector shutter in a movie theater. In a television system, each frame is captured and reproduced by horizontal scanning lines. In a NTSC television system, used in North America and East Asia, new frames occur at a rate of 30 per second. The number of horizontally scanned lines in each frame is 525. To reduce the gap between the scanning lines on a screen and to reduce flickering, each frame is scanned twice into two separate fields that are shifted vertically with the height of half a scanning line as shown in figure 6.1.

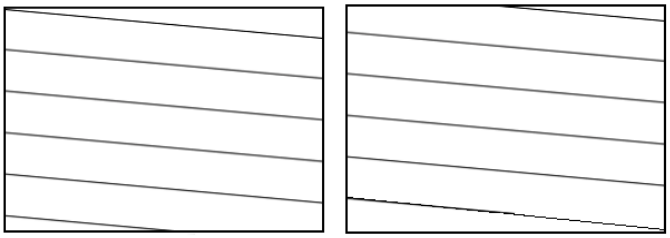

Figure 6.1. Illustration of the difference between the two fields in one frame.

The first field begins with a full line and ends on half a line. The second field starts with a half line and ends with a full line. Each field will contain 262.5 lines and the fields' repetition rate is about 60 Hz or 60 fields per second. However, neither all the lines, nor the entire part of a line is used to carry the picture information. The standard number of lines used for picture information in a frame is 485. The line period is 64 μs, for which 52 μs is used as picture space. In this case, the number of lines used for the thermal imagery from the FBI Nightstalker FLIR sensor is about 416. There are several different video system in use around the world, and the FLIR system is designed to RS-170 that is an EIA standard for 60 Hz monochrome (grey scale) video. RS-170A (SMPTE 170M) is the standard for 60 Hz color video (NTSC). In Europe, the most commonly used system is PAL. The main difference between NTSC and PAL is that PAL in Europe has a 50 Hz field rate, 25 Hz frame rate, and 625 lines in each frame, and 312.5 lines in each field. The system for color reproduction is also different for NTSC and PAL. The frame and field rate of RS-170 and RS-170A that are commonly specified as 30 respectively 60 Hz, are in

fact 29.97 respectively 59.94 Hz. Specifications for different video systems can be found in ITU-R (formally CCIR) reports.

A normal TV set or a low-cost monitor will not display the entire picture due to over scanning. The amount of picture information that is outside the visible area depends, for example, on how well the monitor or TV set is aligned. As a result, there is picture information just outside the visible screen. In the forensic case, the "hidden" information can be of great importance. There are also computer frame grabbers and other digitizing products on the market which have limitations in capturing the full picture area.

6.1.2 Video Signal

The video signal itself is a continuous stream of complex information, which contains a wealth of information that needs to be distributed. For example, the illumination level, vertical (field/frame) synchronization, horizontal (line) synchronization and in the case of color reproduction, color information and color synchronization are contained in the video signal. Every new field starts with a vertical synchronization pulse. Between two consecutive vertical synchronization pulses, there is 262.5 horizontal synchronization pulses. Every line starts with a horizontal synchronization pulse. Between two consecutive horizontal synchronization pulses there is image information.

The standard level of video signal used by video equipment is 1-volt peak to peak, where both vertical and horizontal synchronization signals are pulses between 0 and 286 mV. The image information has an amplitude variation from 286 mV to 714 mV, where 286 mV is black information and 714 mV correspond to 100% white. The synchronization signal is thereby distributed at a level that is lower than black image information, and serves not only as reference to a new field or a new line, but also as a level reference for the luminance information. It is very important that the above mentioned relationship between synchronization and video signal is kept unchanged through a distribution chain, or through a copying process. If the synchronization signal is restored with a different level, for example by using misaligned mixers or time base correctors (TBC), or if the synchronization level has been changed by any other external processing, it will affect the level of the video signal. Consequently the original video signal level will not be correctly represented in captured or digitized video, if the synchronization level has been changed.

6.1.3 Recording of Video

Analog recording of a video signal is performed in a different way than analog recording of audio signals. This difference is due to the higher bandwidth needed for video signals. The main difference in mechanical arrangements is that the video signal is recorded or played back by two record/playback heads. The record/playback heads are mounted on the periphery of a rotating drum, on opposite sides, figure 6.2. When the videotape is loaded into the mechanism, it wraps a little bit more than halfway around the drum as shown in figure 6.2.

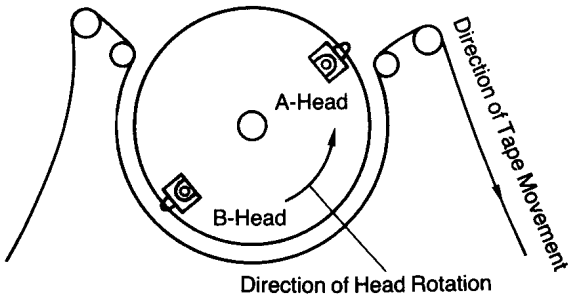

Figure 6.2. Helical scanning, from [Panasonic, Basic video guide] p. 7.

During recording, the rotation of the drum is locked in speed and phase to the actual frame-rate of the supplied video signal. In case of NTSC, for which the frame rate is about 30 Hz, the drum will make 30 revolutions per second. Thus, one revolution will correspond to two fields. The drum is also angled so that half way around the drum corresponds to approximately the width of the videotape, as showed in figure 6.3. This angle between the drum and the videotape is called helix angle.

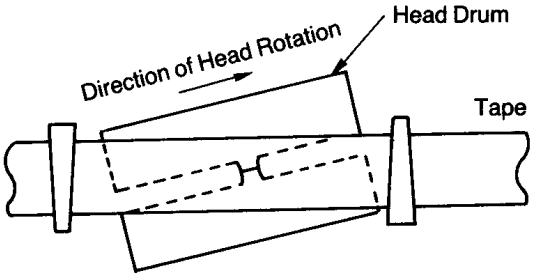

Figure 6.3. Helix angle, from [Panasonic, Basic video guide] p. 7.

The resulting recording of the video signal on the tape will be diagonal tracks as shown in figure 6.4. Each track starts with a new field only if the drum is synchronized at a correct speed and phase during recording. Since the videotape wraps a little bit more than halfway around the rotating drum and the video heads are connected in parallel during recording, each track will end with the same information as the next track starts with. The recorded signal on these tracks is a Radio Frequency (RF) carrier that is frequency modulated (FM) by the luminance part of a video signal. Under normal circumstances there is also a chrominance part to record, and this chrominance signal is distributed as a carrier in the composite video signal. This chrominance carrier will be down converted by electronics inside the video machine from 3.58 MHz (NTSC) to 627 kHz. The converted signal will be used by recording circuits to amplitude modulate the luminance RF-signal.

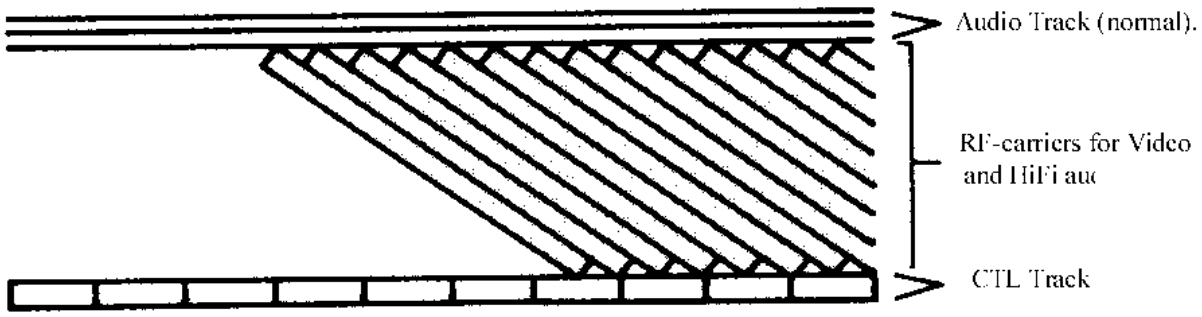

Figure 6.4. Tapepath, from [Panasonic, Basic video guide] p. 9.

In this case, when the video signal was generated by the FBI Nightstalker FLIR system, the FLIR sensor information was recorded as luminance signal. The frequency of the RF-carrier varies between 3.8 MHz and 4.8 MHz, where 3.8 MHz represent the lowest level (0 volt) and 4.8 MHz the highest level (1 volt) of the video signal that modulates the carrier. "Black" in an FLIR image will correspond to approximately 4.0 MHz.

During recording, a Control signal (CTL) is created from the video signal's vertical synchronization of the first field in a frame, and formed into a square wave signal, that is recorded into a longitudinal CTL-track into the lower edge of videotape, figure 6.4. During playback the CTL-pulse serves as a reference for the drum servo circuit, which will cause the video heads to match the recorded track on the videotape. The recording format of a CTL-track is similar to a normal audio track, but the CTL-track is recorded without a bias current. Thus, the recording of a square wave will end up as spikes. A typical playback CTL-pulse is illustrated in fig 6.5.

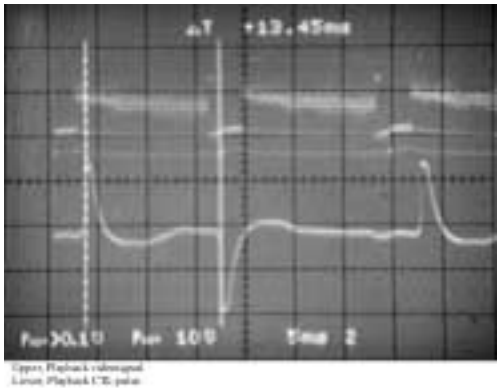

Figure 6.5. Playback CTL-pulse from videotape Q-4 playback video signal (upper) and playback CTL-pulse (lower).

If a video machine is equipped with a hi-fi track for high quality audio reproduction, there are two more recording/playback heads mounted on the video drum. Those extra heads are used for two frequency modulated RF carrier signals, which are required for recording and playback of high quality audio. The carrier frequency specification for VHS format in NTSC television-standard is 1.3 MHz for left channel audio and 1.7 MHz for right channel audio. Recording these RF-carriers deep into the magnetic coating of a videotape, before recording the RF-carrier that contains the picture, will result in a layer that is permanent and not erased by the recording current of the picture signal, figure 6.6.

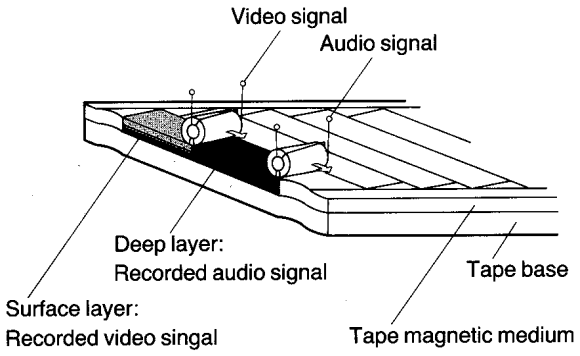

Figure 6.6. Deep modulated FM layer from [Panasonic, Basic video guide] p. 8.

6.2 Analytical Methods

One of the two main parts of this investigation was to determine whether the April 19, 1993, FLIR videotapes Q-1 – Q-7 are original and authentic. To answer this question the following electrical signals have been analyzed to determine if there has been any kind of alteration of the FLIR videotapes, and also to ensure that a single recording source was used for each FLIR videotape;

- RF-envelope for the video signal.
- RF-signal carrier for video signal.
- RF-envelope for FM-audio signal.
- RF-signal carrier frequencies for FM-audio signal.
- Dihedral error.
- CTL-pulses.

A visual inspection of the playback picture on the FLIR videotapes was also performed.

No attempt was made to expose the magnetic layer on FLIR videotapes as this might damage the videotapes.

6.2.1 RF-envelope for the Video Signal

This is the playback RF signal for one drum revolution exposed on an oscilloscope. Each video recorder has a slightly different helix angle and recording current. This will cause variations in the playback RF envelope and level if different video machines where used to record a videotape. These machine specific differences are identifiable in the playback RF envelope. A typical view of the playback RF-envelope from FLIR videotape Q-1 is seen in figure 6.7.

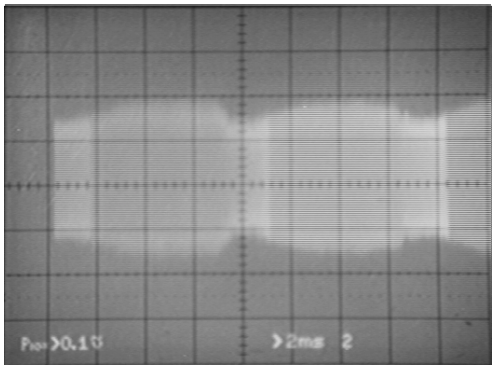

Figure 6.7. Oscilloscope picture viewing playback envelope from FLIR videotape Q-1. The picture shows the signal from one drum revolution, the head switch occurs in the middle of the picture.

6.2.2 RF-signal Carrier Frequency for Video Signal

The RF-carrier frequency can vary between 3.8 MHz and 4.8 MHz. 3.8 MHz represents the lowest part of the video signal and has been used for analyzing the FLIR videotapes.

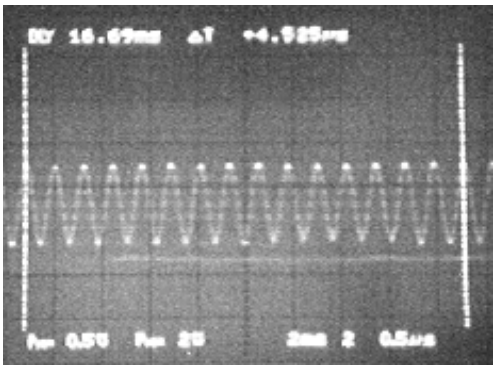

Figure 6.8. Oscilloscope picture viewing the RF-carrier from FLIR videotape Q-6. The picture is

captured during a vertical synchronization pulse, where the RF-carrier is nearly stable.

A typical view of the playback RF-carrier from FLIR videotape Q-6 is seen in figure 6.8.

Adjustment for this RF-carrier is done when manufacturing and also during service. This RF-carrier is seldom adjusted by anything more sophisticated than a potentiometer, and the precision is approximate. The lowest stable frequency available for examination occurs during the vertical synchronization area of the video signal. By using an oscilloscope to capture several cycles of the RF-carrier during vertical synchronization it is possible to calculate the frequency, and detect changes that could indicate a different recording video machine.

6.2.3 RF-envelopes for the FM-audio Signals

These two signals were treated in the same manner as the RF-envelope for video signal. A typical oscilloscope view showing audio RF-envelopes are in figure 6.9.

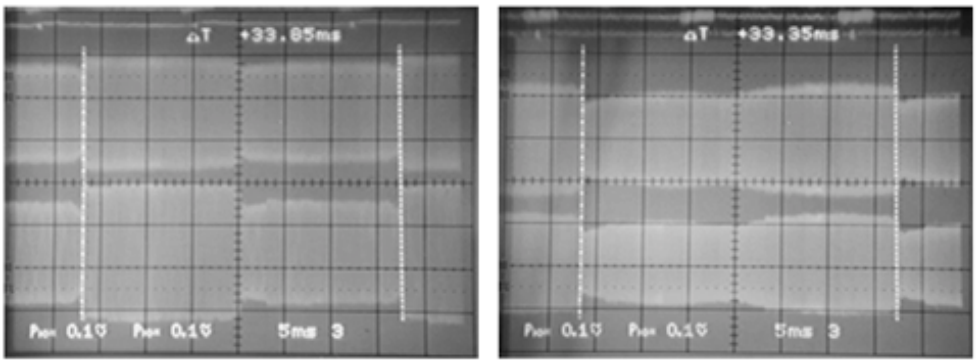

Figure 6.9. Oscilloscope picture viewing audio RF-envelope from videotape Q-3 and Q-4. The upper signal is from left channel, and the lower signal is from the right channel. Between the cursors there are one drum revolution, and in the middle of each picture the heads are shifted.

6.2.4 RF-signal Carrier Frequency for the FM-audio Signal

The RF-carriers were monitored with a frequency counter during playback. The purpose was to detect variations in the carrier frequencies that could indicate different recording equipment.

6.2.5 Dihedral Error

During recording, the record/playback heads are connected in parallel. In playback mode the heads must be electronically shifted when one track has been scanned. The head switch is adjusted in a playback video machine to occur at the end of a track, in a portion similar to the beginning of the next track. This position is just outside the visible area of the screen, at the end of a field to avoid picture disturbance.

Since every recorded video-line only corresponds to 0.685º of a drum revolution, the heads on the video drum needs to be mounted in a precise manner to keep the signal as accurate as possible to allow accurate playback by different video machines. The difference error is normally about 0.01º. A misalignment between different video machines of the head mounting position on the drum by 0.1º from 180º gives a time shift to the video signal in the head switch point of about 20% of the picture width.

Measuring this time shift during playback of a questioned videotape gives a signature that is related to the difference between the recorder machine and the laboratory machine. It is normal that there are variations in this time shift during playback of a videotape. These variations normally depend on ambient temperature, back-tension fluctuations and tape friction among other factors. These changes vary at a slow rate. This method is the most effective test that can be used to track a master recording video machine from a second generation copy. A switch signature from the head switch is added to the video signal during playback. During additional copying processes, these additional switch signatures will be recorded to the videotape. The number of switch signatures will then normally indicate the number of copying processes, the copying order. A typical view showing the results created by a dihedral error is in figure 6.10.

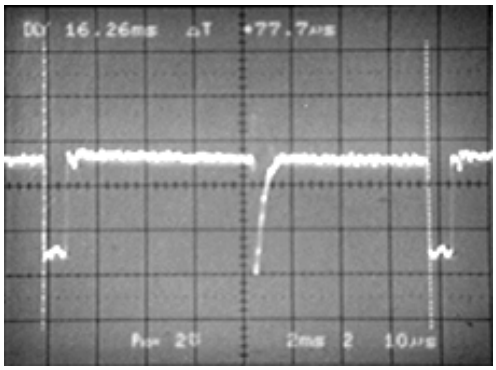

Figure 6.10 is an oscilloscope picture viewing the video line where the head switch occurs. The line period has been expanded from 64 µs to 77.7 µs, caused by the difference between the recording and the playback video machine. The cursors are adjusted to the falling edge of horizontal synchronization for measuring the line period, and in middle of the picture there is a glitch from the head switch.

6.2.6 CTL-pulse

The parameters examined were; the duty cycle, pulse level, rise and fall time, time between CTL-pulses and vertical synchronization pulses. Different manufacturers use different values for the duty cycle within different types of video recorders and there are often differences in the rise and fall time between different models. Variations during playback are normally dependent on ambient temperature, back-tension fluctuations, and tape friction. However, this change occurs slowly without any step functions. Typical CTL-pulses are shown in figure 6.11.

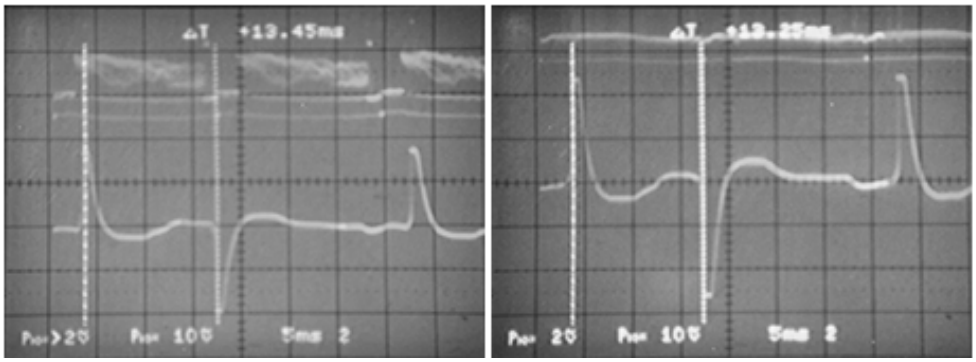

Figure 6.11. Oscilloscope pictures viewing typical CTL-pulses from FLIR-videotape Q-3 (left) and FLIR-videotape Q-6 (right).

6.3 Preprocessing

Each tape was copied onto a working copy tape for use in some of the measurement procedures. These working copies recorded the video signal and two hi-fi sound tracks. The ordinary longitudinal soundtrack was omitted as Mr. Chris Mills, Network International Forensic Science Division, investigated it. On these working copies, the original CTL-pulse track from the FLIR videotapes has been recorded into one hi-fi soundtrack to be used for examination of authenticity, and the original sound hi-fi tracks from FLIR videotapes were mixed together and recorded into the second hi-fi sound track. During the preparation process two FLIR videotapes Q-6 and Q-7, gave indications of not being original recordings. One indication is the fact that the video signal contained color synchronization, which is a facility that the FLIR sensor did not support. Secondly, Q-6 and Q-7 did not have hi-fi sound tracks, which should have been present if they were recorded on same type of video recorders that produced Q-1 to Q-5. Thirdly, there is a trace of an earlier head switch that has been added by a playback video machine during the copying process.

As a result of these observations the recorded video signal on FLIR videotape Q-6 and Q-7 was compared to the recorded signal on FLIR videotape Q-1 – Q-5. When Q-6 and Q-7 were produced, the video signal underwent some significant signal processing. First, the synchronization portions have been changed to a signal that contains color synchronization. Secondly, the synchronization part of the video signal recorded on Q-6 and Q-7 does not match the video signal amplitude, of Q-1 – Q-5. Thirdly, an aperture facility has been used. In practice this means that every edge of fast action is amplified and thereby deviates from the original level. This has caused the trailing edge of every action to be enhanced, which can be seen both in the picture and as a measurable signal. Fourth, the copying process has also fed a discernable amplitude variation in the vertical direction. The noise levels have been increased, not only due to an aperture facility, but by virtue of the copying process. Figure 6.12 shows averaged video line information.

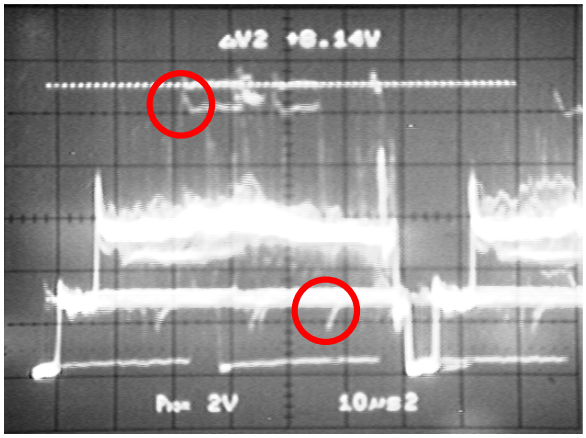

Figure 6.12. An oscilloscope picture viewing averaged line information from tape Q-6. The enhanced edges are clearly observable (red circles).

In short, FLIR videotapes Q-6 and Q-7 were determined to be copies and were instead used to investigate the authenticity of their masters. Consequently, the video signals recorded on FLIR videotapes Q-6 and Q-7 are not to be used for image measurements.

6.4 Analysis and Result

Results from the analysis are summarized in section 7.

6.4.1 Visual Inspection of Playback Picture

The airborne FBI Nightstalker FLIR system initially generated the recorded video signal on FLIR videotapes Q-1 to Q-7. Since the FBI Nightstalker slowly circled above the compound, the recorded subject itself and the slow image motion were a perfect object for visual inspection, as a jump or any fast change in the picture will be clearly observable. Initially, a visual inspection of the playback picture was performed to determine if there were any abnormal changes or jumps in the picture that could indicate some kind of editing or erasure. The results from this visual examination were:

- FLIR videotape Q-1. The first frame of the actual sequence starts at 05:58:11, and the actual sequence ends with 08:00:02. However, in the initial part of the videotape, frames with at least three different dates and time information were found, 05:19:00 04/17/93, 03:06:39 04/18/93 and 05:51:43 04/19/93. All three portions have been recorded over by the recorded portion 05:58:11 – 08:00:02. There are no indications of breaks or edited parts on the recorded portion 05:58:11 – 08:00:02.

- FLIR videotape Q-2. There were no indications of breaks or edited parts on the recorded portion 07:57:42 – 09:28:20.

- FLIR videotape Q-3. There were no indications of breaks or edited parts on the recorded portion 05:58:09 – 07:57:00.

- FLIR videotape Q-4. The recording of the video sequence was interrupted between 10:47:16 and 10:51:57, according to the time information displayed in picture. There is no sign that this interruption is an edit or erasure. It appears to only be a stop during recording that probably was induced by the operator. There are no other indications of breaks or edited parts, beside this interruption, on the recorded portion 10:41:57 – 12:16:13.

- FLIR videotape Q-5. There were no indications of breaks or edited parts on the recorded portion 12:16:37 – 13:39:07.

- FLIR videotape Q-6. In the beginning of the videotape there was a sequence with color bars and the text "30421013E QE". There are no indications of breaks or edited parts on the recorded portion 12:41:25 – 14:01:38. By comparing the picture and recorded length to videotape Q-5, it is further concluded that the master for this recording is not FLIR videotape Q-5.

- FLIR videotape Q-7. In the beginning of the videotape there was a sequence with color bars and the text "30421013E QE". The recorded video sequence is interrupted between 10:47:15 – 10:51:57, according to the time information displayed in picture. There is no sign that this interruption is an edit or erasure. It appears to only be a stop during recording that probably was induced by the operator. There are no indications of other breaks or edited parts on the recorded portion 10:41:57 – 12:41:07. By comparing the picture and recorded length to videotape Q-4, it is concluded that the master for this recording is not FLIR videotape Q-4.

6.4.2 RF-envelope and Carrier Frequency for Recorded Video Signal

The playback RF-envelope on the entire recorded part, for each of the FLIR videotapes, was observed using an oscilloscope. This aim was to determine if there were any changes or level fluctuations that could indicate an attempt to tamper with the recorded material. The lowest frequency of the video signal's RF-carrier has been monitored with an oscilloscope to detect if there were abnormal changes in carrier frequency. Such a change would indicate the use of other recording devices. The lowest stable frequency available for examination occurs during vertical synchronization. By using an oscilloscope to capture several cycles of the RF-carrier it was possible to calculate the frequency, and also to exclude changes that would indicate a different video machine.

The results from this inspection were:

- FLIR videotape Q-1. Only normal variations have been detected. Carrier frequency is about 3.44 MHz.

- FLIR videotape Q-2. Only normal variations have been detected. Carrier frequency is about 3.43 MHz.

- FLIR videotape Q-3. Only normal variations have been detected. Carrier frequency is about 3.43 MHz.

- FLIR videotape Q-4. A fast disturbance in RF-envelope occurs at 10:47:16, according to the time information displayed in picture. Both the RF-envelope and carrier frequency remained similar, before and after the disturbance. The disturbance was identified as a stop during recording. Referring to the time information displayed in the picture there is an interrupt in recording that last between 10:47:16 and 10:51:57. Carrier frequency is about 3.44 MHz.

- FLIR videotape Q-5. Only normal variations have been detected. Carrier frequency is about 3.42 MHz.

- FLIR videotape Q-6. Only normal variations have been detected. Carrier frequency is about 3.31 MHz.

- FLIR videotape Q-7. Only normal variations have been detected. Carrier frequency is about 3.31 MHz.

The results from analyzing the RF-envelope and carrier frequency is that only normal variations in RF-envelope and carrier frequency recorded on FLIR videotapes Q-1 – Q-7 were observed through the entire recorded portions of the FLIR videotapes.

The visible break in recording that occurs on FLIR videotape Q-4 from 10:47:16 to 10:51:57 is with a disturbance in the RF-signal. Both the RF-envelope and carrier frequency signals remained similar before and after the disturbance. This indicates that Q-4 was made utilizing the same video machine.

The break in recording that occurs on FLIR videotape Q-7 at 10:47:15 and lasts until 10:51:57 does not have a disturbance in the RF-signal. This indicates that Q-7 is a copy and that the recording was continuous during the copying process.

6.4.3 RF-envelope and Carrier Frequency for FM-audio

Since the recorded sound on videotapes Q-1 – Q-5 are FM-type and deeply modulated into the surface of the videotape, it is not possible to edit or erase this track without also tampering with the video

signal. Therefore, this part of the analysis was performed in conjunction with the analysis of the RF-envelope for the video signal. The carrier's average center frequency of both channels has also been measured during playback.

The results from this inspection were;

- FLIR videotape Q-1. Only normal variations of the playback envelope have been detected. Carrier frequency: left channel = 1306.5 kHz, right channel = 1705.3 kHz.

- FLIR videotape Q-2. Only normal variations of the playback envelope have been detected. Carrier frequency: left channel =1305.3 kHz, right channel = 1704.8 kHz.

- FLIR videotape Q-3. Only normal variations of the playback envelope have been detected. Carrier frequency: left channel =1303.5 kHz, right channel = 1703.8 kHz.

- FLIR videotape Q-4. A disturbance in RF-envelopes occurs at 10:47:16. Both the RF-envelopes and carrier frequencies remained similar, before and after the disturbance. The disturbance was identified as a stop during recording. According to the time information displayed in picture the stop lasts between 10:47:16 and 10:51:57. Carrier frequency: left channel =1307.0 kHz, right channel = 1705.5 kHz.

- FLIR videotape Q-5. Only normal variations of the playback envelope have been detected. Carrier frequency: left channel =1306.0 kHz, right channel = 1705.0 kHz.

- FLIR videotape Q-6. No carriers were recorded.

- FLIR videotape Q-7. No carriers were recorded.

The conclusion after analyzing the FLIR videotapes Q 1 – Q-5 is that the recorded audio FM - carrier on FLIR videotapes Q-1 – Q-5 are original recordings without any erased or edited parts. The visible break in the recording that occurs on FLIR videotape Q-4 at 10:47:16 and lasts until 10:51:57 has a simultaneous disturbance in the RF-signals. Both RF-envelopes and carrier frequencies signals remained similar before and after the disturbance. This indicates that a single video recorder made Q-4.

Videotapes Q-6 and Q-7 were not recorded with deep modulated FM-carriers for hi-fi sound.

6.4.4 Dihedral Error Measurement

It is possible to estimate the dihedral error from the time shift in the video signal that occurs at the head switch position. By measuring the time shift related to the specific recording and the playback video machine a "time shift" signature is produced. Variations in this signature could indicate if more than one

machine has been used for recording a particular tape, or if there have been edits subsequently produced by another machine. For each videotape the time shift has been monitored during the recorded portion. The measurements are from field one, at a midpoint of the recorded portion. The numerical value is for the line period where the head switch occurs. The results from analyzing the dihedral error were;

- FLIR videotape Q-1. In the head switch point, the line period is expanded to 77.7 µs.
- FLIR videotape Q-2. In the head switch point, the line period is expanded to 83.3 µs.
- FLIR videotape Q-3. In the head switch point, the line period is expanded to 83.6 µs.
- FLIR videotape Q-4. A fast disturbance in the video signal occurs at 10:47:16, according to the time information displayed in picture. The disturbance is identified as a break during recording, and according to the time information the break lasts between 10:47:16 and 10:51:57. The dihedral error remained similar throughout the entire recording indicating that a single video recorder made Q-4. In the head switch point, the line period is expanded to 78.6 µs.
- FLIR videotape Q-5. In the head switch point, the line period is expanded to 69.4 µs.
- FLIR videotape Q-6. In the head switch point, the line period is expanded to 70.2 µs. There is also a sign of an additional head switch caused by another playback video machine during the copying process.
- FLIR videotape Q-7. In the head switch point, the line period is expanded to 70.2 µs. There is also a sign of an additional head switch caused by another playback video machine during the copying process.

There were no indications that more than one video machine per FLIR videotapes Q-1 – Q-7 should have been used for recording.

6.4.5 CTL-pulses

The CTL-pulses that were recorded on the working copies of FLIR videotapes Q-1 – Q-7 were examined. Different manufacturers use different standards for CTL-pulses. In practice, this means that the recorded CTL-pulses will vary between different types of video machines. Variations can also occur between individual video machines. For each of the videotapes the CTL-pulses have been monitored among the recorded portion on the working copies.

The results from analyzing the CTL-pulses were;

- FLIR videotape Q-1. Only normal variations among the recorded portion were detected.
- FLIR videotape Q-2. Only normal variations among the recorded portion were detected.
- FLIR videotape Q-3. Only normal variations among the recorded portion were detected.
- FLIR videotape Q-4. A double CTL-pulse occurs at 10:47:16, according to the time information displayed in picture. By analyzing the CTL-pulses, it can be seen that the recording have been interrupted, and only one frame have been over recorded, i.e. there was no earlier recordings that have been over recorded.
- FLIR videotape Q-5. Only normal variations among the recorded portion were detected.
- FLIR videotape Q-6. Only normal variations among the recorded portion were detected.
- FLIR videotape Q-7. Only normal variations among the recorded portion were detected.

The double CTL-pulse that occurs on FLIR videotape Q-4 does not constitute an edit point created in an edit video machine, since such an edit operation do not affect the flow of CTL-pulses.

The break during recording that appears in images on FLIR videotape Q-7, does not appear on the CTL-track. This is because the video signal was restored during the copy process, and there was no interrupt or variations in the synchronization signal that was fed to the recording video machine.

The recorded CTL-pulses on the FLIR videotape Q-1 – Q-5 are similar, which indicates that similar sources have been used for recordings, such as video machines of the same type. The result also shows that recorded CTL-pulses on the FLIR videotape Q-6 – Q-7 are similar, which indicates that similar sources have been used for recordings, such as video machines of the same type.

7. RESULTS AND CONCLUSIONS

Section 7.1 summarizes the results from the image analysis part of the investigation, while section 7.2 deals with the results from investigating the authenticity.

7.1 Image Analysis

Several flashes are seen on FLIR videotape Q-4 recorded by the FBI Nightstalker surveillance aircraft on April 19, 1993, between 10:41 a.m. -12:16 p.m. In order to determine the cause of the flashes, a sophisticated computer hard and software systems solution was used to analyze the FLIR imagery, specially designed to maintain the image quality and limit further degradations.

In the case of alleged gunfire in open areas close to the complex, it is reasonable to assume that persons present to fire the subject weapons would be possible to detect on the FLIR imagery. Dr. Allard explained the lack of persons on the FLIR imagery as an inability to resolve the temperature differences, (app. 2, item 53). According to (app.2, item 71), Paul Beaver also concluded gunmen to be hard to detect if wearing Kevlar suits. Differences in radiated temperature from suits can occasionally be seen on the Fort Hood flight trial imagery from March 19, 2000. The Nightstalker imagery is of better spatial resolution and thermal sensitivity than the Lynx FLIR. The Lynx FLIR is very similar in performance to the FLIR used on April 19, 1993.

Moving persons are however possible to detect, at least partially, whenever the contrast relative to the wide temperature range of the background provides. From analyzing sequences from FLIR videotapes Q-1 and Q-5 and the March 19, 2000, Fort Hood flight trial imagery, it was verified that the FBI Nightstalker FLIR could resolve persons. Even if persons on the FLIR images momentarily appeared “thermally invisible,” it is highly implausible that a moving person, regardless suit worn, would have the same temperature as all of the complex background, at all times, on the FLIR imagery.

To determine if anything of consequence or if any persons were present in relation to each of the flashes, sequences of the FLIR imagery were enhanced in the area surrounding the flashes. When moving objects were identified proximate to a flash, analytical methods were employed to determine whether the movement was human in form or nature. The detected motion patterns were analyzed by tracing the movements. The moving objects were measured in size and grey levels. If the motion pattern seemed human-like, yet another method to analyze the motion pattern was to be applied. However, no human-like motion was found in the area surrounding the flashes, only moving debris. A further search for activity within low contrast areas in the FLIR imagery was performed, but without any findings that can be concluded to be persons. Neither have any persons been detected on the reviewed duplicate photos and copies of videotapes that were exposed close in time to the flashes.

From these results it is concluded with a reasonable level of certainty that all detected moving

objects are debris. The appearance of persons between 10:41 a.m. -12:16 p.m. on April 19, 1993, cannot be entirely excluded from analyzing FLIR videotape Q-4, the duplicate photos and videotapes, due to the limitations in resolution, field of view and presence of image artifacts as these are factors contributing to the low quality of the imagery. No human type movement or activity was however detected proximate to any of the flashes on the April 19, 1993, FLIR videotape Q-4. In fact nothing of consequence was detected proximate to any of the flashes.

During one of the first visual review of the FLIR videotapes, it was discovered that several of the flashes appeared at fixed positions and on a regular basis that agreed with the FBI Nightstalker's circular movements over the Branch Davidian complex. This result strongly suggested that the majority of the flashes were caused by solar reflections. To confirm these findings the reflection geometry was reconstructed utilizing a 3D model based on the physical laws of reflections. The 3D model incorporated the positions of the Branch Davidian complex, the sun and the FBI Nightstalker.

Based upon the striking correlation of the theoretical model and physical laws of reflections in comparison to the reconstructed geometry, it is concluded with a confident level of certainty that solar specular reflections on the FLIR videotapes are not only possible but have caused the majority of flashes on the April 19, 1993, FLIR videotapes. These findings were further confirmed by an additional experiment, which confirmed that solar reflections could, in fact, be captured by the FLIR sensor. The experiment also confirmed the model used to reconstruct the geometry of the flashes. It is also concluded with a reasonable level of certainty that some flashes were caused by heat reflections.

Four flashes of a pulsating nature could not be explained to reflections solely from the reconstructed data. The core of the FBI Nightstalker FLIR, the infrared SPRITE/TED detector elements and scanning mechanisms were believed to have contributed in causing undesired image artifacts on the FLIR videotapes. The interlaced video format used for recording the FLIR imagery were also believed to have contributed in distorting small objects like the flashes on the FLIR videotapes. The results from studying the characteristics of FBI Nightstalker FLIR detectors and the interlaced video format, confirmed that small flashes of short duration cannot be assumed to be correctly represented on the FLIR videotapes.

The Fort Hood flight trials were analyzed, as well, and pulsating flashes from reflecting debris were detected on the videotapes from the March 19, 2000, imagery. These pulsating specular solar reflections are distinctly similar to the flashes on the FLIR videotape from April 19, 1993. The muzzle blast flashes seen on the Fort Hood flight trial imagery from March 19, 2000 were different in appearance compared to the flashes on the FLIR videotape from April 19, 1993.

Many contradictory opinions exist on the cause of the flashes seen on the FLIR videotape from April 19, 1993. Due to the contradictory conclusions by experts concerning the cause of the flashes, these reports and statements were carefully reviewed. Dr. Allard and Mr. Maurice Cox, among others, conclude that the flashes are gunfire. Dr. Allard and Mr. Cox's gunfire hypothesis is not only based on wrongful assumptions, but also suffers from neglecting several important scientific parameters.

The Maryland Advanced Development Laboratory concluded that gunfire could be eliminated based solely on duration in all but 4 of the 90 events they analyzed, (app. 2, item 58). Their conclusion was based on an extensive analysis on muzzle blasts in the far IR, (app. 2, item 59) and (app. 2, item 60-61). From a contextual analysis and the strong correlation to other flashes from the same position, they judged these 4 events to be caused by other phenomena than small arm fire and strongly suggested specular solar reflections. Moreover, Duane Burchick, Maryland Advanced Development Laboratory, proved solar specular reflections on a watery surface at 10:53:25 on the FLIR videotape Q-4, (app. 2, item 62). Burchick also confirmed the potential of solar specular reflections in the far IR from a video recording, (app. 2, item 15).

Dr. Allard and Mr. Cox contend that the FBI Nightstalker FLIR could not record solar reflections. In the visual band sun glints are well known phenomena. Normally, sun glints does not cause too much of a problem in thermal images in the far IR band, $7 - 13$ μm. In the mid IR $3 - 5$ μm sun glints are more likely to add to the complexity of image interpretation. The appearances of sun glints in the far IR band are, however, well documented in the literature. Two examples are [HolstIR] and [Cuthbertson]. The large amount of glass from broken windows and the large amount of reflective debris from the demolished complex are factors that have contributed to a significant increased possibility of specular solar reflections then would have been the case at an earlier stage of the siege. Vector Data Systems (U.K.) Ltd. conducted a thorough review of the FLIR videotapes and the corresponding collateral imagery from which they accurately identified several of the reflecting objects, (app. 2, item 65). The appearance of sun glints on the FLIR imagery during the Fort Hood flight trials further verified that reflections are possible.

Contributing to Mr. Cox misinterpretations is his wrongful assumptions regarding the Nightstalker's speed and its position relative to the Branch Davidian complex. Variations in the flight path are compensated for by the on board operator in order to obtain imagery of the complex. Mr. Cox also disregards the effects of the wind that substantially affected the flight path. The wind caused the FBI Nightstalker's ground speed to vary significantly and thereby the duration time of the solar specular reflections. Therefore, constant airspeed cannot be used as in Mr. Cox calculations. Moreover, the surfaces of reflective objects can not be assumed to be aligned with the ground plane, but his assumption regarding reflections to be arbitrarily directed is correct. However, neither of these two reflection models makes any sense after the wrongful assumption about misplacement of aircraft's position.

Therefore, misplacements in the aircraft's circular movements from an ideal and constant flight path cannot be used in the reflection geometry model to prove that solar specular reflections are impossible. Misplacements from an ideal circular flight path would have been a more correct assumption if the FLIR sensor was instead fixed to the aircraft and directed by the fuselage. From the reconstructed flight paths in this investigation, section 5.4, it was seen that such precision can not be assumed. In practice, under the conditions on April 19, 1993, it is extremely difficult to keep the aircraft on track with such precision needed to keep the Branch Davidian complex in a fixed FLIR sensor field of view. This is mainly due to FBI Nightstalker FLIR system's narrow field of view, the distance to the complex and the

strong wind.

Dr. Allard stated "*nothing in nature could do this*" regarding the pulsating nature of thermal signatures. Multiple reflective objects and the characteristics of the FLIR imaging systems have within this work been concluded, with a reasonable level of confidence, to have created pulsating flashes. Neglecting the FLIR sensor scanning mechanisms and the interlaced format of used video standard, are factors contributing to Dr. Allard's and Mr. Cox's misinterpretation of the flashes seen on the FLIR videotapes from April 19, 1993.

The presence of solar specular reflections has been very well confirmed. The Maryland Advanced Development Laboratory conclusions gives a much more accurate and correct explanation of the flashes seen on the April 19, 1993, FLIR imagery. Dr. Allard's and Mr. Cox's conclusion that the FBI Nightstalker FLIR cannot record solar reflections has been proven wrong. In short, the reviewed reports and declarations confirm that solar reflections are the major source of the flashes seen on the FLIR videotapes from April 19, 1993.

The results from investigating the start and spread of the fire have been provided to Ulf Wickstöm, SP, Swedish National Testing and Research Institute, Borås, Sweden and were used in his Report to the Office of Special Counsel.

7.2 Video Authentication

The following electrical signatures have been analyzed; RF-envelope for video signal, RF-signal carrier frequency for video signal, RF-envelope for FM-audio signal, RF-signal carrier frequency for FM-audio signal, dihedral error measurements and CTL-pulses.

FLIR videotape Q-1 has at least three previous recordings found in the beginning of the tape, which all three have been over-recorded. The recording made at 05:58:11-08:00:02 on April 19, 1993, is an original recording with no signs of edit or erasure to the recorded portions.

FLIR videotape Q-2 is an original recording with no signs of edit or erasure to the recorded portions.

FLIR videotape Q-3 is an original recording with no signs of edit or erasure to the recorded portions.

FLIR videotape Q-4 is an original recording with no signs of edit or erasure to the recorded portions. Although the recording is interrupted between 10:47:16 – 10:51:57 there is no sign that this portion of the tape was edited or erased.

FLIR videotape Q-5 is an original recording with no signs of edit or erasure to the recorded portions.

FLIR videotape Q-6 is a first generation copy from an original master. There is no sign that the FLIR imagery has been edited. The master for this recording is not FLIR videotape Q-1 – Q-5.

FLIR videotape Q-7 is a first generation copy from an original master. Although the video sequence is interrupted between 10:47:15 and 10:51:57 there is no sign that this interruption in recording is an edit point. There is no sign that any other part of the FLIR imagery has been edited or erased. The master for this recording is not FLIR videotapes Q-1 – Q-5.

7.3 Conclusions

Finally, it is concluded with a confident level of certainty that all of the analyzed flashes seen on FLIR videotapes from the April 19, 1993, between 10:41 a.m. - 12:16 p.m. are caused by solar or heat reflections from single or multiple objects. The characteristics of the SPRITE/TED detectors and scanning mechanisms and the interlaced video format are factors that have contributed to distort the appearance of the flashes on the April 19, 1993, FLIR videotapes. Moreover, no humans were detected on the FLIR videotapes in any area in the vicinity of any of the flashes. Only moving debris were detected. The results from this investigation have shown, with a confident level of certainty, that the flashes on the FLIR videotapes from the April 19, 1993, between 10:41 a.m. - 12:16 p.m. cannot form evidence of gunfire.

It is also concluded, with a confident level of certainty, that FLIR videotapes Q-1 – Q-5, are original recordings. There is no sign that the recorded portions on FLIR videotapes Q-1 – Q-5 have been edited or erased after they were produced. It is concluded, with a confident level of certainty that the interrupt on FLIR videotape Q-4, between 10:47:16 and 10:51:57, was not created afterwards but during the time of recording. It is also concluded, with a confident level of certainty, that FLIR videotapes Q-6 – Q-7 are copies.

October 4, 2000

Mrs. Lena KLASÉN
Orlunda Agro & IT
Skänninge, SWEDEN

Mr. Sten MADSEN
Aservice i Linköping
Linköping, SWEDEN

REFERENCES

[AA] Astronomical Applications Dept. U.S. Naval Observatory, Washington, DC Internet: http://aa.usno.navy.mil/AA/data/docs/AltAz.html.

[Baker] Baker I. M., Hastings M. P., Hipwood L. G., Jones C. L. and Knowles P., "Infra-red Detectors for the year 2000", GEC REVIEW, Vol. 10, No. 31, p. 148-160, 1995.

[Bear] Bear M. F., Connors B. W. and Paradiso M. A., "Neuroscience, exploring the brain", Williams & Wilkins, 1996.

[Cuthberthson] Cuthberthson G. M. "Thermal Imaging", GEC REVIEW, Vol. 2, No. 1, p. 21-31, 1986.

[Elliott] Elliott C. T., "The SPRITE Detector". In: Institution of Electrical Engineering, Conference Publication "Advanced Infrared Detectors and Systems", 29-30 October 1981, p 1-6, 1981.

[Fraden] Fraden J., "AIP Handbook of Modern Sensors. Physics, Design and Applications", AIP Press, New York, 1993.

[Guichard] Guichard F. and Rudin L., "Velocity Estimation from Image Sequence and Application to Super Resolution". In: IEEE Proceeding on International Conference on Image Processing, Vol. 3, p. 527-531, 1999.

[HolstCCD] Holst C., "CCD Arrays, Cameras and Displays", SPIE Press, 1998.

[HolstIR] Holst C., "Testing and Evaluating Infrared Imaging Systems", SPIE Press, 1998.

[Klasén] Klasén L., "Image Analysis". In: Proceedings of the 12th INTERPOL Forensic Science Symposium, October 20-23 1998, Lyon, France, p. 261-301, 1999.

[Panasonic] "Basic Video Guide", Panasonic Matsushita Electric Industrial Co., Ltd., unknown year for publication.

[Philips] "Camera tubes and accessories, Image Intensifiers, IR detectors", Data Handbook, Electronic Components and Materials, T10-05-83, Part 10, 1983.

[Rudin] Rudin L. and Osher S., "Total Variation Based Image Restoration with Free Local Constraints" In: IEEE Proceeding on International Conference on Image Processing, Vol. 1, p 31-31, 1994.

[SWGIT] Scientific Working Group of Imaging Technologies, “Definitions and guidelines for the use of Imaging Technologies in the Criminal Justice System”, Version 2.1 6/8/99. Internet publication, Scientific Working Group of Imaging Technologies, http://www.for-swg.org/it_files/swgit_guidelines.html.

[Watkinson] Watkinson J., chapter 9 “Rotary-Head Tape Transport”. In: “The Art of Digital Video”, Focal Press, 1990.

[Vince] Vince J., “Virtual Reality Systems”, Addison-Wesley Publishing Company, 1995.

APPENDIX 1. AUTHOR BIOGRAPHIES

Mrs. Lena M. WIDIN KLASÉN.

Mrs. Klasén has worked for the Swedish government since 1988, both for the Swedish Defence and the Swedish National Police. After receiving her MSc in Computer Science and Technology at University of Linköping in 1988, Mrs Klasén worked 1988-1995 as a flight test engineer at the Testing Directorate, Defence Material Administration in Malmslätt, Sweden. Testing airborne reconnaissance, registration and surveillance systems, she come to work with CCD-, IR- as well as CMOS sensors, video of varying TV- and video format, digital and digitized video as well as still images. One of the tasks was to analyze image sequences using image analysis systems and software specialized for the purpose. She has also operated as an onboard engineer during flight tests. During one year from August 1994, she was stationed at Saab Military Aircraft to assist in image analysis within the Swedish fighter aircraft JAS39 Gripen test program. She has also been stationed at several Swedish Airforce air wings for shorter periods. In 1995 she received a new position as a systems engineer and worked with integration of the JAS39 avionics systems, which included the reconnaissance, sensing and recording systems among others.

Since January 1996, until August 2000 she was employed by the National Laboratory of Forensic Science, SKL, Sweden where she worked as a forensic engineer and also joined the Image Coding Group at Department of Electrical Engineering University of Linköping as a Ph.D. student. At SKL she established the image lab and several of the analytical methods in operative use. From May 1998 until September last year, she was head of the Information Technology group. The group dealt with casework in the area computer evidence, audio processing, and photography as well as image analysis. Since January this year she has devoted her full attention on her Ph.D. project on “3D reconstruction of shape and motion of non-rigid objects”, or in common language “tracking and measuring persons from video”. Since 1995 she have been investigating about two hundred cases, either in charge or as co-operating investigator. Measurement from images, identification from facial images, authentication of video and still images, technical investigations of video, imaging- or recording devices were some of the analytical methods she was involved in. She has also published book chapters and conference papers, on her research topic as well as on image analysis for forensic applications.

In January 2000 she established a small company to work on this investigation on a part time basis. Since September 1, 2000, she works as a researcher at the Defence Research Establishment, Division of Sensor Technology.

Mr. Sten K. MADSEN

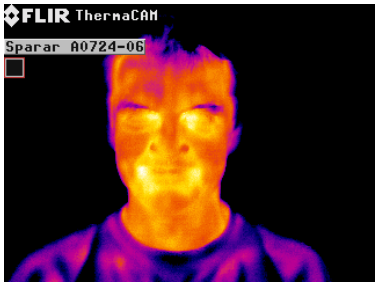

Since 1977 Mr. Madsen has run his own company Aservice i Linköping, mainly in the field of video support, products and consultations. His company supports productions companies and industries using video equipment for documentation and research. Mr. Madsen has a many years of experience from service and alignment of different videotape formats and auxiliary equipment such as video mixers, time base correctors, text-generators and digital video effect generators. Mr. Madsen has also been involved on several occasions, in specifying and constructing video-recording studios. He has also participated in numerous short training courses and workshops arranged by manufacturers. This experience has lead to a vast knowledge of videotape format such as VHS, SVHS, V8, Hi8, U-matic, highband/SP U-matic, Betacam, Betacam SP and also digital video (DV) format. One of Mr Madsen's special skills is to modify system components to suit special purpose applications, such as systems for airborne or underwater applications, to meet the customer’s requirements.

Between February 1996 and December 1999 Mr. Madsen worked as a forensic engineer at the National Laboratory of Forensic Science in Sweden. In this job, Mr Madsen investigated cases concerning technical investigations of video. Some examples are tracing imaging or recording devices, video authenticity, copying order and editing.

Among his customers are Saab Military Aircraft, Saab Dynamics, Swedish National Police, Defence Research Establishment, Defence Material Administration, Swedish Army, Swedish Airforce and Bofors Underwater Technology.

APPENDIX 2: SOURCE OF DATA

Videotapes

1.	Videotape Q-1, VHS "Nightstalker - 4/19/93 Tape#1 -5:57 Am-8:00 Am Q-1"
2.	Videotape Q-2, VHS "Nightstalker - 4/19/93 Tape #2 7:57A-9:30 AM Q-2"
3.	Videotape Q-3, VHS "Q-3 Nightstalker 4/19/93 Tape #1 -5:57AM-7:57AM"
4.	Videotape Q-4, VHS "Tape 1 ORIGINAL 4/19/93 appx 1:30 Q-4"
5.	Videotape Q-5, VHS "4/19/93 Tape II Waco ORIGINAL appx 45 min Q-5"
6.	Videotape Q-6, VHS "Tape #16 FBI aerial infra-red recording of Mt. Carmel's Branch Davidian Compound on 4/19/93, 12:41 p.m. through 2:01 p.m. (2 of 2). Elsur #1B-319"
7.	Videotape Q-7, VHS "Tape #15 FBI aerial infra-red recording of Mt. Carmel's Branch Davidian Compound on 4/19/93, 10:41 a.m. through 12:41 p.m. (1 of 2). Elsur #1B-319"

Copies of Videotapes

8.	Videotape, BASF VHS U. S. Postal Inspection Service, "Direct copy Qc1., Lab date 12/21/99".
9.	Videotape, BASF VHS U. S. Postal Inspection Service, "Direct copy Qc2., Lab date 12/21/99".
10.	Videotape, BASF VHS U. S. Postal Inspection Service, "Direct copy Qc3., Lab date 12/21/99".
11.	Videotape, BASF VHS U. S. Postal Inspection Service, "Direct copy Qc4., Lab date 12/21/99".
12.	Videotape Maxell VHS, Reference video from FLIR "FLIR from March 26, 1993. Copied for Lena Klassen"
13.	Videotape "Waco Gunfire footage", Maxell VHS
14.	Videotape "Major Network News", Maxell VHS
15.	Videotape, VHS

	"Maryland Advanced Development Laboratory Solar Specular Reflections in the far IR spectrum • VDS •"
16.	Videotape NS-1, VHS "NS-1 Direct copy 3/29/00", copy of video recording during Fort Hood flight trials, Night Stalker.
17.	Videotape Lynx-1, VHS "Lynx 1 Direct copy 3/29/00", copy of video recording during Fort Hood flight trials, Lynx.
18.	Videotape Lynx-2, VHS " Lynx 2 Direct copy 3/29/00", copy video recording during Fort Hood flight trials, Lynx.
19.	Videotape, VHS, ThermaCAM video from Forth Hood flight trials "U. S. Postal Inspection Service, Direct copy FLIR videotape #1, 3/19/00"
20.	Videotape, VHS, ThermaCAM video from Forth Hood flight trials "U. S. Postal Inspection Service, Direct copy FLIR videotape #2, 3/19/00"
21.	Videotape, VHS "U. S. Postal Inspection Service, Direct copy V-3 #1, 3/19/00"
22.	Videotape, VHS "U. S. Postal Inspection Service, Direct copy V-3 #2, 3/19/00"
23.	Videotape, VHS "U. S. Postal Inspection Service, Direct copy Camera 1 Tape 1 of 2, 3/19/00"
24.	Videotape, VHS "U. S. Postal Inspection Service, Direct copy Camera 1 Tape 2 of 2, 3/19/00"
25.	Videotape, VHS "U. S. Postal Inspection Service, Direct copy Camera 2 Tape 1, 3/19/00"
26.	Videotape, VHS "U. S. Postal Inspection Service, Direct copy Camera 2 Tape 2, 3/19/00"

Digital Images

27.	DVD CLONE, Copy of a DVD, "FLIR footage" from April 19, 1993, Forensic Video Inc., Minneapolis.
28.	TDK CD, "Photographs from FBI of Davidian Compound 4/19/93".
29.	SONY CD-R. Copy of CD containing "Photographs from FBI of Davidian Compound 4/19/93".
30.	CD-RW IMATION "Folder FBI 4-19-93; 77 files"
31.	Kodak DS Photo CD "Scanned photos"

32.	Kodak DS Photo CD “Scanned photos”
33.	Zip-diskette “Fire Pixs, 39 files” FBI1210067, WACMUR Roll 2608
34.	Zip-diskette “Tactical Pixs, 46 files” FBI1210067, WACMUR Roll C 040943
35.	Hard drive containing results of 2000 FLIR trials
36.	CD Maxell, ThermaCAM primary digital images from ground position during Fort Hood flight trials and related software

Photos and Duplicate Photos

37.	Four photos from Fort Hood flight trials, aerial view United States Postal Inspection Service, roll #1 A00031087
38.	Four photos from Fort Hood flight trials, aerial view United States Postal Inspection Service, roll #2 A00031087
39.	Twenty-four photos from Fort Hood flight trials, aerial view United States Postal Inspection Service, roll #3 A00144476
40.	Twenty photos from Fort Hood flight trials, debris United States Postal Inspection Service, roll #4 A00144477
41.	Twenty-four photos from Fort Hood flight trials, debris United States Postal Inspection Service, roll #5 A00144477
42.	Three copies of photos taken from a black side sniper position showing the demolished catwalk roof
43.	Five pages duplicate images taken from a black side sniper position showing the demolished catwalk roof and the fire at the cafeteria

Maps and Drawings

44.	OSC Group I, Packet A: Mt. Carmel Floor Plan, Floors 1-4
45.	OSC Group I, Packet B: Branch Davidian Cause of Death Color Coding Grid/Bunker Recovery Grid
46.	OSC Group I, Packet C: Mt. Carmel Side Views
47.	OSC Group I, Packet D: Mt. Carmel First and Second Floor Plans
48.	OSC Group I, Packet E: Maps and Diagrams of Mt. Carmel and Surrounding Area
49.	OSC Group I, Packet F: Mt. Carmel Side Views

50.	Stake positions of Mount Carmel Compound generated by the FBI 6 days after the siege ended and a drawing of first floor plane revised 4/22/93.
51.	A 3D model of the complex, <*Mount Carmel.DFX*>.
52.	Six drawings of the complex external and interior views.

Reports

53.	Allard E. F., “Analysis of the April 19, 1993 Waco FLIR Videotapes”, March 1, 2000.
54.	Cox M., ”Sun Reflection Geometry”, technical report, revision 1, 22 March 1999.
55.	Johnson F., System Engineering and Laboratories Corporation, “Mount Carmel Complex Structural Damage Evaluation”. Prepared for Caddell & Chapman, Houston, Texas.
56.	Ziegel F., Radian Inc., “Report of Ferdinand Ziegel”, 29 February 2000.
57.	Zimmelman J. B., “Report of Jack B. Zimmelman”.
58.	Ertem M. C., Pierson R., Burchick D., Maryland Advanced Development Laboratory, “Analysis of Flashes by an Infrared Sensor”, report to US Department of Justice, February 28, 2000.
59.	Ertem M. C., Pierson R., Burchick D., Maryland Advanced Development Laboratory, “Long Wave Infrared Muzzle Flash Duration Experiment”, report to US Department of Justice, February 28, 2000.
60.	Ertem M. and Burchick D., Maryland Advanced Development Laboratory, “Muzzle flash detection by Infra-red Cameras”, report to US Department of Justice, February 28, 2000.
61.	Pierson R., Maryland Advanced Development Laboratory, notes prepared for Office of Special Counsel from “IR Video review of Fire Development Analysis report”, report to US Department of Justice, February 28, 2000.
62.	Burchick D., Maryland Advanced Development Laboratory, “Potential for Solar Reflections”, report to US Department of Justice, February 28, 2000.
63.	Ginsberg I. W., “Technical Review of Allard Report”, report to US Department of Justice, February 29, 2000.
64.	Corley G. W., Kosel H. C., Stejskal B. G., Construction Technology Laboratory Inc., “Analysis of Structural and Egress Issues Relating to Events of April 19, 1993 at the Branch Davidian Compound, Waco, Texas”, report to US Department of Justice, February 29, 2000.
65.	Oxley D. D., Evans N. M., Ayres P., Vector Data Systems (U.K.) Ltd., “Imagery Analysis Report The Events at Waco Texas 19 April 1993, prepared for Office of Special Counsel.

Related Literature

66.	A summary of NIIRS scale.
67.	Sea Owl Passive Identification Device, product specification GEC V5040, 1 page.
68.	Flight trial protocol. "Protocol for a Forward Looking Infra-red Imagery Trial", prepared for Office of Special Counsel and the United States District Court for the Western District of Texas.
69.	Aircraft handbook. Duplicate of the Nightstalker's Airplane Flight Manual, requested from Office of Special Counsel.
70.	Audio transcripts from videotape Q-1, Q-2, Q-4 and Q-5. Network International Forensic Science Division, "FLIR (Nightstalker) Tape Transcripts", prepared for The Office of Special Counsel.
71.	A summary of public statements made by experts regarding flashes at FLIR videotape Q-4.

Miscellaneous

72.	Climatic data for April 1993. U.S. Department of Commerce, Asheville, N. C., prepared for The Office of Special Counsel.
73.	Surface weather observations for March 18-19, 2000, Fort Hood, TX.
74.	Activity list from Vector Data Systems (U.K.) Ltd. An early and abbreviated version of the events by Vector Data Systems (U.K.) Ltd.